UNIVERSIDADE FEDERAL DO PARANÁ

VICTOR JUAN BENITES

CALCULATION OF TRANSPORT COEFFICIENTS OF GASEOUS MIXTURES AT LOW DENSITY BASED ON *AB INITIO* POTENTIALS

CURITIBA
2018

VICTOR JUAN BENITES

CALCULATION OF TRANSPORT COEFFICIENTS OF GASEOUS MIXTURES AT LOW DENSITY BASED ON *AB INITIO* POTENTIALS

Tese apresentada ao Curso de Pós-Graduação em Física do Setor de Ciências Exatas da Universidade Federal do Paraná, como requisito parcial à obtenção do grau de Doutor em Física.

Orientador: Prof. Dr. Felix Sharipov.

CURITIBA
2018

Catalogação na Fonte: Sistema de Bibliotecas, UFPR
Biblioteca de Ciência e Tecnologia

B467c Benites, Victor Juan
Calculation of transport coefficients of gaseous mixtures at low density based on ab initio potentials / Victor Juan Benites. – Curitiba, 2018.

Tese - Universidade Federal do Paraná, Setor de Ciências Exatas, Programa de Pós-Graduação em Física, 2018.

Orientador: Felix Sharipov .

1. Teoria do transporte. 2. Boltzmann, Equação de. 3. Teoria quântica. 4. Ab initio potential. I. Universidade Federal do Paraná. II. Sharipov, Felix. III. Título.

CDD: 530.132

Bibliotecário: Elias Barbosa da Silva CRB-9/1894

MINISTÉRIO DA EDUCAÇÃO
SETOR CIÊNCIAS DE CIÊNCIAS EXATAS
UNIVERSIDADE FEDERAL DO PARANÁ
PRÓ-REITORIA DE PESQUISA E PÓS-GRADUAÇÃO
PROGRAMA DE PÓS-GRADUAÇÃO FÍSICA

TERMO DE APROVAÇÃO

Os membros da Banca Examinadora designada pelo Colegiado do Programa de Pós-Graduação em FÍSICA da Universidade Federal do Paraná foram convocados para realizar a arguição da tese de Doutorado de **VICTOR JUAN BENITES** intitulada: **"Calculation of transport coefficients of gaseous mixtures at low density based on ab initio potentials"** , após terem inquirido o aluno e realizado a avaliação do trabalho, são de parecer pela sua aprovação no rito de defesa.
A outorga do título de doutor está sujeita à homologação pelo colegiado, ao atendimento de todas as indicações e correções solicitadas pela banca e ao pleno atendimento das demandas regimentais do Programa de Pós-Graduação.

Curitiba, 02 de Outubro de 2018.

FELIX SHARIPOV
Presidente da Banca Examinadora (UFPR)

JOSÉ DANILO SZEZECH JÚNIOR
Avaliador Externo (UEPG)

WILSON MARQUES JÚNIOR
Avaliador Interno (UFPR)

JOAO LUIZ FILGUEIRAS DE AZEVEDO
Avaliador Externo (IAE)

RESUMO

Os coeficientes de transporte para misturas binárias de gases monoatômicos foram calculados utilizando o método de Chapman-Enskog, na 10^a aproximação de polinômios de Sonine, considerando a teoria quântica para interações intermoleculares. Tal método permite expandir a função distribuição de velocidades do gás, considerando que o sistema esteja próximo do equilíbrio. As misturas consideradas são hélio-neônio, hélio-argônio e neônio-argônio. A interação entre as partículas é descrita em termos de potenciais *ab initio*, os quais não dependem de parâmetros experimentais. Tais potenciais são calculados utilizando conceitos básicos da física, como a lei de Coulomb e a equação de Schrödinger. Os coeficientes de transporte, ou seja, viscosidade, condutividade térmica, difusão e fator de termodifusão, foram calculados em um amplo intervalo de temperatura e no intervalo inteiro de fração molar. Uma inversão do sinal do fator de termodifusão para duas das misturas consideradas foi observada. A exatidão numérica dos coeficientes de transporte calculados nesse trabalho é mais alta que pode ser atingida no momento. A incerteza relacionada aos potenciais interatômicos representa a maior contribuição na incerteza total. Com base em comparações dos resultados relatados nesse trabalho com aqueles publicados na literatura aberta, podemos afirmar que os resultados relatados são os mais precisos até o momento.

Palavras-Chave: Teoria do transporte, Equação de Boltzmann, Teoria quântica, Potencial *ab initio*.

ABSTRACT

The transport coefficients of binary mixtures of monatomic gases have been calculated applying the Chapman-Enskog method, using the 10^{th} order of approximation with respect to the Sonine polynomials, considering a quantum approach to intermolecular collisions. This method allows us to expand the velocity distribution function of the gas, considering that the system is close to the equilibrium. The studied mixtures are helium-neon, helium-argon and neon-argon. The interactions between the particles are described using the *ab initio* potentials, which does not depend on experimental parameters. Such potentials are calculated using only basic principles of physics, such as Coulomb's law and Schrödinger's equation. The transport coefficients, namely, viscosity, thermal conductivity, diffusion and thermal diffusion factor, have been calculated in a wide range of the temperature and in the whole range of the mole fraction. A sign inversion of the thermal diffusion factor of two mixtures considered here has been detected. The numerical accuracy of the transport coefficients calculated in the present work is as high as it can be achieved at the moment. The uncertainty related to interatomic potentials used here represents the main contribution into the total uncertainty. Comparing the results reported in the present work with those published in the open literature, one can conclude that the reported results are the most precise at the moment.

Key-words: Transport theory, Boltzmann equation, Quantum theory, *Ab initio* potential.

AGRADECIMENTOS

Agradeço ao Laboratório Central de Processamento de Alto Desempenho (LCPAD) da UFPR, por disponibilizar suas máquinas para uso.

À CAPES pela bolsa de pesquisa.

Ao professor Dr. Felix Sharipov pela excelente orientação ao longo de todo o mestrado e doutorado.

A todos que de alguma forma estiveram envolvidos com este trabalho.

List of Figures

List of Tables

Nomenclature

$\boldsymbol{A}_i$	vector representing perturbation function, Eq.(4.27)
A_{pq}	matrix elements, Eq.(4.75)
a_0	Bohr radius
$\mathbb{B}_i$	tensor representing perturbation function, Eq.(4.27)
b	impact parameter
B_{pq}	matrix elements, Eq.(4.55)
$\boldsymbol{c}_i$	particle velocity of species i
$\boldsymbol{C}_i$	peculiar velocity of species i, Eq.(2.13)
$\boldsymbol{\mathscr{C}}_i$	dimensionless velocity of species i, Eq.(4.24)
$\boldsymbol{d}_{ij}$	vector of molar fraction gradient, Eq.(4.25)
$\boldsymbol{D}_i$	vector representing perturbation function, Eq.(4.27)
D_{12}	diffusion coefficient, Eq.(2.21)
$\mathcal{E}$	dimensionless energy, Eq.(4.105)
EFP	equivalent free path, Eq.(2.43)
E	energy of interaction particles, Eq.(4.105)
f	scattering amplitude
f_i	distribution function of species i, Eq.(2.2)
f_i^0	local Maxwellian function of species i, Eq.(4.7)

$\boldsymbol{G}$	velocity of center of mass, Eq.(2.33)
$\boldsymbol{g}$	relative velocity, Eq.(2.28)
$\hat{H}$	Hamiltonian, Eq.(2.46)
$\hbar$	reduced Planck constant
I_{ij}	linearized collision integral, Eq.(4.21)
j_l	spherical Bessel function
Kn	Knudsen number, Eq.(2.44)
k	wave number, Eq.(4.114)
k_{B}	Boltzmann constant
k_{T}	thermal diffusion ratio, Eq.(2.20)
MFP	mean free path, Eq.(2.40)
M	standard atomic weight in u
M_i	atomic weight of isotope in u
m_i	molecular mass of species i
m_r	reduced mass, Eq.(4.106)
N_L	Loschmidt constant
n_l	spherical Neumann function
n	number density of mixture
n_i	number density of species i
$\mathbb{P}$	pressure tensor, Eq.(2.14)
p	pressure, Eq.(2.15)
P_l	Legendre polynomials

$\boldsymbol{q}$ heat flow vector, Eq.(2.16)

$Q_{ij}^{(l)}$ transport cross section, Eq.(4.107)

$\boldsymbol{r}$ position vector

r_0 zero-point of potential

r_m point of phase shift calculation

$\mathbb{S}$ rate of shear tensor, Eq.(2.18)

$S_m^{(n)}$ Sonine polynomials, Eq.(4.52)

T temperature of mixture, Eq.(2.12)

t time

T^* reduced temperature, Eq.(2.39)

$\boldsymbol{v}_i$ bulk velocity of species i, Eq.(2.9)

$\boldsymbol{v}$ hydrodynamic velocity of mixture, Eq.(2.10)

V intermolecular potential, Eq.(2.34)

$\boldsymbol{w}$ average velocity of mixture, Eq.(2.11)

x_i molar fraction of ith species, Eq.(2.5)

α_{T} thermal diffusion factor, Eq.(2.22)

δ_{ij} Kronecker delta

δ_l phase shift

ϵ well-depth of potential

ε angle of the collision plane

κ thermal conductivity, Eq.(2.20)

μ viscosity, Eq.(2.17)

ρ	mass density of mixture, Eq.(2.7)
ρ_i	mass density of species i, Eq.(2.6)
σ	differential collision cross-section
σ_t	total cross section, Eq.(2.41)
χ	deflection angle
ψ	wave function
$\Omega_{ij}^{(l,r)}$	omega integral, Eq.(4.104)

Contents

*

Chapter 1

INTRODUCTION

1.1 Transport coefficients and their applications

Transport phenomena in gases play an important role in theoretical modeling of many technological processes, e.g., heat exchangers [1], mixing of gases [2], separation of gases [3], gaseous sensors [4], aerothermodynamics [5], etc. When all assumptions of continuous medium mechanics [6–8] are met, a description of transport phenomena can be based on the Navier-Stokes equations containing the transport coefficients [9] as input data. In case of single gas, the viscosity relating a shear stress to a velocity gradient and thermal conductivity relating a temperature gradient to a heat flux vector completely determine a behavior of the gas. The diffusion and thermal diffusion coefficients must be considered in addition if one deals with binary gaseous mixtures. Thus, the four transport coefficients, namely, viscosity, thermal conductivity, diffusion, and thermal diffusion, are needed to obtain solutions of the Navier-Stokes equations. An availability of reliable data on these coefficients is important for precise modeling of transport phenomena in continuous media. Moreover, the viscosity coefficient of single gases and their mixtures is used as an input parameter in rarefied gas dynamics [10–16] in order to determine the rarefaction parameter. It can be said that the transport coefficients are fundamental quantities for fluid mechanics in general.

The viscosity is the easiest coefficient to measure so that the list of papers reporting experimental data on this quantity is rather long, see e.g. Refs. [17–35]. It is harder to measure the thermal conductivity. Some experimental methods of such measurement and data on this coefficients are reported in Refs. [20–22, 36–40]. Experimental data on the binary diffusion in gases are very poor. Some data on this coefficient are given in Refs. [41, 42]. The thermal diffusion factor has not been measured till now. It can be

seen that a measurement of the transport coefficients is a hard task especially for gaseous mixtures. Under such circumstances, a necessity in developing reliable numerical methods to calculate the transport coefficients is very high.

Calculations of the transport coefficients are based on the kinetic Boltzmann equation [9–13, 43–45]. There are several approaches to solve this equation. The Chapman-Enskog method [44, 45] consists of an expansion of the velocity distribution function with respect to a small parameter which leads to the linearized Boltzmann equation for the perturbation function. The latter is represented via the Sonine polynomials and then the transport coefficients are calculated using a variational principle. The Boltzmann equation can also be solved by the discrete velocity method [13, 46, 47] which is used to calculate rarefied gas flows too [47]. The direct simulation Monte Carlo (DSMC) method is one more alternative to calculate rarefied gas flows. Considering some simple flows, like Couette flow or planar heat transfer, the transport coefficients can be extracted from numerical results obtained by this method, see e.g. Refs. [48, 49]. However, the discrete velocity and DSMC methods require significant computational efforts and are not justified for the unique purpose to calculate the transport coefficients. Thus, the Chapman-Enskog method [44, 45] is employed in the present work.

1.2 Importance of intermolecular potentials

To solve numerically the Boltzmann equation [46, 50] or to apply the DSMC method [51–53] we need an intermolecular potential as input data. All of them can be divided in two groups: phenomenological and *ab initio*. Phenomenological potentials, usually, represent a simple relation of the potential energy to the intermolecular distance. They contain several adjustable parameters which are extracted from some experimental data. For instance, the hard sphere model contains the molecular diameter as the unique adjustable parameter. The Lennard-Jones potential contains two adjustable parameters, namely, the well-depth and zero-point of potential. A typical way to extract these parameters is to calculate the viscosity coefficient as a function of the adjustable parameters and then to fit the parameters so as to have the best agreement between the numerical results of viscosity and experimental data. Then, the obtained adjustable parameters can be used to calculate the other transport coefficients, i.e., thermal conductivity, diffusion and thermal diffusion. Since it is not possible using few parameters to fit theoretical results

to experimental data over a wide range of the gas temperature, the phenomenological potentials leads to significant errors in prediction of the transport coefficients.

Ab initio potentials are obtained from main physical principles solving the Schrödinger equation for atomic nucleus and electrons. The potential energy of interatomic interaction is tabulated as a function of the interatomic distance. Using these data, some interpolating formula is usually proposed in order to make the use of the *ab initio* potential easier. Nowadays, the *ab initio* potentials are available practically for all noble gases and their mixtures, see e.g. Refs. [54–71]. Thereby, solving the Boltzmann equation based on *ab initio* potentials, we obtain the transport coefficients without using any experimental data.

Once the *ab initio* potential is chosen, the Boltzmann equation can be solved by two approaches to interatomic interaction: classical and quantum. The first approach is based on calculation of trajectories of interacting particles applying the classical mechanics. As a result, we obtain the deflection angle and relate the post-collision velocities to those before a collision. This approach is justified for heavy gases, e.g. argon, or in case of room temperature and higher. In case of light gases, e.g. helium, and at low temperatures, say 10 K, the classical approach fails. Therefore, the quantum approach based on the Schrödinger equation must be applied. However, we do not know *a priori* the contribution of the quantum effects. Moreover, techniques to measure the transport coefficients are always improved so that the experimental uncertainty can be of the order of the quantum effects even for heavy gases like argon. To obtain more reliable results, the quantum approach is applied for all mixtures considered here. Some particular calculations are carried out using the classical theory in order to have an idea about the discrepancy of the two approaches.

Some numerical results on the transport coefficients of single gases based on *ab initio* potentials can be found in Refs. [72–75]. Numerical results concerning gaseous mixtures are still very poor. We should mention that such results reported in the Refs. [76–79] contain a significant uncertainty because only few terms in the Sonine expansion were taken into account. Recently published work [71] provides the transport coefficients for the mixture helium - krypton.

1.3 Proposal of the present work

The proposals of the present work are as follows:

- *To calculate the transport coefficients with a high numerical accuracy for mixtures of noble gases using ab initio potentials.* The transport coefficients are calculated for helium-neon, helium-argon, and neon-argon mixtures for a wide range of the temperature and several values of the mole fraction. These mixtures have been chosen because they are frequently used in experiments [26, 80] and have the most accurate potential at the moment. Moreover, their potentials are well known and can be found in the open literature. All sources of numerical errors are analyzed and it is shown that the total numerical error is much smaller than the uncertainty related to *ab initio* potentials. Our aim is to keep the relative numerical error close to the order of 10^{-6} by analysing all contributions like errors of integration, finite difference scheme, transition between the quantum and semi-classical scheme, etc. The estimated uncertainty due to the potential of each transport coefficient depends on temperature and chemical composition of mixtures.

- *To implement the quantum approach to calculate the transport cross sections for all gases considered here.* In fact, the transport coefficients are calculated via the so-called Omega integrals where the cross sections are integrants. In turn, these cross sections depend on the relative velocity of two colliding molecules and are expressed in terms of the phase shifts. In order to achieve the desirable accuracy of the transport coefficient, the phase shift should be calculated with a high accuracy combining the purely quantum method and the semi-classical Wentzel-Kramers-Brillouim (WKB) method.

1.4 Organization of this work

In Chapter 2, we define the basic concepts of transport phenomena and kinetic theory of gases. The transport coefficients are defined from the macroscopic viewpoint. The velocity distribution function is introduced and the kinetic Boltzmann equation is written down. In Chapter 3, a bibliographic survey about *ab initio* potentials is given. The most reliable *ab initio* potentials found in the open literature are pointed out. A review about experimental data and theoretical results on the transport coefficients is presented with an

estimation of their uncertainties. In Chapter 4, we describe the methodologies used in this work, focusing on the Chapman-Enskog method used to solve the Boltzmann equation in order to have analytical expressions for the transport coefficients. The methods employed to calculate the transport cross sections and phase shifts are described in details. In Chapter 5, we explain the numerical scheme used in the present work with an analysis of the numerical error of our results. The transport coefficients for the mixtures considered in this work are tabulated for many values of the temperature and molar fraction. A comparison with previously published results is performed. Finally, in Chapter 6 we give our conclusions about this work. In Appendix A, the universal constants used in this work are presented.

Chapter 2

BASIC CONCEPTS OF KINETIC THEORY OF GASES

2.1 Main assumptions of kinetic theory

The kinetic theory of gases [9,12,13,44,45,81] describes the motion and the interactions of a huge number of particles under the assumption that there is no correlation between moving particles. In other words, the particles are in free motion independent of each other during practically all time. A particle undergoes an interaction with another one only during a very short time. Such a condition can be fulfilled if the average distance between particles is much larger than their size. Under standard conditions, i.e. when the pressure is equal to 10^5 Pa and the temperature is 273.15 K, the average distance estimated via the Loschmidt constant N_L (see Table A.1) is about $1/N_L^{1/3} \approx 3$ nm, while the molecular size is one order smaller.

In addition, here the free-motion of particles is considered to be classical. This assumptions is valid when the de Broglie wavelength is much smaller than the interatomic distance. Mathematically, this non-degeneracy condition reads [15, 82, 83]

$$\frac{nh^3}{(2\pi m k_{\mathrm{B}} T)^{3/2}} \ll 1, \tag{2.1}$$

where n is the gas number density, h is the Planck constant, m is the atomic mass of the gas, k_{B} is the Boltzmann constant (see Table A.1) and T is the gas temperature. This condition is well satisfied under the standard conditions. Using the state equation, $p = nk_{\mathrm{B}}T$, one can estimate the maximum pressure when the condition (2.1) is met for any gas temperature T.

We will consider only monatomic non-ionized gases so that their internal structure is disregarded and no external force acting on particles is taken into account. Below,

main definitions of the kinetic theory of gases are given with basis on the textbooks [9, 12, 13, 44, 45, 81].

2.2 Velocity distribution function

First of all, we need to define a quantity that gives the number of particles d^6N of a species i expected within the physical space d^3r close to $\boldsymbol{r}$, and in the velocity space d^3c_i close to $\boldsymbol{c_i}$ at the instant t. The quantity that determines such a number under the assumption listed in the previous section is the *distribution function* $f_i(t, \boldsymbol{r}, \boldsymbol{c_i})$ defined as

$$f_i(t, \boldsymbol{r}, \boldsymbol{c_i}) := \frac{\mathrm{d}^6N}{\mathrm{d}^3r\mathrm{d}^3c_i}. \tag{2.2}$$

This distribution function contains all information about a mixture flow. For instance, its integration over the whole velocity space leads to the *number density* $n_i(t, \boldsymbol{r})$ of the corresponding species, i.e.,

$$n_i(t, \boldsymbol{r}) := \int f_i(t, \boldsymbol{r}, \boldsymbol{c_i})\mathrm{d}^3c_i. \tag{2.3}$$

The total number density n of the mixture is defined as the sum of the number density of each species of the mixture:

$$n(t, \boldsymbol{r}) := \sum_i n_i(t, \boldsymbol{r}). \tag{2.4}$$

The molar fraction of species i is defined by the ratio

$$x_i := \frac{n_i}{n}. \tag{2.5}$$

It is obvious that $\sum_i x_i = 1$ so that the molar fraction of the first species determines completely the chemical composition of a binary mixture.

The *mass density* of each species $\rho_i(t, \boldsymbol{r})$ is given as

$$\rho_i := n_i m_i, \tag{2.6}$$

where m_i is the molecular mass of the corresponding species. The total mass density ρ of the mixture is calculated by summing the mass density of each species:

$$\rho := \sum_i \rho_i = \sum_i n_i m_i. \tag{2.7}$$

2.3 Macroscopic quantities

To define other concepts, let us introduce the notation for the average of any quantity $\varphi_i(\boldsymbol{c}_i)$ as

$$\overline{\varphi}_i := \frac{1}{n_i} \int f_i(t, \boldsymbol{r}_i, \boldsymbol{c}_i) \varphi_i(\boldsymbol{c}_i) \, \mathrm{d}^3 c_i. \tag{2.8}$$

A macroscopic velocity of mixture can be defined by various ways described in this section. First, let us define the bulk velocity of species i as

$$\boldsymbol{v}_i := \overline{\boldsymbol{c}}_i. \tag{2.9}$$

The *hydrodynamic* velocity $\boldsymbol{v}$ of a mixture as whole is defined as:

$$\boldsymbol{v} := \frac{1}{\rho} \sum_i \rho_i \boldsymbol{v}_i, \tag{2.10}$$

which is that velocity usually measured in practice. The *average* velocity $\boldsymbol{w}$ of the mixture is defined as:

$$\boldsymbol{w} := \frac{1}{n} \sum_i n_i \boldsymbol{v}_i. \tag{2.11}$$

The *temperature* of a mixture is related to the average kinetic energy of chaotic motion of particles in the reference frame related to the hydrodynamic velocity of the mixture

$$T := \frac{1}{3nk_\mathrm{B}} \sum_i n_i m_i \overline{C_i^2}, \tag{2.12}$$

where

$$\boldsymbol{C}_i := \boldsymbol{c}_i - \boldsymbol{v}, \tag{2.13}$$

is the *peculiar velocity*, i.e., the particle velocity in the reference frame related to the hydrodynamic velocity $\boldsymbol{v}$. Physically, Eq. (2.12) means that the temperature is a measure of kinetic energy of the thermal agitation. Moreover, this definition leads to the energy equation of perfect gases used in thermodynamics.

The pressure tensor is defined as

$$\mathbb{P} := \sum_i n_i m_i (\overline{\boldsymbol{C}_i \boldsymbol{C}_i}). \tag{2.14}$$

Note that $\boldsymbol{C}_i\boldsymbol{C}_i$ is a tensor of the second rank determining the flux of the ith momentum component in the j direction in the reference frame related to the hydrodynamic velocity $\boldsymbol{v}$. The *hydrostatic pressure* can be calculated by taking the trace of the pressure tensor:

$$p := \frac{1}{3}\left(P_{11} + P_{22} + P_{33}\right). \tag{2.15}$$

The heat flow vector is defined as:

$$\boldsymbol{q} := \frac{1}{2}\sum_i n_i m_i \overline{C_i^2 \boldsymbol{C}_i}. \tag{2.16}$$

2.4 Definition of transport coefficients

The main purpose of the present work is to calculate the transport coefficients for mixtures. Below, these coefficients are defined from the macroscopic viewpoint.

2.4.1 Viscosity

First, we will define the *viscosity* coefficient μ, which relates the pressure tensor $\mathbb{P}$, see Eq.(2.14), and the rate-of-shear tensor $\mathbb{S}$ by *Newton's Law*:

$$\mathbb{P} = p\mathbb{I} - 2\mu\mathbb{S}, \tag{2.17}$$

where $\mathbb{I}$ is the identity matrix. The rate-of-shear tensor is defined in terms of the gradient of the hydrodynamic velocity, and its components are given by:

$$S_{\alpha\beta} := \frac{1}{2}\left(\frac{\partial v_\alpha}{\partial r_\beta} + \frac{\partial v_\beta}{\partial r_\alpha}\right) - \frac{1}{3}\delta_{\alpha\beta}\nabla\cdot\boldsymbol{v}. \tag{2.18}$$

Here, $\alpha, \beta = 1, 2, 3$, $\delta_{\alpha\beta}$ is de Kronecker delta and ∇ is a vector defined as:

$$\nabla := \left[\frac{\partial}{\partial r_1}, \frac{\partial}{\partial r_2}, \frac{\partial}{\partial r_3}\right]. \tag{2.19}$$

2.4.2 Thermal conductivity, diffusion and thermal diffusion

The heat flow vector for a binary mixture in the hydrodynamic regime reads

$$\boldsymbol{q} = -\kappa\nabla T + pk_{\mathrm{T}}\left(\boldsymbol{v}_1 - \boldsymbol{v}_2\right) + \frac{5}{2}p\left(\boldsymbol{w} - \boldsymbol{v}\right), \tag{2.20}$$

where κ is the *thermal conductivity* coefficient, k_{T} is the thermal diffusion ratio of species 1 in species 2. The quantities $\boldsymbol{v}_1$ and $\boldsymbol{v}_2$ are the mean velocity of each species, see Eq.(2.9), while $\boldsymbol{v}$ and $\boldsymbol{w}$ are defined for the mixture by Eqs.(2.10) and (2.11), respectively.

In a mixture, two species move relatively to each other due to gradients of molar fraction, pressure and temperature. Thus, the relative velocity is given as

$$\boldsymbol{v}_1 - \boldsymbol{v}_2 = -D_{12}\left[\frac{1}{x_2}\nabla \ln x_1 + \frac{n}{\rho}\left(m_2 - m_1\right)\nabla \ln p + \alpha_{\mathrm{T}}\nabla \ln T\right], \tag{2.21}$$

where D_{12} is the diffusion coefficient, and α_{T} is the thermal diffusion factor related by the thermal diffusion ratio by

$$\alpha_{\mathrm{T}} := \frac{k_{\mathrm{T}}}{x_1 x_2}. \tag{2.22}$$

Thus, the set of coefficients μ, κ, D_{12}, and α_{T} completely determine the constitutive equations for a binary mixture, i.e. relations between two physical quantities (especially kinetic quantities as related to kinematic quantities) that are specific to a material or substance, and approximate the response of that material to external stimuli.

The transport coefficients are calculated via the distribution function (2.2), as shown below.

2.5 Boltzmann equation

The distribution functions f_i obey the kinetic Boltzmann equation which describes their evolution due to the intermolecular collisions. Under the assumptions listed in Sec.2.1, the Boltzmann equation can be written as:

$$\mathcal{D}f_i = \sum_j J(f_i f_j), \tag{2.23}$$

where $\mathcal{D}f_i$ is the streaming term

$$\mathcal{D}f_i = \left(\frac{\partial}{\partial t} + \boldsymbol{c}_i \cdot \nabla\right) f_i(t, \boldsymbol{r}, \boldsymbol{c}_i) \tag{2.24}$$

and $J(f_i f_j)$ is the collision integral between species i and j

$$J(f_i f_j) = \int\int\int (f_i' f_j' - f_i f_j) g\sigma(g, \chi) \sin\chi \,\mathrm{d}\chi \,\mathrm{d}\varepsilon \,\mathrm{d}^3 c_j. \tag{2.25}$$

Here, the following abbreviations have been use:

$$f_i = f_i(t, \boldsymbol{r}, \boldsymbol{c}_i), \quad f_j = f_j(t, \boldsymbol{r}, \boldsymbol{c}_j), \tag{2.26}$$

$$f_i' = f_i(t, \boldsymbol{r}, \boldsymbol{c}_i'), \quad f_j' = f_j(t, \boldsymbol{r}, \boldsymbol{c}_j'), \tag{2.27}$$

where $\boldsymbol{c}_i$ and $\boldsymbol{c}_j$ are velocities before a collision, $\boldsymbol{c}_i'$ and $\boldsymbol{c}_j'$ are velocities after a collision, σ is the differential collision cross-section, χ is the deflection angle, ε is the angle of the plane in which the collision occurs, and $\boldsymbol{g}$ is the relative velocity of colliding particles

$$\boldsymbol{g} := \boldsymbol{c_i} - \boldsymbol{c_j}. \tag{2.28}$$

The relative velocity after a collision $\boldsymbol{g}'$ is determined by the angles χ and ε

$$g_1' = g_1 \cos\chi + \sqrt{g_2^2 + g_3^2}\, \sin\varepsilon\, \sin\chi, \tag{2.29}$$

$$g_2' = g_2 \cos\chi + \frac{g g_3 \cos\varepsilon - g_1 g_2 \sin\varepsilon}{\sqrt{g_2^2 + g_3^2}}\, \sin\chi, \tag{2.30}$$

$$g_3' = g_3 \cos\chi - \frac{g g_2 \cos\varepsilon + g_1 g_3 \sin\varepsilon}{\sqrt{g_2^2 + g_3^2}}\, \sin\chi. \tag{2.31}$$

The post-collision velocities are calculated via the relative velocity $\boldsymbol{g}'$ and the velocity of center of mass $\boldsymbol{G}$

$$\boldsymbol{c}_i' = \boldsymbol{G} + \frac{m_j}{m_i + m_j}\boldsymbol{g}', \quad \boldsymbol{c}_j' = \boldsymbol{G} - \frac{m_i}{m_i + m_j}\boldsymbol{g}', \tag{2.32}$$

being

$$\boldsymbol{G} := \frac{m_i \boldsymbol{c}_i + m_j \boldsymbol{c}_j}{m_i + m_j}. \tag{2.33}$$

The differential cross section $\sigma(g, \chi)$ is defined as the ratio of the number of particles scattered into a solid angle $\sin\chi\, \mathrm{d}\chi\, \mathrm{d}\varepsilon$ to the incident number of particles. This quantity depends on the relative velocity g and it is determined by the intermolecular potential.

2.6 Intermolecular potential

The intermolecular potential $V(r)$ is defined so that the potential energy of two particles separated by a distance r is equal to V. If this potential is known, then the interaction force F between these two particles is calculated as

$$F(r) = -\frac{\mathrm{d}V(r)}{\mathrm{d}r}. \tag{2.34}$$

An exact calculation of the potential $V(r)$ is a very hard task, and that is why many simplified models were proposed.

The most simple potential is the hard sphere (HS) model given as

$$V(r) = \begin{cases} \infty & \text{at} \quad r < d, \\ 0 & \text{at} \quad r > d, \end{cases} \tag{2.35}$$

where d is the sphere diameter. Physically, it means that two particles cannot be closer than their diameter, but when they are separated by a distance $r > d$, then the interaction force is zero. The differential cross section for this model is constant and expressed via the diameter as

$$\sigma = \frac{d^2}{4}, \tag{2.36}$$

which simplifies significantly the solution of the Boltzmann equation.

The authors of Refs. [84] solved the Boltzmann equation for hard spheres by the method proposed in Ref. [85] and obtained the following expressions of the viscosity and heat conductivity for a single gas

$$\mu = 1.01603\frac{5}{16}\frac{\sqrt{\pi m k_{\mathrm{B}} T}}{\pi d^2}, \quad \kappa = 1.02522\frac{75 k_{\mathrm{B}}}{64 m}\frac{\sqrt{\pi m k_{\mathrm{B}} T}}{\pi d^2}. \tag{2.37}$$

A direct numerical solution of the Boltzmann equation [46] confirmed this result. Thus, the molecular diameter d can be extracted from experimental data on the viscosity. However, if one calculates the diameter d from the gas viscosity at two different temperatures, one obtains two different values of the diameter. It means that we cannot calculate the diameter once at one temperature and then to use it for any other temperature. However, the hard sphere model works pretty well in situations where the temperature variation is small. That is why it is used in many applications [52, 86–88].

Tipton et al. [89, 90] calculated all transport coefficients of several binary mixtures applying the Chapman-Enskog procedure to the Boltzmann equation of hard spheres.

These results cannot be expressed by a simple formula, but they are presented in details by the authors of Refs. [89,90] in tables.

According to Eq.(2.37), the viscosity μ of hard sphere gas is proportional to $\sqrt{T}$, while empirical data, see for example, the review by Kestin et al. [91], indicate a different dependence of viscosity on the temperature. Such a discrepancy is explained by neglecting the attractive force between particles when they are separated by a distance $r > d$, due to mutual polarization. Moreover, the repulsive force arising at a short distance is really large but not infinite as for the hard sphere potential. These two factors are taken into account by the Lennard-Jones (LJ) potential given as

$$V(r) = 4\epsilon \left[\left(\frac{r_0}{r} \right)^{12} - \left(\frac{r_0}{r} \right)^{6} \right]. \tag{2.38}$$

The first term describes the repulsion between the particles and the second one describes the attraction between them. In the expression, the parameter ϵ is the well-depth of the potential and r_0 is its zero point where $V(r_0) = 0$.

The viscosity and heat conductivity of a single gas can be calculated by solving the Boltzmann equation with the LJ potential as a function of the reduced temperature

$$T^* = k_{\mathrm{B}} T/\epsilon \tag{2.39}$$

as was done in Ref. [46]. Then, this function can be used to fit the parameters ϵ and r_0 of Eq.(2.38) to experimental data on viscosity. The LJ potential is more physical than the hard sphere one and it is also widely used. However, it contains parameters that must be extracted from some kind of experimental data. In other words, it contains adjustable parameters.

Our aim is to calculate the transport coefficient without any adjustable parameter so that we will use the so-called *ab initio* potentials, which are obtained by using basic physical principles. This means that they do not depend on any experimental data. More detailed information about such potentials will be given in Sec. 3.1.

2.7 Knudsen number

The mean free path (MFP) [13] is defined as the mean distance travelled by a particle between two successive collisions, and for a single gas in equilibrium, it can be written as

$$\mathrm{MFP} = \frac{1}{\sqrt{2} n \sigma_t}, \tag{2.40}$$

where σ_t is the total cross-section defined via the differential cross-section as

$$\sigma_t := 2\pi \int_0^\pi \sigma(g, \chi) \sin\chi \mathrm{d}\chi. \tag{2.41}$$

It is important to notice that, if a cut-off is not defined for a potential like that given by Eq.(2.38), the MFP can be zero for classical interactions. It occurs because in the frame of the classical theory of interaction, gaseous particles are always colliding if a potential is nonzero at any distance. Mathematically this means that $\lim_{\chi\to 0}\sigma(g,\chi) \to \infty$. Thus, the total cross-section will be infinite, and the MFP will be zero. In order to avoid that, the intermolecular potential must have a cut-off, i.e. we assume that two particles do not interact with each other when the distance r between them exceeds some limit quantity r_m. In this case, the total cross section is equal to $\sigma_t = \pi r_m^2$. We also may assume that when the deflection angle is smaller than some cut-off value χ_0 ($\chi_0 \ll 1$), no collision happens, Then, the total cross-section is calculated as

$$\sigma_t = 2\pi \int_{\chi_0}^\pi \sigma(g, \chi) \sin\chi \mathrm{d}\chi, \tag{2.42}$$

and it is not infinite. However, both ways to cut-off do not define clearly how to determine the values r_m or χ_0. A consideration of intermolecular collision using a quantum approach leads to a finite and well-defined value of the total cross section which is not constant, but it depends on the relative velocity g.

Thus, the use of the MFP concept to describe non-equilibrium phenomena in gases is not convenient. The equivalent free path, defined as

$$\mathrm{EFP} := \frac{\mu}{p}\sqrt{\frac{2k_\mathrm{B}T}{xm_1 + (1-x)m_2}}, \tag{2.43}$$

is free from the above mentioned defects. This quantity is used to define the Knudsen number

$$\mathrm{Kn} := \frac{\mathrm{EFP}}{a}, \tag{2.44}$$

where a denote the characteristic size of gas flow. For boundless flows, the size a has the distance of significant variations of macroscopic quantities. In Sec. 4.1, the parameter Kn is used to expand the distribution function in order to solve the Boltzmann equation.

2.8 Schrödinger equation

As has been mentioned above, the free motion of particles is considered to be classical. However, an interaction of two particles will be considered in the framework of quantum

theory of scattering so that some concepts of quantum mechanics [92–94] will be given here.

The main concept of quantum theory is the wave function $\Psi = \Psi(\boldsymbol{r}, t)$, which determines completely the behaviour of a quantum particle. The quantity $|\Psi|^2 \, \mathrm{d}^3 r$ is the probability to meet a particle in the elementary volume $\mathrm{d}\boldsymbol{r}$ around the point $\boldsymbol{r}$. The wave function obeys the Schrödinger equation

$$i\hbar \frac{\partial}{\partial t} \Psi(\mathbf{r}, t) = \hat{H}\Psi, \tag{2.45}$$

where $i = \sqrt{-1}$ is the imaginary unit, $\hbar = h/2\pi$ is the reduced Planck constant (see Table A.1) and $\hat{H}$ is is the Hamiltonian operator.

When a moving particle of mass m is subject to a potential $V(\mathbf{r})$, the Hamiltonian is given as

$$\hat{H} = -\frac{\hbar^2}{2m}\Delta + V(\mathbf{r}), \tag{2.46}$$

where Δ is the Laplacian operator

$$\Delta = \frac{\partial^2}{\partial x^2} + \frac{\partial^2}{\partial y^2} + \frac{\partial^2}{\partial z^2}. \tag{2.47}$$

Thus, the Schrödinger equation takes the form

$$i\hbar \frac{\partial}{\partial t} \Psi(\mathbf{r}, t) = -\frac{\hbar^2}{2m}\Delta\Psi(\mathbf{r}, t) + V(\mathbf{r})\Psi(\mathbf{r}, t), \tag{2.48}$$

The energy E of a stationary state is calculated as

$$\hat{H}\Psi = E\Psi, \tag{2.49}$$

which leads to the following dependence on time

$$\Psi(\boldsymbol{r}, t) = e^{-iEt/\hbar}\psi(\boldsymbol{r}). \tag{2.50}$$

The function $\psi(\boldsymbol{r})$ obeys the stationary Schrödinger equation

$$\frac{\hbar^2}{2m}\Delta\psi + (E - V)\,\psi = 0, \tag{2.51}$$

which will be used to calculate the differential cross section.

Since we have established all basic concepts necessary for the understatement of this work, on the next chapter we will define the state of art of the calculation and measurement of transport coefficients.

Chapter 3

BIBLIOGRAPHIC REVIEW

3.1 *Ab initio* potentials

3.1.1 General remarks

Intermolecular potentials used in the present work are known as *ab initio* potentials because they are calculated from basic principles of physics, such as Coulomb's law and Schrödinger's equation. Unlike phenomenological potentials such as the Lennard-Jones expression [95] and the hard spheres model, these potentials do not contain any kind of adjustable parameter extracted from experimental results. First, the potential is tabulated, i.e. the potential, $V(r)$, is calculated for many values of the separation r, then it is interpolated using several sophisticated formulas. Below, the main potentials used in the present works are analyzed. The interpolating formulas are given and interpolating coefficients are tabulated. The main characteristics of all potentials are the well-depth, ϵ, the zero-point of potential ,r_0, where the potential is zero, $V(r_0) = 0$, and the well-position point ,r_ϵ. The latter is also called the equilibrium point because the attractive and repulsive forces are equal to each other in this position. These characteristics, which have been calculated in various papers, will be compared to each other in order to have and idea about the potential uncertainty.

3.1.2 Helium-helium potential

The first results on the *ab initio* potential for helium-helium interaction were obtained in 1995 by Aziz et al. [55] on the basis of the Hartree-Fock dispersion model. In 1997, Korona et al. [96] calculated the interaction potential using the symmetry-adapted perturbation theory (SAPT). At the same year, Janzen et al. [56] optimized the results given by Korona et al. In 1999, Cybulski and Toczyowski [57] calculated the potential for some no-

ble gases using the supermolecule single and double excitation coupled-cluster theory with non-iterative perturbational treatment of triple excitations CCSD(T). In 2000, Hurly and Moldover [97] calculated the *ab initio* potential, being the most precise authors until 2007, when Hurly and Mehl [98] used different methods for specific intervals of intermolecular distances to calculate it with a better precision. In the same year, Hellmann et al. [62] calculated the interaction potential with a higher precision. The potential proposed by Przybytek et al. [67] in 2010 was computed including relativistic and quantum electrodynamics contributions as well as improved accuracy adiabatic ones. Moreover, accurate asymptotic expansions were used for large distances. Some improvements and analysis of uncertainties of this potential are described by Cencek et al. [75]. The supplementary material of this work contains numerical codes to calculate the potential that is considered the most precise at the moment.

The interpolating formula elaborated in Ref. [67] can be written as:

$$V(r) = V_{tot}(r) + V_{ret}(r), \tag{3.1}$$

where the expression for V_{tot} represents a total of four terms, see Eq. (1) of Ref. [67], which is interpolated by a unique formula

$$V_{tot}(r) = e^{-ar}(P_0 + P_1 r + P_2 r^2) + e^{-br}(Q_0 + Q_1 r) - \sum_n f_n(\eta r)\frac{C_n}{r^n}, \tag{3.2}$$

and $f_n(x)$ is the Tang-Toennies damping function [99]:

$$f_n(x) = 1 - e^{-x}\sum_{k=0}^{n}\frac{x^k}{k!}. \tag{3.3}$$

The second term in Eq. (3.1) represents a small retardation correction and is written as:

$$V_{ret}(r) = \frac{C_3}{r^3} + \frac{C_4}{r^4} + [1 - g(\alpha r)]\,\frac{C_6^{BO}}{r^6}, \tag{3.4}$$

where $\alpha = 1/137.035999679$ according to Ref. [75] and $g(x)$ is given by:

$$g(x) = \frac{1 + \sum_{n=1}^{5} A_n x^n}{1 + \sum_{n=1}^{6} B_n x^n}. \tag{3.5}$$

The parameters of the interpolating formulas (3.1)-(3.5) are calculated in Ref. [67] and summarized in Table 3.1.

According to the estimation given in Ref. [75], the uncertainty of the potential (3.1) implies an relative uncertainty to the viscosity and the thermal conductivity of pure helium is 5×10^{-4} for $T \leq 50$ K and 2×10^{-5} for $T > 50$ K.

Table 3.1: Interpolating coefficients for Eqs.(3.2),(3.4), and (3.5) reported in Refs. [67] for helium-helium potential. The distance r is measured in Bohr radius a_0 and the potential is calculated in Hartree energy E_h.

a	3.6489030365283	A_1	8.454 943 177 941 253
b	2.36824871743591	A_2	15.552 570 228 545 543
η	4.09423805117871	A_3	7.556 443 185 698 804
P_0	-4.09423805117871	A_4	1.417 737 689 876 350
P_1	269.244425630616	A_5	0.142 506 077 478 301
P_2	-56.3879970402079	B_1	8.454 943 177 941 253
Q_0	38.7957487310071	B_2	16.006 586 066 260 556
Q_1	-2.76577136772754	B_3	10.378 373 954 734 820
C_3	0.577235×10^{-6}	B_4	3.515 803 817 223 855
C_4	-0.35322×10^{-4}	B_5	0.591 502 377 533 792
C_5	0.1377841×10^{-5}	B_6	0.059 455 768 329 599
C_6	1.461830	C_6^{BO}	1.460 977 837 725
C_8	14.12350		
C_{10}	183.7497		
C_{11}	-0.7674×10^2		
C_{12}	0.3372×10^{-4}		
C_{13}	-0.3806×10^4		
C_{14}	0.8534×10^5		
C_{15}	-0.1707×10^{-6}		
C_{16}	0.286×10^7		

Table 3.2: Well-depth ϵ, well-position r_ϵ, and zero-point r_0 for helium-helium potentials (3.1) and (3.6). The relative difference Δ is calculated between maximum and minimum values.

	Eq.(3.1), [67]	Eq.(3.6), [62]	Δ
ϵ/k_B (K)	10.996 427	10.997 898	1.3×10^{-4}
r_ϵ/a_0	5.607 951	5.608 068	2.1×10^{-5}
r_0/a_0	4.990 743	4.990 672	1.4×10^{-5}

In order to analyse the uncertainty of the potential, we will use the potential given in [62], which can be written as

$$V(r) = A\exp\left[a_1 r + a_2 r^2 + a_{-1} r^{-1} + a_{-2} r^{-2} + d_1 \sin(d_2 r + d_3)\right]$$

$$- \sum_{n=3}^{8} f_{2n}(br)\frac{C_{2n}}{r^{2n}}. \tag{3.6}$$

The interpolating coefficients are given in Table 6 of Ref. [62].

The well-depth ϵ, well-position r_ϵ, and zero-point r_0 for both potentials (3.1) and (3.6) are given in Table 3.2. It can be seen that these characteristics are very close to each other so that the additional effects taken into account in Ref. [67] just slightly changed the potential.

3.1.3 Neon-neon potential

In 1991, Eggenberger et al. [100] calculated the interaction energies for the neon-neon collisions *ab initio*, but they did not interpolated the results. In 1998, Grochola et al. [101] calculated the potential using the Moller-Plesset perturbation theory MP4(SDTQ). Cybulski and Toczylowski [57] calculated the interatomic potential for several species including the neon-neon one. In 2008, Hellmann and Bich [63] used the CCSDT(Q) method to calculate the interaction potential and interpolated it by the formula

$$V(r) = A\exp(a_1 r + a_2 r^2 + a_{-1} r^{-1} + a_{-2} r^{-2}) - \sum_{n=3}^{8} f_{2n}(br)\frac{C_{2n}}{r^{2n}}. \tag{3.7}$$

The fitting coefficients are given in Table 3.3, and the units are K and nm for Ref. [63] and E_h (Hartree energy) and a_0 (Bohr radius) for Ref. [57].

The well-depth ϵ, well-position r_ϵ, and zero-point r_0 for both potentials obtained in Refs. [57,63] are given in Table 3.4. It can be seen that the discrepancy of the well-depth is about 2%, while the points r_ϵ and r_0 deviate in these two works for about 0.3%.

Table 3.3: Interpolating coefficients for Eq. (3.7) reported in Refs. [57, 63] for neon-neon potential. The distance r is measured in nm and the potential in K in Ref. [63]. The distance r is measured in Bohr radius a_0 and the potential in the Hartree energy E_h in Ref. [57].

	Ref. [63]	Ref. [57]
A	$0.402915058383 \times 10^{8}$	88.5513
a_1	$-0.428654039586 \times 10^{2}$	-2.20626
a_2	$-0.333818674327 \times 10^{1}$	-2.49851×10^{2}
a_{-1}	$-0.534644860719 \times 10^{-1}$	0
a_{-2}	$0.501774999419 \times 10^{-2}$	0
b	$0.492438731676 \times 10^{2}$	1.85166
C_6	$0.440676750157 \times 10^{-1}$	6.28174
C_8	$0.164892507701 \times 10^{-2}$	90.0503
C_{10}	$0.790473640524 \times 10^{-4}$	1679.45
C_{12}	$0.485489170103 \times 10^{-5}$	4.18967×10^{4}
C_{14}	$0.382012334054 \times 10^{-6}$	1.36298×10^{6}
C_{16}	$0.385106552963 \times 10^{-7}$	5.62906×10^{7}

Table 3.4: Well-depth ϵ, well-position r_ϵ, and zero-point r_0 for neon-neon potentials given by Eq.(3.7). The relative difference Δ is calculated between maximum and minimum values.

	Ref. [63]	Ref. [57]	Δ
ϵ/k_{B} (K)	42.152521	41.153	2.4×10^{-2}
r_ϵ/a_0	5.838225	5.8559	3.0×10^{-3}
r_0/a_0	5.218004	5.2343	3.1×10^{-3}

3.1.4 Argon-argon potential

At 1993, Aziz [102] calculated the *ab initio* potential for the argon collisions using Hartree Fock Dispersion-B (HFD-B). Cybulski and Toczylowski [57] also determined the interaction potential for the argon collisions using the same method as that used by then for the helium and neon potentials. In 2003, Slavicek et al. [60] used the CCSD(T) method to determine their interaction potential. In 2006, Nasrabad and Laghaei [103] improved the CCSD(T) method used by Cybulski applying it to a Monte Carlo simulation using the Gibbs ensemble (GEMC). In 2009, Jager and Vogel [66,74] calculated the interaction potential using the CCSDT(Q) theory, obtaining results with an extremely high precision. In 2010, Patkowski and Szalewicz [104] considered more terms in the sum of the intermolecular energies than Jager and Vogel, obtaining the most accurate potential known at the moment for the argon-argon interaction.

In our calculations, we used the potential obtained in Refs. [57, 66], which can be interpolated by the formula (3.7) with the parameters given in Table 3.5. The units are K and nm for Ref. [66] and E_h and a_0 for Ref. [57].

Table 3.5: Interpolating coefficients for Eq. (3.7) reported in Refs. [57,69] for argon-argon potential. The distance r is measured in nm and the potential in K in Ref. [69]. The distance r is measured in Bohr radius a_0 and the potential in the Hartree energy E_h in Ref. [57].

	Ref. [66]	Ref. [57]
A	4.61330146×10^{7}	82.9493
a_1	-29.8337630	-1.45485
a_2	-9.71208881	-3.79929×10^{2}
a_{-1}	$2.75206827 \times 10^{-2}$	0
a_{-2}	$-1.01489050 \times 10^{-2}$	0
b	40.2517211	1.62365
C_6	0.442812017	63.7520
C_8	$3.26707684 \times 10^{-2}$	1556.46
C_{10}	$2.45656537 \times 10^{-3}$	4.94379×10^{4}
C_{12}	$1.88246247 \times 10^{-4}$	2.07289×10^{6}
C_{14}	$1.47012192 \times 10^{-5}$	1.105297×10^{8}
C_{16}	$1.17006343 \times 10^{-6}$	7.24772×10^{9}

The well-depth ϵ, well-position (equilibrium point) r_ϵ, and zero-point r_0 for both potentials obtained in Refs. [57,66] are given in Table 3.6. It can be seen that the discrepancy of the well-depth is about 2.6 %, while the points r_ϵ and r_0 deviate in these two works for about 0.5%.

Table 3.6: Well-depth ϵ, well-position r_ϵ, and zero-point r_0 for argon argon potentials given by Eq.(3.7). The relative difference Δ is calculated between maximum and minimum values.

	Ref. [66]	Ref. [57]	Δ
$\epsilon/k_{\rm B}$ (K)	143.123	139.52	2.6×10^{-2}
r_ϵ/a_0	7.10881	7.1492	5.6×10^{-3}
r_0/a_0	6.34459	6.3774	5.1×10^{-3}

3.1.5 Helium-neon, helium-argon and neon-argon potentials

The potentials for helium-neon, helium-argon and neon-argon interactions were calculated by Cybulski and Toczylowski [57]. In 2004, Cacheiro et al. [61] calculated the same potentials without estimation of their accuracy, but it seems that these results are more accurate than those by Cybulski and Toczylowski [57]. All potentials calculated in Refs. [57, 61] can be interpolated by the formula

$$V(r) = A\exp(-a_1 r + a_2 r^2) - \sum_{n=3}^{8} f_{2n}(br)\frac{C_{2n}}{r^{2n}}. \tag{3.8}$$

The interpolating coefficients are given in in Tables 3.7-3.9. The present results have been obtained by using both works [57, 61] in order to estimate the uncertainty related to the potentials. The main results of the present work are based on the paper Cacheiro et al. [61] being more accurate.

The well-depth ϵ, well-position r_ϵ, and zero-point r_0 for both potentials obtained in Refs. [57, 61] are given in Table 3.10. It can be seen that for the helium-neon interactions, the discrepancy in the well-depth is about 5%, while for r_0 and r_ϵ is close to 0.9%. For the helium-argon interactions, the divergence in the well-depth is close to 0.1%, for r_ϵ is about 0.02% and for r_0 is 0.0085%. For neon-argon collisions, one can notice a discrepancy close to 0.3% for all parameters.

Table 3.7: Interpolating coefficients for Eq. (3.8) reported in Refs. [57, 61] for helium-neon interactions. The distance r is measured in Bohr radius a_0 and the potential in the Hartree energy E_h in both works.

	Ref. [61]	Ref. [57]
A	24.39281476	24.4219
a_1	2.06719912	2.05766
a_2	−0.03101869	−0.0323443
b	2.59345555	2.65628
C_6	3.06231479	3.05239
C_8	31.679810	31.6787
C_{10}	427.73150	427.732
C_{12}	7725.1599	7725.16
C_{14}	1.8194500×10^5	1.81945×10^5
C_{16}	5.440120×10^6	5.44012×10^6

Table 3.8: Interpolating coefficients for Eq. (3.8) reported in Refs. [57, 61] for helium-argon interactions. The distance r is measured in Bohr radius a_0 and the potential in the Hartree energy E_h by the authors of both works.

	Ref. [61]	Ref. [57]
A	23.03058634	23.1693
a_1	1.63051044	1.63329
a_2	−0.04680016	−0.0462008
b	1.62747925	1.63719
C_6	9.40835513	9.38701
C_8	165.523018	165.522
C_{10}	3797.15796	3797.16
C_{12}	1.165179999×10^5	1.16518×10^5
C_{14}	4.66258×10^6	4.66258×10^6
C_{16}	2.36861×10^8	2.36861×10^8

Table 3.9: Interpolating coefficients for Eq. (3.8) reported in Refs. [57, 61] for neon-argon interactions. The distance r is measured in Bohr radius a_0 and the potential in the Hartree energy E_h by the authors of both works.

	Ref. [61]	Ref. [57]
A	75.46127492	75.4390
a_1	1.74950215	1.74939
a_2	−0.03696981	−0.0367715
b	1.62629958	1.63079
C_6	19.00663350	19.0098
C_8	392.862647	392.861
C_{10}	1.056270065×10^4	1.05627×10^4
C_{12}	3.798789997×10^5	3.79879×10^5
C_{14}	1.78160×10^7	1.78160×10^7
C_{16}	1.06075×10^9	1.06075×10^9

Table 3.10: Well-depth ϵ, well-position r_ϵ, and zero-point r_0 for helium-neon, helium-argon and neon-argon potentials given by Eq.(3.8). The relative difference Δ is calculated between maximum and minimum values.

	Ref. [61]	Ref. [57]	Δ
	helium - neon		
ϵ/k_B (K)	21.0357	22.145	5.0×10^{-2}
r_ϵ/a_0	5.72200	5.6697	9.1×10^{-3}
r_0/a_0	5.09994	5.0534	9.3×10^{-3}
	helium - argon		
ϵ/k_B (K)	29.7599	29.730	1.0×10^{-3}
r_ϵ/a_0	6.59786	6.5997	2.8×10^{-4}
r_0/a_0	5.89016	5.8921	8.5×10^{-5}
	neon - argon		
ϵ/k_B (K)	65.0267	65.008	2.9×10^{-4}
r_ϵ/a_0	6.59964	6.6015	2.8×10^{-4}
r_0/a_0	5.89989	5.9017	3.1×10^{-4}

Table 3.11: Isotope composition x_i, atomic weight of isotopes M_i, and average atomic weight M. Weights are given in atomic unit u.

gas	isotope	x_i, [105]	M_i, [106]	M, Eq.(3.9), [107]
helium	^{3}He	0.000 001 343(13)	3.016 029 3094(12)	4.002 602(2)
	^{4}He	0.999 998 657(13)	4.002 603 2497(15)	
neon	^{20}Ne	0.904 838(90)	19.992 440 176(3)	20.179 7(6)
	^{21}Ne	0.002 696(5)	20.993 846 74(4)	
	^{22}Ne	0.092 465(90)	21.991 385 50(25)	
argon	^{36}Ar	0.003 336 1(35)	35.967 546 26(27)	39.948(1)
	^{38}Ar	0.000 628 9(12)	37.962 732 2(5)	
	^{40}Ar	0.996 035 0(42)	39.962 383 124(5)	

3.2 Isotopic composition

As is known, any noble gas represents a mixture of its isotopes so that one never deals with a single isotope. It means that the transport coefficients must be calculated for a single gas considering its average atomic weight for a typical isotopic composition given as

$$M = \sum_{i=1}^{n} x_i M_i, \tag{3.9}$$

where x_i is the isotope fraction and M_i is the atomic weight of each isotope. The Commission on Isotopic Abundances and Atomic Weights of the International Union of Pure and Applied Chemistry has revised the Table of Isotopic Compositions of the Elements. The observed interval of isotope-abundance variation in natural gases are reported in Ref. [105]. The best measured results of the isotope fraction are given in the third column of Table 3.11. The atomic weights of each isotopes reported in Ref. [106] are given in the fourth column of the same table. The average atomic weight calculated by Eq.(3.9) is given in the fifth column of Table 3.11. These values are recommended in Ref. [107] as the standard atomic weight and are used in the present work.

3.3 Data on transport coefficients

Now, we will discuss about some results given by authors that measured or calculated the transport coefficients for helium, neon, argon and mixtures with these gases. The results from theoretical and experimental approach are divided in two subsections.

3.3.1 Viscosity

Experimental results

In 1959, Kestin and Leidenfrost [19] measured the transport coefficients for pure helium with an uncertainty of 0.5%. In 2000, Wilhelm and Vogel [27] measured the viscosity for pure argon with an uncertainty of 0.2%, but they had to admit the uncertainty of 3% close to the critical density point. In spite of the results have a good precision, we cannot compare our results with theirs because all pressures considered in their work are above 1 atm.

In 2002, Evers, Lösch and Wagner [29] measured the viscosity for pure helium, pure neon and pure argon with and uncertainty of 0.15% for the low density case, and 0.4% for higher densities. In 2006, May et al. [30] measured the ratio between the viscosity from helium at some temperatures and at 25°C. Also, they measured the ratio between the viscosity from argon and the viscosity from helium at the same temperatures. Using a reference viscosity, one could determine the viscosity for pure helium and pure argon at some temperatures between 200K and 400K. The uncertainty of those ratios are close to 0.084%.

In 2009, Seibt et al. [108] measured the viscosity of the helium, obtaining an uncertainty of 0.25%, but it was measured for pressures above 1 atm. In 2010, Vogel [31] measured the viscosity for pure argon with an uncertainty of 0.15%. In 2012, Berg and Burton [33] measured the viscosity for pure helium, pure neon and pure argon at 25 °C with an uncertainty of 0.032%. In 2014, Lin et al. [35] measured the viscosity of the argon, with an uncertainty of 0.062%. In the same year, Berg et al. [34] made a review of the experimental results using capillary viscometers at 25 °C. In this work, they claim that the best result for the viscosity of helium has an uncertainty of 0.001%, 0.032% for neon, and 0.027% for argon.

There is no reliable measurements for mixtures.

Tables 3.12, 3.13 and 3.14 show some of the obtained values from the authors cited above.

Semi-empirical results

In 1984, Kestin et al. [91] determined the viscosity for helium, neon, argon, krypton, and xenon, in a wide range of temperature, using a formula obtained empirically. More

Table 3.12: Experimental values of μ for helium vs. T.

	μ (μPa $\cdot$ s)	
T(K)	Ref. [34]	Ref. [29]
293.15	-	19.612
298.15	19.8253	-
Uncertainty (%)	0.001	0.4

Table 3.13: Experimental values of μ for neon vs. T.

	μ (μPa $\cdot$ s)	
T(K)	Ref. [34]	Ref. [29]
298.15	31.7088	31.691
348.15	-	35.225
Uncertainty (%)	0.032	0.4

than 400 reference values were used in order to interpolate the omega integrals, which are necessary to determine the transport coefficients. For example, the formula used to determine the viscosity for pure gases is given by:

$$\mu = \frac{5}{16}\left(\frac{mk_{\mathrm{B}}T}{\pi}\right)^{1/2}\frac{f_\mu}{r_0^2\Omega^{(2,2)*}}, \qquad \Omega^{(2,2)*} = \frac{\Omega^{(2,2)}}{\Omega^{(2,2)}_{HS}}, \tag{3.10}$$

where $\Omega^{(2,2)*}$ is the reduced omega integral, $\Omega^{(2,2)}_{HS}$ is the omega integral for hard spheres of diameter r_0, and f_μ is a factor that was adjusted. Since the interpolated expressions for the data are cumbersome, they are omitted here. Kestin el al. obtained results for a wide range of temperature and three different mole fractions. Some of the results and the uncertainties listed in their work are given in Tables 3.15-3.20.

Theoretical results

In 1993, Eggenberger et al. [109] calculated the viscosity of neon using a potential given in Ref. [100]. In the same year, Aziz [102] calculated the viscosity coefficient for argon with an uncertainty of 0.5%. Then, in 1995, Aziz calculated the viscosity for helium in Ref. [55]. In 1996, Xiufeng and Xi [110] calculated the viscosity for helium-neon mixture, but they do not specify the uncertainty of their results.

In 2000, Hurly and Moldover [97] calculated the viscosity of helium using an *ab initio* potential developed by themselves. In 2007, Hurly and Mehl [98] calculated the viscosity again, but now using their new *ab initio* potential, obtaining an uncertainty of 0.35%. Some of their results are given in Table 3.15.

Table 3.14: Experimental values of μ for argon vs. T.

	μ (μPa $\cdot$ s)			
T(K)	Ref. [34]	Ref. [31]	Ref. [29]	Ref. [30]
293.15	-	-	22.321	-
298.15	22.5666	-	-	22.578
350.34	-	25.760	-	-
565.36	-	37.177	-	-
681.82	-	42.496	-	-
Uncertainty (%)	0.027	0.15	0.4	0.084

Also in 2007, Bich, Hellmann and Vogel [72] calculated the viscosity for helium using the potential given in Ref. [62], obtaining an uncertainty of 0.02% for temperatures above 15K, and 0.2% for temperatures below 15K. Some of their results are given in Table 3.15

In 2008, Bich, Hellmann and Vogel [73] calculated the viscosity coefficient for neon using the potential given in [63], obtaining results with an uncertainty of 0.1%. Some of their results are presented in Table 3.16.

In 2009, Tipton, Tompson and Loyalka [89] calculated the viscosity coefficient for the noble gases, and the binary mixtures between then, in a wide range of temperature and mole fraction. The coefficients were calculated using the hard spheres potential, which implies that the results are not so realists. But, the method used by them, shown in Ref. [111], allows the calculation of the transport coefficients for any order of approximation in the Sonine polynomials expansion in the Chapman-Enskog method [44,45]. In this paper, the viscosity was calculated up to the 60^{th} order of approximation.

In 2009, Mehl [64] calculated the viscosity of pure helium using the potential given by Jeziorzka et al. in Ref. [112], but the uncertainty of the results is not cited in the paper. In the same year, Sharipov and Bertoldo [46] calculated the viscosity for helium, neon and argon numerically solving the linearized Boltzmann equation. Their results were obtained in terms of a reduced temperature.

The viscosity coefficients for the noble gases and their mixtures were calculated by Song et al. [76]. Some of their results are given in Tables 3.15-3.20. However, they used only the first approximation with respect to the Sonine expansion. As a result, their values for the viscosity and thermal conductivity differ significantly from those obtained for single gases in Refs. [72–74]. Thus, we conclude that the results reported by Song et al. [76] have a large uncertainty.

In 2010, Vogel et al. [74] calculated the viscosity coefficient for argon using the potential

given in [66], obtaining results with an uncertainty of 0.1%. Some of their results are listed in Table 3.17 .

In 2012, Cencek et al. [75] calculated the viscosity for pure helium with a high precision, achieving an uncertainty of 0.002%. This uncertainty of the transport coefficients is related to the potential uncertainty obtained by them. Those are the most precise results at the moment. In the same year, Sharipov and Strapasson [48] calculated the viscosity of the helium-argon mixture using the DSMC method at 300 K, obtaining an uncertainty of 0.5% related to the numerical method.

In 2014, Dodulad et al. [47] calculated the viscosity for helium-argon mixture, obtaining an uncertainty of 0.5%. In the same year, Song et al. [79] calculated the coefficient for helium using the potential given in [61], but the uncertainty was not informed. Some the their results are given in Table 3.15.

In Ref. [113], the transport coefficients for helium-argon mixture were calculated in a wide range of temperature and mole fraction, obtaining an uncertainty of 0.3% for temperature above 150 K. In this work, we used the classical approach to describe the collision between the particles, which leads to an additional uncertainty at low temperatures. However, the data reported in Ref. [113] are the most precise results for helium-argon mixture at the moment.

Tables 3.15-3.20 show some of the results obtained in the works listed above. It can be seen that the theoretical results are in agreement with the experimental data within the uncertainty declared in the corresponding papers.

Table 3.15: Theoretical results of viscosity μ for helium vs. T.

	μ (μPa $\cdot$ s)				
T(K)	Ref. [98]	Ref. [72]	Ref. [76]	Ref. [91]	Ref. [79]
10	2.1023	2.1018	-	-	-
100	9.5519	9.5531	9.5817	9.66	9.4372
200	15.128	15.130	15.319	15.26	15.080
273.15	18.677	18.678	-	18.81	18.644
300	19.908	19.910	20.172	20.04	19.880
400	25.260	24.261	24.569	-	24.240
600	32.196	32.196	32.564	-	32.184
1000	46.358	46.357	46.789	-	46.349
1273.15	-	-	-	55.04	-
2000	77.259	77.253	77.740	-	77.241
Uncertainty (%)	0.35	0.02	-	0.3	-

Table 3.16: Theoretical results of viscosity μ for neon vs. T.

	μ (μPa $\cdot$ s)		
T(K)	Ref. [73]	Ref. [76]	Ref. [91]
25	3.9213	-	-
100	14.399	14.642	14.39
200	24.122	23.982	24.29
273.15	29.900	-	30.13
300	31.860	31.479	32.10
400	38.640	38.083	-
600	50.604	49.783	-
1000	71.141	69.934	-
1273.15	-	-	83.67
2000	113.72	111.85	-
Uncertainty (%)	0.1	-	0.3

Table 3.17: Theoretical results of viscosity μ for argon vs. T.

	μ (μPa $\cdot$ s)		
T(K)	Ref. [74]	Ref. [76]	Ref. [91]
100	8.1271	8.1556	7.97
200	15.858	15.919	15.89
273.15	20.939	-	21.08
300	22.669	22.772	22.83
400	28.613	28.754	-
600	38.774	38.999	-
1000	55.450	55.839	-
1273.15	-	-	65.39
2000	88.604	89.418	-
Uncertainty (%)	0.1	-	0.3

3.3.2 Thermal conductivity

Experimental results

In 1981, Assael et al. [37] measured the thermal conductivity for the noble gases, estimating an uncertainty of 0.2% for their results. Their measurements were made for pressures higher than 1 atm.

In 2006, May et al. [30] used the measured viscosities ratios cited before to determine the thermal conductivity for argon, using the Prandtl number, which is a relation between the viscosity and the thermal conductivity coefficients, and for the the case where the gas is pure, its value is close to 2/3. The uncertainty of the thermal conductivity is close to 0.084%.

There is no reliable measurements for mixtures.

Table 3.18: Theoretical results of viscosity μ for helium-neon mixture at $x_1 = 0.5$ vs. T.

	μ (μPa $\cdot$ s)	
T(K)	Ref. [76]	Ref. [91]
100	12.895	13.27
200	20.786	21.69
273.15	-	26.77
300	27.310	28.50
400	33.143	-
600	43.607	-
1000	61.890	-
1273.15	-	75.44
2000	100.60	-
Uncertainty (%)	-	0.3

Table 3.19: Theoretical results of viscosity μ for helium-argon mixture at $x_1 = 0.5$ vs. T.

	μ (μPa $\cdot$ s)	
T(K)	Ref. [76]	Ref. [91]
100	9.4836	9.44
200	17.007	17.17
273.15	-	22.02
300	23.420	23.67
400	29.052	-
600	38.881	-
1000	55.496	-
1273.15	-	65.49
2000	89.630	-
Uncertainty (%)	-	0.3

Semi-empirical results

As described above, Kestin et al. [91] determined the transport coefficients for the noble gases using an interpolation for the omega integrals. For the thermal conductivity, the uncertainty is estimated to be close to 0.7%. The formula used to determine the thermal conductivity for pure gases is given by:

$$\kappa = \frac{75}{64}\left(\frac{k_B^3 T}{\pi m}\right)^{1/2} \frac{f_\kappa}{r_0^2 \Omega^{(2,2)*}}, \tag{3.11}$$

where $\Omega^{(2,2)*}$ and f_κ were adjusted too. The expressions of the thermal conductivity for mixtures are cumbersome and omitted here.

Table 3.20: Theoretical results of viscosity μ for neon-argon mixture at $x_1 = 0.5$ vs. T.

	μ (μPa $\cdot$ s)	
T(K)	Ref. [76]	Ref. [91]
100	10.832	10.65
200	19.382	19.51
273.15	-	24.92
300	26.409	26.74
400	32.512	-
600	43.110	-
1000	60.957	-
1273.15	-	72.18
2000	97.385	-
Uncertainty (%)	-	0.3

Theoretical results

Aziz calculated the thermal conductivity for pure helium and pure argon in Refs. [55, 102] using the *ab initio* potential.

In 2000, Hurly and Moldover [97] calculated the thermal conductivity for helium using their *ab initio* potential, and in 2007, Hurly and Mehl [98] obtained new results using their new potential, obtaining an uncertainty of 0.35%.

In 2007, Bich et al. [72] also calculated the thermal conductivity of helium using the potential given in [62]. In 2008, Bich et al. [73] obtained the thermal conductivity for pure neon with the potential given in Ref. [63]. The uncertainty of both results is the same that estimated for the viscosity. Some of their results are listed in Tables 3.21 and 3.22.

In 2009, Sharipov and Bertoldo [46] calculated the thermal conductivity for helium, neon and argon numerically solving the linearized Boltzmann equation numerically. In the same year, Mehl [64] obtained the thermal conductivity for pure helium using the potential given in Ref. [112]. In the same year, Song et al. [76] calculated the thermal conductivity for the noble gases and their mixtures. Some of their results are listed in the Tables 3.21-3.23. Like the viscosity, the thermal conductivity data have a large uncertainty because of the coarse approximation commented above. In 2010, Vogel et al. [74] calculated the thermal conductivity for argon using the potential given in Ref. [66]. Some of their results are given in Table 3.23. In 2012, Sharipov and Strapasson [48] also calculated the thermal conductivity for helium argon mixture using the DSMC method. Two years later, Song et al. [79] calculated the thermal conductivity for helium without an estimation of

the uncertainty of their results. In 2015, we calculated the thermal conductivity [113] considering classical interactions for helium-argon mixture.

The Tables 3.21-3.26 give some of the results from the papers cited above.

Table 3.21: Theoretical results of thermal conductivity κ for helium vs. T.

	κ (mW/m·K)				
T(K)	Ref. [98]	Ref. [72]	Ref. [76]	Ref. [91]	Ref. [79]
10	16.427	16.423	-	-	-
100	74.726	74.735	74.905	75.54	73.785
200	118.31	118.32	119.78	119.32	117.91
273.15	146.03	146.04	-	147.04	145.76
300	155.65	155.66	157.71	156.66	155.42
400	189.63	189.64	192.06	-	189.48
600	251.60	251.60	254.50	-	251.50
1000	362.14	362.12	365.53	-	362.06
1273.15	-	-	-	429.84	-
2000	603.20	603.15	607.00	-	603.06
Uncertainty (%)	0.35	0.02	-	0.7	-

Table 3.22: Theoretical results of thermal conductivity κ for neon vs. T.

	κ (mW/m·K)		
T(K)	Ref. [73]	Ref. [76]	Ref. [91]
25	6.0597	-	-
100	22.227	22.668	22.26
200	37.385	37.186	37.63
273.15	46.364	-	46.71
300	49.410	48.833	49.77
400	59.937	59.084	-
600	78.502	77.236	-
1000	110.35	108.48	-
1273.15	-	-	129.72
2000	176.35	173.43	-
Uncertainty (%)	0.1	-	0.7

3.3.3 Diffusion and thermal diffusion

Experimental results

High accuracy experimental results on diffusion and thermal diffusion are very rare. To our knowledge, only Kugler et al. [42] measured the diffusion coefficient for neon-argon mixture, obtaining an uncertainty between 0.4% and 1.4%, depending on the pressure.

Table 3.23: Theoretical results of thermal conductivity κ for argon vs. T.

	κ (mW/m·K)		
T(K)	Ref. [74]	Ref. [76]	Ref. [91]
100	6.3421	6.3660	6.22
200	12.380	12.427	12.41
273.15	16.355	-	16.46
300	17.709	17.789	17.83
400	22.369	22.478	-
600	30.343	30.518	-
1000	43.430	43.734	-
1273.15	-	-	51.23
2000	69.416	70.052	-
Uncertainty (%)	0.1	-	0.7

Table 3.24: Theoretical results of thermal conductivity κ for helium-neon mixture at $x_1 = 0.5$ vs. T.

	κ (mW/m·K)	
T(K)	Ref. [76]	Ref. [91]
100	38.172	39.93
200	61.450	64.74
273.15	-	79.66
300	81.070	84.96
400	98.776	-
600	130.83	-
1000	187.51	-
1273.15	-	229.05
2000	309.49	-
Uncertainty (%)	-	0.7

Semi-empirical results

Kestin obtained the diffusion coefficient and thermal diffusion factor using the same interpolation formula then before. For the diffusion, the uncertainty is 1% and for the thermal diffusion faction is close to 3%. Some of their results are given in Tables 3.27-3.32. The formulas used are:

$$D_{12} = \frac{3}{8}\left[\frac{k_{\mathrm{B}}^3 T^3 (m_1 + m_2)}{2\pi m_1 m_2}\right]^{1/2} \frac{(1+\Delta)}{p r_0^2 \Omega_{12}^{(1,1)*}(T_{12}^*)}, \tag{3.12}$$

$$\alpha_{\mathrm{T}} = (6C_{12}^* - 5)\left(\frac{x_1 S_1 - x_2 S_2}{x_1^2 Q_1 + x_2^2 Q_2 + x_1 x_2 Q_{12}}\right), \tag{3.13}$$

where $\Omega_{12}^{(1,1)*}(T_{12}^*)$, C_{12}^*, S_1, S_2, Q_1, Q_2, Q_{12} and Δ were interpolated.

Table 3.25: Theoretical results of thermal conductivity κ for helium-argon mixture at $x_1 = 0.5$ vs. T.

	κ (mW/m·K)	
T(K)	Ref. [76]	Ref. [91]
100	23.654	24.06
200	39.566	40.38
273.15	-	50.74
300	52.976	54.36
400	64.984	-
600	86.523	-
1000	124.24	-
1273.15	-	147.94
2000	204.79	-
Uncertainty (%)	-	0.7

Table 3.26: Theoretical results of thermal conductivity κ for neon-argon mixture at $x_1 = 0.5$ vs. T.

	κ (mW/m·K)	
T(K)	Ref. [76]	Ref. [91]
100	12.207	12.04
200	21.493	21.68
273.15	-	27.55
300	29.094	29.52
400	35.717	-
600	47.271	-
1000	66.840	-
1273.15	-	79.51
2000	107.00	-
Uncertainty (%)	-	0.7

Theoretical results

Song et al. [77] obtained in 2011 the diffusion coefficient and thermal diffusion factor for binary mixtures involving helium, neon and argon. Some of their results are given in Tables 3.27-3.32.

In 2012, Sharipov and Strapasson [48] also calculated the diffusion and thermal diffusion factor for helium-argon mixture using the DSMC method. In the next year, Song et al. [78] calculated the thermal diffusion for the noble gases using the Prandtl number, with an uncertainty of 0.25%. In our paper [113], theoretical results on the diffusion and thermal diffusion factor for helium-argon mixture based on the classical collision are reported.

Some of the above mentioned results are given in Tables 3.27-3.32.

Table 3.27: Theoretical results of diffusion coefficient D_{12} for helium-neon mixture at $x_1 = 0.5$ vs. T.

	D_{12} (10^{-4} m^2/s)	
T(K)	Ref. [77]	Ref. [91]
100	0.1697	0.1739
200	0.5556	0.5627
273.15	-	0.9480
300	1.1044	1.1079
400	1.7980	-
600	3.5791	-
1000	8.5608	-
1273.15	-	12.5178
2000	28.279	-
Uncertainty (%)	-	1

Table 3.28: Theoretical results of diffusion coefficient D_{12} for helium-argon mixture at $x_1 = 0.5$ vs. T.

	D_{12} (10^{-4} m^2/s)	
T(K)	Ref. [77]	Ref. [91]
100	0.1120	0.1139
200	0.3726	0.3810
273.15	-	0.6447
300	0.7425	0.7543
400	1.2085	-
600	2.4007	-
1000	5.7168	-
1273.15	-	8.4977
2000	18.742	-
Uncertainty (%)	-	1

3.3.4 General comments

From the review, one can notice that it is hard to measure the diffusion coefficients for any temperature and pressure since results for this coefficient are scarce. Even for other coefficients, reliable measurements have been done only for some specific temperatures and for pure gases. This indicates that theoretical results with a high precision are fundamental, because they can be determined with a modest computational effort for any temperature and for any molar fraction. The coefficients calculated numerically can be used as input data for other experiments or calculations.

Table 3.29: Theoretical results of diffusion coefficient D_{12} for neon-argon mixture at $x_1 = 0.5$ vs. T.

	D_{12} (10^{-4} m^2/s)	
T(K)	Ref. [77]	Ref. [91]
100	0.0448	0.0444
200	0.1594	0.1597
273.15	-	0.2771
300	0.3240	0.3262
400	0.5311	-
600	1.0578	-
1000	2.5075	-
1273.15	-	3.7203
2000	8.1031	-
Uncertainty (%)	-	1

Table 3.30: Theoretical results of thermal diffusion factor $-\alpha_{\mathrm{T}}$ for helium-neon mixture at $x_1 = 0.5$ vs. T.

	α_{T}	
T(K)	Ref. [77]	Ref. [91]
100	0.2673	0.2741
200	0.2948	0.3097
273.15	-	0.3206
300	0.2967	0.3227
400	0.2945	-
600	0.2882	-
1000	0.2769	-
1273.15	-	0.2894
2000	0.2574	-
Uncertainty (%)	-	3

Table 3.31: Theoretical results of thermal diffusion factor $-\alpha_{\mathrm{T}}$ for helium-argon mixture at $x_1 = 0.5$ vs. T.

	α_{T}	
T(K)	Ref. [77]	Ref. [91]
100	0.3114	0.2731
200	0.3802	0.3656
273.15	-	0.3845
300	0.3941	0.3865
400	0.3966	-
600	0.3935	-
1000	0.3826	-
1273.15	-	0.3699
2000	0.3599	-
Uncertainty (%)	-	3

Table 3.32: Theoretical results of thermal diffusion factor $-\alpha_{\mathrm{T}}$ for neon-argon mixture at $x_1 = 0.5$ vs. T.

	α_{T}	
T(K)	Ref. [77]	Ref. [91]
100	0.0832	0.0654
200	0.1629	0.1379
273.15	-	0.1642
300	0.1907	0.1710
400	0.2021	-
600	0.2095	-
1000	0.2099	-
1273.15	-	0.1995
2000	0.2019	-
Uncertainty (%)	-	3

Chapter 4

METHODOLOGIES

4.1 Chapman-Enskog method

In order to obtain the transport coefficients for a mixture, we will use the Chapman-Enskog method. This chapter is based on Refs. [44, 45, 89, 90] and provides just the main steps to derive the expressions of the transport coefficients omitting many mathematical details.

First, the distribution function for each component of the mixture is expanded with respect to the Knudsen number Kn defined by (2.44), i.e. we assume that Kn $\ll 1$. Physically, this means that a spacious variation of the distribution function is very small along a distance equal to the mean-free-path. Moreover, we consider only steady states, i.e., the distribution functions do not depend explicitly on time, i.e.

$$\frac{\partial f_i}{\partial t} = 0. \tag{4.1}$$

In other words, a significant variation of the distribution function occurs during a time much longer than the time between two successive collisions. Mathematically, these two assumptions mean that the ratio of the streaming term (2.24) to the collision integral (2.25) has the order of the Knudsen number

$$\mathcal{D}f_i \sim c_i \frac{f_i}{a}, \quad J(f_i f_j) \sim n c_i f_i \sigma_t \approx c_i \frac{f_i}{\mathrm{EFP}}, \tag{4.2}$$

where a is a characteristic size of gas flow and EFP$\approx 1/n\sigma_t$ is the equivalent free path. Now, the distribution functions of a binary mixture are represented as

$$f_1 = f_1^{(0)} + \mathrm{Kn} f_1^{(1)} + \mathrm{Kn}^2 f_1^{(2)} + ..., \tag{4.3}$$

$$f_2 = f_2^{(0)} + \mathrm{Kn} f_2^{(1)} + \mathrm{Kn}^2 f_2^{(2)} ..., \tag{4.4}$$

and substituted into the Boltzmann equation (2.23). Considering the terms of the same order and taking into account Eqs.(4.1) and (4.2), we obtain the recurrent equations relating the functions $f_i^{(n+1)}$ to $f_i^{(n)}$. Thus, the functions $f_i^{(0)}$ obey the following equations

$$\sum_{j=1}^{2} J(f_i^{(0)} f_j^{(0)}) = 0, \quad i = 1, 2, \tag{4.5}$$

while the functions $f_i^{(1)}$ are related to $f_i^{(0)}$ as

$$\boldsymbol{c}_i \cdot \nabla f_i^{(0)} = \sum_{j=1}^{2} \left[J(f_i^{(0)} f_j^{(1)}) + J(f_i^{(1)} f_j^{(0)}) \right]. \tag{4.6}$$

The solutions of Eq.(4.5) are Maxwellian [45]

$$f_1^{(0)} = n_1 \left(\frac{m_1}{2\pi k T} \right)^{\frac{3}{2}} \exp\left[-\frac{m_1}{2kT} (\boldsymbol{c}_1 - \boldsymbol{v})^2 \right], \tag{4.7}$$

$$f_2^{(0)} = n_2 \left(\frac{m_2}{2\pi k T} \right)^{\frac{3}{2}} \exp\left[-\frac{m_2}{2kT} (\boldsymbol{c}_2 - \boldsymbol{v})^2 \right], \tag{4.8}$$

where the densities n_i, temperature T, and the bulk velocity $\boldsymbol{v}$ are functions of the spatial coordinates $\boldsymbol{r}$. The distributions (4.7) and (4.8) lead to the Euler equations on the hydrodynamic level

$$\frac{1}{\rho_i} \frac{\mathrm{d}\rho_i}{\mathrm{d}t} = -\nabla \cdot \boldsymbol{v}_i, \tag{4.9}$$

$$\rho \frac{\mathrm{d}\boldsymbol{v}}{\mathrm{d}t} = -\nabla p, \tag{4.10}$$

$$\frac{\mathrm{d}\left(\rho T^{-3/2}\right)}{\mathrm{d}t} = 0, \tag{4.11}$$

Applying the Maxwellian function to determine the pressure tensor, heat flow vector and diffusion velocities, one obtains

$$\mathbb{P}^{(0)} = p\mathbb{I}, \tag{4.12}$$

$$\boldsymbol{q}^{(0)} = 0, \tag{4.13}$$

and

$$\boldsymbol{v}_1^{(0)} - \boldsymbol{v}_2^{(0)} = 0, \tag{4.14}$$

respectively. Further, we will use the perturbation functions defined as

$$f_i = f_i^{(0)}(1 + \phi_i + ...), \tag{4.15}$$

related to the distribution functions as

$$\mathrm{Kn}\, f_1^{(1)} = f_1^{(0)}\phi_1, \tag{4.16}$$

$$\mathrm{Kn}\, f_2^{(1)} = f_2^{(0)}\phi_2. \tag{4.17}$$

Substituting (4.16) and (4.17) into (4.6), we obtain the linearized Boltzmann equation:

$$\boldsymbol{c}_1 \cdot \nabla f_1^{(0)} = -n_1^2 I_1(\phi_1) - n_1 n_2 I_{12}(\phi_1 + \phi_2), \tag{4.18}$$

$$\boldsymbol{c}_2 \cdot \nabla f_2^{(0)} = -n_2^2 I_2(\phi_2) - n_1 n_2 I_{21}(\phi_1 + \phi_2). \tag{4.19}$$

where the following notation have been introduced

$$n_i^2 I_i(F) = \int\int f_i^{(0)} f^{(0)}(F_i + F - F_i' - F')g\sigma_{ii}(g,\chi)\sin\chi\,\mathrm{d}\chi\,\mathrm{d}\varepsilon\,\mathrm{d}^3c, \tag{4.20}$$

$$n_i n_j I_{ij}(K) = \int\int f_i^{(0)} f_j^{(0)}(K - K')g\sigma(g,\chi)\sin\chi\,\mathrm{d}\chi\,\mathrm{d}\varepsilon\,\mathrm{d}^3c_j. \tag{4.21}$$

Using the Euler equations (4.9-4.11), we can rewrite the left side of the Boltzmann equation in terms of the peculiar velocity

$$\boldsymbol{c}_1 \cdot \nabla f_1^{(0)} = f_1^{(0)}\left\{\left(\mathscr{C}_1^2 - \frac{5}{2}\right)\boldsymbol{C}_1 \cdot \nabla \ln T + \frac{1}{x_1}\boldsymbol{d}_{12} \cdot \boldsymbol{C}_1 + 2\boldsymbol{\mathscr{C}}_1\boldsymbol{\mathscr{C}}_1 : \nabla\boldsymbol{v}\right\}, \tag{4.22}$$

$$\boldsymbol{c}_2 \cdot \nabla f_2^{(0)} = f_2^{(0)} \left\{ \left(\mathscr{C}_2^2 - \frac{5}{2} \right) \boldsymbol{C}_2 \cdot \nabla \ln T + \frac{1}{x_2} \boldsymbol{d}_{21} \cdot \boldsymbol{C}_2 + 2\boldsymbol{\mathscr{C}}_2 \boldsymbol{\mathscr{C}}_2 : \nabla \boldsymbol{v} \right\}, \tag{4.23}$$

where the symbol ":" represents the double product of tensors and the quantity $\boldsymbol{\mathscr{C}}_i$ represents the dimensionless velocity

$$\boldsymbol{\mathscr{C}}_i := \sqrt{\frac{m_i}{2k_{\mathrm{B}}T}} \boldsymbol{C}_i, \tag{4.24}$$

and the vectors $\boldsymbol{d}_{12}$, $\boldsymbol{d}_{21}$ can be represented as:

$$\boldsymbol{d}_{12} = -\boldsymbol{d}_{21} = \nabla x_1 + x_1 x_2 (m_2 - m_1) \frac{n}{\rho} \nabla \ln p. \tag{4.25}$$

Since the left-hand sides of Eqs. (4.18) and (4.19) have the form (4.22) and (4.23), the unknown functions can be expressed as

$$\phi_1 = -\boldsymbol{A}_1 \cdot \nabla \ln T - \boldsymbol{D}_1 \cdot \boldsymbol{d}_{12} - 2\mathbb{B}_1 : \nabla \boldsymbol{v}, \tag{4.26}$$

$$\phi_2 = -\boldsymbol{A}_2 \cdot \nabla \ln T - \boldsymbol{D}_2 \cdot \boldsymbol{d}_{12} - 2\mathbb{B}_2 : \nabla \boldsymbol{v}. \tag{4.27}$$

Then, the system of Eqs(4.22) and (4.23) is split in three independent systems. The vectors $\boldsymbol{A}_1$ and $\boldsymbol{A}_2$ obey the following system

$$f_1^{(0)} \left(\mathscr{C}_1^2 - \frac{5}{2} \right) \boldsymbol{C}_1 = n_1^2 I_1(\boldsymbol{A}_1) + n_1 n_2 I_{12}(\boldsymbol{A}_1 + \boldsymbol{A}_2), \tag{4.28}$$

$$f_2^{(0)} \left(\mathscr{C}_2^2 - \frac{5}{2} \right) \boldsymbol{C}_2 = n_2^2 I_2(\boldsymbol{A}_2) + n_1 n_2 I_{21}(\boldsymbol{A}_1 + \boldsymbol{A}_2). \tag{4.29}$$

Moreover, these vectors must satisfy the relation

$$\int f_1^{(0)} m_1 \boldsymbol{C}_1 \cdot \boldsymbol{A}_1 \mathrm{d}\boldsymbol{c}_1 + \int f_2^{(0)} m_2 \boldsymbol{C}_2 \cdot \boldsymbol{A}_2 \mathrm{d}\boldsymbol{c}_2 = 0, \tag{4.30}$$

that follows from the fact that the center of mass of the mixtures is at rest. The vectors $\boldsymbol{D}_1$ and $\boldsymbol{D}_2$ are related to each other via the relations

$$\frac{1}{x} f_1^{(0)} \boldsymbol{C}_1 = n_1^2 I_1(\boldsymbol{D}_1) + n_1 n_2 I_{12}(\boldsymbol{D}_1 + \boldsymbol{D}_2), \tag{4.31}$$

$$-\frac{1}{1-x} f_2^{(0)} \boldsymbol{C}_2 = n_2^2 I_2(\boldsymbol{D}_2) + n_1 n_2 I_{21}(\boldsymbol{D}_1 + \boldsymbol{D}_2), \tag{4.32}$$

and satisfy the condition of the center of mass being at rest,

$$\int f_1^{(0)} m_1 \boldsymbol{C}_1 \cdot \boldsymbol{D}_1 \mathrm{d}\boldsymbol{c}_1 + \int f_2^{(0)} m_2 \boldsymbol{C}_2 \cdot \boldsymbol{D}_2 \mathrm{d}\boldsymbol{c}_2 = 0. \tag{4.33}$$

The tensors $\mathbb{B}_1$ and $\mathbb{B}_2$ are obtained from the system

$$f_1^{(0)} \boldsymbol{\mathscr{C}}_1 \boldsymbol{\mathscr{C}}_1 = n_1^2 I_1(\mathbb{B}_1) + n_1 n_2 I_{12}(\mathbb{B}_1 + \mathbb{B}_2), \tag{4.34}$$

$$f_2^{(0)} \boldsymbol{\mathscr{C}}_2 \boldsymbol{\mathscr{C}}_2 = n_2^2 I_2(\mathbb{B}_2) + n_1 n_2 I_{21}(\mathbb{B}_1 + \mathbb{B}_2). \tag{4.35}$$

The physical space isotropy leaves us the only manner to construct the vectors and tensors using the peculiar velocity

$$\boldsymbol{A} = \boldsymbol{C} A(C), \quad \boldsymbol{D} = \boldsymbol{C} D(C), \quad \mathbb{B} = \boldsymbol{C}\boldsymbol{C} B(C). \tag{4.36}$$

Now, the problem has been reduced to the unknown functions $A(C)$, $D(C)$ and $B(C)$.

Let us define the bracket integrals:

$$n^2\{F, G\} = n_1^2 [F, G]_1 + n_1 n_2 [F_1 + F_2, G_1 + G_2]_{12} + n_2^2 [F, G]_2, \tag{4.37}$$

$$[F, G]_1 := \int G_1 I_1(F) \mathrm{d}\boldsymbol{c}_1, \tag{4.38}$$

$$[F, G]_2 := \int G_2 I_2(F) \mathrm{d}\boldsymbol{c}_2, \tag{4.39}$$

$$[F_1 + G_2, H_1 + K_2]_{12} := \int F_1 I_{12}(H_1 + K_2) \mathrm{d}\boldsymbol{c}_1 + \int G_2 I_{21}(H_1 + K_2) \mathrm{d}\boldsymbol{c}_2. \tag{4.40}$$

Using these definitions and the relations (4.28)-(4.35), we obtain the following expressions:

$$n^2\{\boldsymbol{A}, \boldsymbol{a}\} = \int f_1^{(0)} \left(\mathscr{C}_1^2 - \frac{5}{2} \right) \boldsymbol{C}_1 \cdot \boldsymbol{a}_1 \mathrm{d}\boldsymbol{c}_1 + \int f_2^{(0)} \left(\mathscr{C}_2^2 - \frac{5}{2} \right) \boldsymbol{C}_2 \cdot \boldsymbol{a}_2 \mathrm{d}\boldsymbol{c}_2, \tag{4.41}$$

$$n^2\{\boldsymbol{D}, \boldsymbol{a}\} = \frac{1}{x_1} \int f_1^{(0)} \boldsymbol{C}_1 \cdot \boldsymbol{a}_1 \mathrm{d}\boldsymbol{c}_1 - \frac{1}{x_2} \int f_2^{(0)} \boldsymbol{C}_2 \cdot \boldsymbol{a}_2 \mathrm{d}\boldsymbol{c}_2, \tag{4.42}$$

$$n^2\{\mathbb{B}, \mathbb{b}\} = \int f_1^{(0)} \boldsymbol{\mathscr{C}}_1 \boldsymbol{\mathscr{C}}_1 : \mathbb{b}_1 \mathrm{d}\boldsymbol{c}_1 + \int f_2^{(0)} \boldsymbol{\mathscr{C}}_2 \boldsymbol{\mathscr{C}}_2 : \mathbb{b}_2 \mathrm{d}\boldsymbol{c}_2, \tag{4.43}$$

where $\boldsymbol{a}$ could be any vector and $\mathbb{b}$ could be any tensor defined in both velocity spaces.

4.2 Expression of viscosity

To calculate the viscosity coefficient, we need to start from the pressure tensor expression (2.14). Substituting (4.15) into (2.14) we obtain

$$\mathbb{P} = \mathbb{P}^{(0)} + \mathbb{P}^{(1)} + ... \tag{4.44}$$

The first term is calculated on the basis of $f_i^{(0)}$ given by (4.8) as

$$\mathbb{P}^{(0)} = p\mathbb{I}, \tag{4.45}$$

while the second term is based on ϕ_i

$$\mathbb{P}^{(1)} = 2m_1 \int f_1^{(0)} \phi_1 \boldsymbol{C}_1 \boldsymbol{C}_1 \, \mathrm{d}\boldsymbol{c}_1 + 2m_2 \int f_2^{(0)} \boldsymbol{C}_2 \boldsymbol{C}_2 \, \mathrm{d}\boldsymbol{c}_2. \tag{4.46}$$

The perturbation function in this case is given by the last terms of Eqs.(4.26) and (4.27) so that Eqs.(4.46) takes the form

$$\mathbb{P}^{(1)} = -2m_1 \int f_1^{(0)} \boldsymbol{C}_1 \boldsymbol{C}_1 (\mathbb{B}_1 : \nabla \boldsymbol{v}) \mathrm{d}\boldsymbol{c}_1 - 2m_2 \int f_2^{(0)} \boldsymbol{C}_2 \boldsymbol{C}_2 (\mathbb{B}_2 : \nabla \boldsymbol{v}) \mathrm{d}\boldsymbol{c}_2, \tag{4.47}$$

In terms of the bracket integrals (4.43), this expression can be written down in a compact form

$$\mathbb{P}^{(1)} = -\frac{4}{5} k_{\mathrm{B}} n^2 T \{\mathbb{B}, \mathbb{B}\} \, \mathbb{S}, \tag{4.48}$$

where the tensor $\mathbb{S}$ is defined by Eq. (2.18). Comparing this result and Eqs.(4.44), (4.45) with Newton's law (2.17), we conclude that viscosity coefficient takes the form

$$\mu = \frac{2}{5} k_{\mathrm{B}} n^2 T \{\mathbb{B}, \mathbb{B}\}. \tag{4.49}$$

In order to solve the bracket integrals, we will expand the tensor $\mathbb{B}$ in terms of the Sonine polynomials

$$\mathbb{B}_1 = \sum_{p=1}^{N} b_p \mathbb{b}_1^{(p)}, \quad \mathbb{B}_2 = \sum_{p=1}^{N} b_{-p} \mathbb{b}_2^{(p)}, \tag{4.50}$$

where

$$\mathbb{b}_1^{(p)} = S_{5/2}^{(p-1)}(\mathscr{C}_1^2) \boldsymbol{\mathscr{C}}_1 \boldsymbol{\mathscr{C}}_1, \quad \mathbb{b}_2^{(p)} = S_{5/2}^{(p-1)}(\mathscr{C}_2^2) \boldsymbol{\mathscr{C}}_2 \boldsymbol{\mathscr{C}}_2, \tag{4.51}$$

and $S_m^{(n)}(x)$ are the Sonine polynomials:

$$S_m^{(n)}(x) := \sum_{p=0}^{n} \frac{(m+n)!}{(p)!(n-p)!(m+p)!} (-x)^p. \tag{4.52}$$

The exact solution is taken in the limit $N \to \infty$.

If we define the coefficients

$$\beta_q = \frac{2}{5} n\{\mathbb{B}, \mathbb{b}^{(q)}\}, \tag{4.53}$$

then using (4.43) we obtain

$$\beta_1 = x_1, \quad \beta_{-1} = x_2, \quad \beta_q = 0 \quad \text{for} \quad q \neq \pm 1. \tag{4.54}$$

Combining Eqs.(4.50) and (4.53), the system of algebraic equations for the coefficients b_p is derived

$$\sum_{\substack{p=-N, \\ p\neq 0}}^{N} B_{pq} b_p = \beta_q, \quad q = \pm 1, \pm 2 \ldots \pm N \tag{4.55}$$

where

$$B_{pq} = \{\mathbb{b}^{(p)}, \mathbb{b}^{(q)}\}, \quad p, q = \pm 1, \pm 2 \ldots \pm N. \tag{4.56}$$

Once the coefficients b_p are known, the expressions (4.50) are substituted in the viscosity expression (4.49) leading to

$$\mu = \frac{5}{2} k_{\mathrm{B}} T \left(x_1 b_1 + x_2 b_{-1}\right). \tag{4.57}$$

4.3 Expressions of thermal conductivity, diffusion and thermal diffusion

The diffusion coefficient is related to the difference of mean velocities of species which is related to the perturbation function as

$$\boldsymbol{v}_1 - \boldsymbol{v}_2 = \frac{1}{n_1} \int f_1^{(0)} \phi_1 \boldsymbol{C}_1 \mathrm{d}\boldsymbol{c}_1 - \frac{1}{n_2} \int f_2^{(0)} \phi_2 \boldsymbol{C}_2 \mathrm{d}\boldsymbol{c}_2, \tag{4.58}$$

where Eqs.(2.9) and (4.15) have been used. A substitution of Eqs. (4.26) and (4.27) without the last terms into (4.58) leads to

$$\boldsymbol{v}_1 - \boldsymbol{v}_2 = -\frac{1}{3} \left\{ \left[\frac{1}{n_1} \int f_1^{(0)} C_1^2 D_1(C_1) \mathrm{d}\boldsymbol{c}_1 - \frac{1}{n_2} \int f_2^{(0)} C_2^2 D_2(C_2) \mathrm{d}\boldsymbol{c}_2 \right] \boldsymbol{d}_{12} \right.$$

$$\left. + \left[\frac{1}{n_1} \int f_1^{(0)} C_1^2 A_1(C_1) \mathrm{d}\boldsymbol{c}_1 - \frac{1}{n_2} \int f_2^{(0)} C_2^2 A_2(C_2) \mathrm{d}\boldsymbol{c}_2 \right] \nabla \ln T \right\}. \tag{4.59}$$

This expression is written down in a compact form using the bracket definition (4.37)

$$\boldsymbol{v}_1 - \boldsymbol{v}_2 = \frac{1}{3} n[\{\boldsymbol{D}, \boldsymbol{D}\}\boldsymbol{d}_{12} + \{\boldsymbol{D}, \boldsymbol{A}\}\nabla \ln T]. \tag{4.60}$$

Comparing this expression with (2.21) and taking into account (4.25), the diffusion coefficient and the thermal diffusion factor are obtained as

$$D_{12} = \frac{x_1 x_2}{3} n\{\boldsymbol{D}, \boldsymbol{D}\}, \tag{4.61}$$

and

$$\alpha_{\mathrm{T}} = \frac{1}{x_1 x_2} \frac{\{\boldsymbol{D}, \boldsymbol{A}\}}{\{\boldsymbol{D}, \boldsymbol{D}\}}. \tag{4.62}$$

To calculate the thermal conductivity coefficient, we will start from the expression for the heat flow vector (2.16). Using the distribution function in the form (4.15), the heat flow vector takes the form

$$\boldsymbol{q} = \boldsymbol{q}^{(0)} + \boldsymbol{q}^{(1)} = \frac{1}{2} m_1 \int f_1^{(0)} \phi_1 C_1^2 \boldsymbol{C}_1 \mathrm{d}\boldsymbol{c}_1 + \frac{1}{2} m_2 \int f_2^{(0)} \phi_2 C_2^2 \boldsymbol{C}_2 \mathrm{d}\boldsymbol{c}_2. \tag{4.63}$$

Substituting (4.26) and (4.27) without the last term into (4.63) we derive

$$\boldsymbol{q} = -\frac{1}{3} k_{\mathrm{B}} T n^2 \left[\{\boldsymbol{A}, \boldsymbol{A}\}\nabla \ln T + \{\boldsymbol{A}, \boldsymbol{D}\}\boldsymbol{d}_{12}\right] + \frac{5}{2} p(\boldsymbol{w} - \boldsymbol{v}). \tag{4.64}$$

Comparing this expression with (2.20), the thermal conductivity coefficient is derived

$$\kappa = \frac{1}{3} k_{\mathrm{B}} n^2 \left[\{\boldsymbol{A}, \boldsymbol{A}\} - \frac{\{\boldsymbol{A}, \boldsymbol{D}\}^2}{\{\boldsymbol{D}, \boldsymbol{D}\}}\right] = \frac{1}{3} k_{\mathrm{B}} n^2 \{\widetilde{\boldsymbol{A}}, \widetilde{\boldsymbol{A}}\}, \tag{4.65}$$

where

$$\widetilde{\boldsymbol{A}}_1 = \boldsymbol{A}_1 - k_{\mathrm{T}} \boldsymbol{D}_1, \quad \widetilde{\boldsymbol{A}}_2 = \boldsymbol{A}_2 - k_{\mathrm{T}} \boldsymbol{D}_2. \tag{4.66}$$

To calculate the brackets (4.65), we expand $\widetilde{\boldsymbol{A}}$ and $\boldsymbol{D}$ in the Sonine polynomials

$$\widetilde{\boldsymbol{A}}_1 = \sum_{p=1}^{N} a_p \boldsymbol{a}_1^{(p)}, \quad \widetilde{\boldsymbol{A}}_2 = \sum_{p=1}^{N} a_{-p} \boldsymbol{a}_2^{(p)}, \tag{4.67}$$

$$\boldsymbol{D}_1 = \sum_{p=0}^{N} d_p \boldsymbol{a}_1^{(p)}, \quad \boldsymbol{D}_2 = \sum_{p=0}^{N} d_{-p} \boldsymbol{a}_2^{(p)}, \tag{4.68}$$

where

$$\boldsymbol{a}_1^{(p)} = S_{3/2}^{(p)}(\mathscr{C}_1^2)\boldsymbol{\mathscr{C}}_1, \quad \boldsymbol{a}_2^{(p)} = S_{3/2}^{(p)}(\mathscr{C}_2^2)\boldsymbol{\mathscr{C}}_2, \quad p > 0 \tag{4.69}$$

$$\boldsymbol{a}_1^{(0)} = M_1^{1/2}\frac{\rho_2}{\rho}\boldsymbol{\mathscr{C}}_1, \quad \boldsymbol{a}_2^{(0)} = -M_2^{1/2}\frac{\rho_2}{\rho}\boldsymbol{\mathscr{C}}_2, \tag{4.70}$$

$$M_i = \frac{m_i}{m_1 + m_2}. \tag{4.71}$$

If we define the coefficients

$$\alpha_q = -\frac{4}{15}\frac{n}{\sqrt{2k_{\mathrm{B}}T}}\{\boldsymbol{A}, \boldsymbol{a}^{(q)}\} \tag{4.72}$$

then using (4.41) we obtain

$$\alpha_1 = \frac{x_1}{\sqrt{m_1}}, \quad \alpha_2 = \frac{x_2}{\sqrt{m_2}}, \quad \alpha_q = 0 \quad \text{for} \quad q \neq \pm 1. \tag{4.73}$$

Using Eq. (4.42), we obtain

$$\frac{2n}{3}\left(\frac{m_0}{2k_{\mathrm{B}}T}\right)^{1/2}\{\boldsymbol{D}, \boldsymbol{a}^{(q)}\} = \delta_{q0}. \tag{4.74}$$

Thus, the quantities d_p obey the system of algebraic equations

$$\sum_{p=-N}^{N} A_{pq}d_p = \delta_{q0}, \quad -N \leq q \leq N, \tag{4.75}$$

and the coefficients a_p are found from the other system

$$\sum_{\substack{p=-N,\\ p\neq 0}}^{N} A_{pq}a_p = \alpha_q, \quad q = \pm 1, \pm 2 \ldots \pm N. \tag{4.76}$$

where and a_{pq} are calculated as:

$$A_{pq} = A_{qp} = \{\boldsymbol{a}^{(p)}, \boldsymbol{a}^{(q)}\}, \quad -N \leq p, q, \leq N. \tag{4.77}$$

Then, the diffusion (4.61), thermal diffusion factor (4.62), and thermal conductivity (4.65) coefficients take the form

$$D_{12} = \frac{3}{2}k_{\mathrm{B}}Td_0\frac{x(1-x)}{n(m_1+m_2)}, \tag{4.78}$$

$$\alpha_{\mathrm{T}} = -\frac{5}{2}\frac{\sqrt{m_1+m_2}}{d_0}\left(\frac{d_1}{(1-x)\sqrt{m_1}} + \frac{d_{-1}}{x\sqrt{m_1}}\right), \tag{4.79}$$

$$\kappa = \frac{75}{8}kT^2\left(\frac{x}{\sqrt{m_1}}a_1 + \frac{1-x}{\sqrt{m_2}}a_{-1}\right), \tag{4.80}$$

respectively.

4.4 Bracket integrals

As shown mathematically in Refs. [89, 90], the terms B_{pq} can be written as follows:

$$B_{pq} = x_1^2 \left[S_{\frac{5}{2}}^{(p-1)}(\mathscr{C}_1^2)\mathscr{C}_1\mathscr{C}_1, S_{\frac{5}{2}}^{(q-1)}(\mathscr{C}_1^2)\mathscr{C}_1\mathscr{C}_1 \right]_1$$

$$+x_1x_2 \left[S_{\frac{5}{2}}^{(p-1)}(\mathscr{C}_1^2)\mathscr{C}_1\mathscr{C}_1, S_{\frac{5}{2}}^{(q-1)}(\mathscr{C}_1^2)\mathscr{C}_1\mathscr{C}_1 \right]_{12}, \tag{4.81}$$

$$B_{p-q} = x_1x_2 \left[S_{\frac{5}{2}}^{(p-1)}(\mathscr{C}_1^2)\mathscr{C}_1\mathscr{C}_1, S_{\frac{5}{2}}^{(q-1)}(\mathscr{C}_2^2)\mathscr{C}_2\mathscr{C}_2 \right]_{12}, \tag{4.82}$$

$$B_{-pq} = x_1x_2 \left[S_{\frac{5}{2}}^{(p-1)}(\mathscr{C}_2^2)\mathscr{C}_2\mathscr{C}_2, S_{\frac{5}{2}}^{(q-1)}(\mathscr{C}_1^2)\mathscr{C}_1\mathscr{C}_1 \right]_{21}, \tag{4.83}$$

$$B_{-p-q} = x_2^2 \left[S_{\frac{5}{2}}^{(p-1)}(\mathscr{C}_2^2)\mathscr{C}_2\mathscr{C}_2, S_{\frac{5}{2}}^{(q-1)}(\mathscr{C}_2^2)\mathscr{C}_2\mathscr{C}_2 \right]_2$$

$$+x_1x_2 \left[S_{\frac{5}{2}}^{(p-1)}(\mathscr{C}_2^2)\mathscr{C}_2\mathscr{C}_2, S_{\frac{5}{2}}^{(q-1)}(\mathscr{C}_2^2)\mathscr{C}_2\mathscr{C}_2 \right]_{21}. \tag{4.84}$$

The A_{pq} read:

$$A_{pq} = x_1^2 \left[S_{\frac{3}{2}}^{(p)}(\mathscr{C}_1^2)\mathscr{C}_1, S_{\frac{3}{2}}^{(q)}(\mathscr{C}_1^2)\mathscr{C}_1 \right]_1$$

$$+x_1x_2 \left[S_{\frac{3}{2}}^{(p)}(\mathscr{C}_1^2)\mathscr{C}_1, S_{\frac{3}{2}}^{(q)}(\mathscr{C}_1^2)\mathscr{C}_1 \right]_{12}, \tag{4.85}$$

$$A_{p-q} = x_1x_2 \left[S_{\frac{3}{2}}^{(p)}(\mathscr{C}_1^2)\mathscr{C}_1, S_{\frac{3}{2}}^{(q)}(\mathscr{C}_2^2)\mathscr{C}_2 \right]_{12}, \tag{4.86}$$

$$A_{-pq} = x_1x_2 \left[S_{\frac{3}{2}}^{(p)}(\mathscr{C}_2^2)\mathscr{C}_2, S_{\frac{3}{2}}^{(q)}(\mathscr{C}_1^2)\mathscr{C}_1 \right]_{21}, \tag{4.87}$$

$$A_{-p-q} = x_2^2 \left[S_{\frac{3}{2}}^{(p)}(\mathscr{C}_2^2)\mathscr{C}_2, S_{\frac{3}{2}}^{(q)}(\mathscr{C}_2^2)\mathscr{C}_2 \right]_2$$

$$+x_1 x_2 \left[S_{\frac{3}{2}}^{(p)}(\mathscr{C}_2^2)\mathscr{C}_2, S_{\frac{3}{2}}^{(q)}(\mathscr{C}_2^2)\mathscr{C}_2 \right]_{21}. \tag{4.88}$$

However, in the case where we use the A_{pq}, the terms p and q can be equal to zero, specially in the case where we calculate the diffusion coefficient. In this case, we cannot define if the values of p and q are positive or negative, in such a way that, if we use those expressions, we do not achieve the same results from [89] and [90]. So, following the sequence proposed by [44], we will modify the expressions above for the case where p is equal to zero:

$$A_{0q} = x_1 x_2 [\boldsymbol{a}_1^{(0)} + \boldsymbol{a}_2^{(0)}, \boldsymbol{a}_1^{(q)}]_{12}. \tag{4.89}$$

Replacing the expressions for $\boldsymbol{a}_1^{(0)}$ and $\boldsymbol{a}_2^{(0)}$ (4.70), we will have:

$$A_{0q} = x_1 x_2 \left[\frac{\sqrt{M_1}\rho_2 \mathscr{C}_1}{\rho} - \frac{\sqrt{M_2}\rho_1 \mathscr{C}_2}{\rho}, \boldsymbol{a}_1^{(q)} \right]_{12}. \tag{4.90}$$

Using the relation given by Ref. [44] where $m_1^{\frac{1}{2}}[\mathscr{C}_1, F]_{12} = -m_2^{\frac{1}{2}}[\mathscr{C}_2, F]_{12}$, we can rewrite the expression as:

$$A_{0q} = x_1 x_2 \left[\frac{\sqrt{M_1}\rho_2 \mathscr{C}_1 + \sqrt{M_1}\rho_1 \mathscr{C}_1}{\rho}, \boldsymbol{a}_1^{(q)} \right]_{12}. \tag{4.91}$$

Knowing that $\rho = \rho_1 + \rho_2$, we will have:

$$A_{0q} = x_1 x_2 \sqrt{M_1} [\mathscr{C}_1, \boldsymbol{a}_1^{(q)}]_{12}. \tag{4.92}$$

Replacing $\boldsymbol{a}_1^{(q)}$ (4.69):

$$A_{0q} = x_1 x_2 \sqrt{M_1} \left[\mathscr{C}_1, S_{\frac{3}{2}}^{(q)}(\mathscr{C}_1^2)\mathscr{C}_1 \right]_{12}. \tag{4.93}$$

In the case where $q < 0$, we only need to invert the subscripts. In the case where $p = q = 0$, we need to apply the same method to q, replacing a_1^q by $a_1^0 + a_2^0$, obtaining:

$$A_{00} = x_1 x_2 M_1 [\mathscr{C}_1, \mathscr{C}_1]. \tag{4.94}$$

Using Eq. (4.55), we can write the matrix form for the expression to calculate the coefficients b_{-1} and b_1 in the first approximation:

$$\begin{pmatrix} B_{-1-1} & B_{-11} \\ B_{1-1} & B_{11} \end{pmatrix} \begin{pmatrix} b_{-1} \\ b_1 \end{pmatrix} = \begin{pmatrix} \beta_{-1} \\ \beta_1 \end{pmatrix}. \tag{4.95}$$

For the viscosity, the matrix of coefficients B_{pq} has always order $2\mathfrak{m}$, where $\mathfrak{m}$ is the approximation order. To calculate a_{-1} and a_1 in the first approximation, we will use Eq. (4.76), being written in the matrix form as follows:

$$\begin{pmatrix} A_{-1-1} & A_{-11} \\ A_{1-1} & A_{11} \end{pmatrix} \begin{pmatrix} a_{-1} \\ a_1 \end{pmatrix} = \begin{pmatrix} \alpha_{-1} \\ \alpha_1 \end{pmatrix}. \tag{4.96}$$

For the thermal conductivity, the matrix of coefficients A_{pq} also has order $2\mathfrak{m}$. For the diffusion in the first approximation order, we will use Eq. (4.75), obtaining:

$$\begin{pmatrix} A_{-1-1} & A_{-10} & A_{-11} \\ A_{0-1} & A_{00} & A_{01} \\ A_{1-1} & A_{10} & A_{11} \end{pmatrix} \begin{pmatrix} d_{-1} \\ d_0 \\ d_1 \end{pmatrix} = \begin{pmatrix} 0 \\ \delta_0 \\ 0 \end{pmatrix}. \tag{4.97}$$

In this case, the matrix of coefficients A_{pq} has order $2\mathfrak{m}+1$, because p and q can be equal to zero. The coefficients A_{pq} and B_{pq} can be calculated integrating the terms inside the brackets, as shown in Eq. (4.38), Eq. (4.39) and Eq. (4.40), however this method requires a greater computational effort for higher approximations. In the situation where one does not want to calculate those integrals, Refs. [9, 44, 45] write the required expressions to calculate the transport coefficients up to third order of approximation, both for pure gases and mixtures of gases. Viehland in Ref. [114] writes the expressions for the bracket integrals up to the fifth order of approximation for pure gases. Tompson in Refs. [111, 115] writes the expressions also up to the fifth order of approximation, but considering a mixture of gases. In order to determine those expressions, Tompson rewrites the bracket integrals in terms of sums, making the calculation of the integrals pretty simple, even for higher orders. In ours calculations, we will use the method given by Tompson, in such a way that the bracket integral will be written as:

$$\left[S_{\frac{3}{2}}^{(p)}(\mathscr{C}_1^2)\mathscr{C}_1, S_{\frac{3}{2}}^{(q)}(\mathscr{C}_1^2)\mathscr{C}_1\right]_{12} = 8 \sum_{l=1}^{(\min[p,q]+1)} \sum_{r=l}^{(p+q+2-l)} A'_{pqrl}\Omega_{12}^{(l,r)}, \tag{4.98}$$

$$\left[S_{\frac{3}{2}}^{(p)}(\mathscr{C}_1^2)\mathscr{C}_1, S_{\frac{3}{2}}^{(q)}(\mathscr{C}_2^2)\mathscr{C}_2\right]_{12} = 8 \sum_{l=1}^{(\min[p,q]+1)} \sum_{r=l}^{(p+q+2-l)} A''_{pqrl}\Omega_{12}^{(l,r)}, \tag{4.99}$$

$$\left[S_{\frac{3}{2}}^{(p)}(\mathscr{C}_1^2)\mathscr{C}_1, S_{\frac{3}{2}}^{(q)}(\mathscr{C}_1^2)\mathscr{C}_1\right]_{1} = 8 \sum_{l=2}^{(\min[p,q]+1)} \sum_{r=l}^{(p+q+2-l)} A'''_{pqrl}\Omega_{11}^{(l,r)}. \tag{4.100}$$

The expressions for A'_{pqrl}, A''_{pqrl} e A'''_{pqrl} can be found in Ref. [115].

$$\left[S_{\frac{5}{2}}^{(p)}(\mathscr{C}_1^2)\mathscr{C}_1\mathscr{C}_1, S_{\frac{5}{2}}^{(q)}(\mathscr{C}_1^2)\mathscr{C}_1\mathscr{C}_1\right]_{12} = \frac{16}{3} \sum_{l=1}^{(\min[p,q]+2)} \sum_{r=l}^{(p+q+4-l)} B'_{pqrl}\Omega_{12}^{(l,r)}, \tag{4.101}$$

$$\left[S_{\frac{5}{2}}^{(p)}(\mathscr{C}_1^2)\mathscr{C}_1\mathscr{C}_1, S_{\frac{5}{2}}^{(q)}(\mathscr{C}_2^2)\mathscr{C}_2\mathscr{C}_2\right]_{12} = \frac{16}{3} \sum_{l=1}^{(\min[p,q]+2)} \sum_{r=l}^{(p+q+4-l)} B''_{pqrl}\Omega_{12}^{(l,r)}, \tag{4.102}$$

$$\left[S_{\frac{5}{2}}^{(p)}(\mathscr{C}_1^2)\mathscr{C}_1\mathscr{C}_1, S_{\frac{5}{2}}^{(q)}(\mathscr{C}_1^2)\mathscr{C}_1\mathscr{C}_1\right]_{1} = \frac{16}{3} \sum_{l=2}^{(\min[p,q]+2)} \sum_{r=l}^{(p+q+4-l)} B'''_{pqrl}\Omega_{11}^{(l,r)}. \tag{4.103}$$

The expressions for B'_{pqrl}, B''_{pqrl} e B'''_{pqrl} can be found in Ref. [111]. The Omega integrals $\Omega_{ij}^{l,r}$ are defined as:

$$\Omega_{ij}^{(l,r)}(T) = \sqrt{\frac{k_\mathrm{B}T}{8\pi m_{ij}}} \int_0^\infty Q_{ij}^{(l)} \mathcal{E}^{r+1} e^{-\mathcal{E}}\, \mathrm{d}\mathcal{E}, \tag{4.104}$$

where $\mathcal{E}$ is the dimensionless energy of interacting particles

$$\mathcal{E} = \frac{E}{k_\mathrm{B}T}, \quad E = \frac{1}{2} m_r |\boldsymbol{v}_i - \boldsymbol{v}_j|^2, \quad i,j = 1,2, \tag{4.105}$$

and m_r is the reduced mass of colliding particles

$$m_r := \frac{m_i m_j}{m_i + m_j}. \tag{4.106}$$

The transport cross sections $Q_{ij}^{(l)}$ are functions of the energy E and calculated via the differential cross section $\sigma(E,\chi)$ as

$$Q_{ij}^{(l)}(E) = 2\pi \int_0^\pi \left(1 - \cos^l \chi\right) \sigma(E,\chi) \sin\chi\, \mathrm{d}\chi, \tag{4.107}$$

where χ is the deflection angle after a binary collision. It is important to note that the the differential cross section $\sigma(E,\chi)$ is determined by the interaction potential.

4.5 Transport cross sections

4.5.1 Classical approach

There are two approaches to calculate transport cross sections $Q_{ij}^{(l)}$: classical and quantum. Following the classical one, the cross sections are written down as

$$Q_{ij}^{(l)}(E) = 2\pi \int_0^\infty \left(1 - \cos^l \chi\right) b \, \mathrm{d}b, \tag{4.108}$$

where b is the impact parameter. Then the deflection angle χ is given by [46]

$$\chi = \arccos\left[-\cos(2\theta)\right], \tag{4.109}$$

where

$$\theta = \frac{b}{r_{mr}} \int_0^1 \left[1 - \left(\frac{bq}{r_{mr}}\right)^2 - \frac{V(r_{mr}/q)}{E}\right]^{-1/2} \mathrm{d}q, \tag{4.110}$$

r_{mr} is the largest root of the following equation:

$$1 - \left(\frac{b}{r}\right)^2 - \frac{V(r)}{E} = 0. \tag{4.111}$$

Thus, the transport cross section is calculated by the integration with respect to the impact parameter in accordance to Eqs.(4.108)-(4.111).

4.5.2 Quantum approach

Input equation

In the quantum approach, the differential cross section is calculated via the scattering amplitude $f(\chi)$ which depends on the energy E of the colliding particles. The function $f(\chi)$ determines the wave function after a collision. Thus, we need to solve the stationary Schrödinger equation (2.51) with a spherically symmetric potential $V(r)$. When two particles interact with each other via a potential $V(r)$, one of them is considered as a bullet, while the other plays a role of target. In this case the mass m in Eq.(2.51) is replaced by the reduced mass of colliding particles (4.106). Then, Eq.(2.51) takes the form

$$\frac{\hbar^2}{2m_r}\Delta\psi + \left[E - V(r)\right]\psi = 0, \quad E = \frac{1}{2}m_r g^2. \tag{4.112}$$

The asymptotic solution at $r \to \infty$ of Eq.(4.112) is given by a combination of plane and spherical waves. In case of elastic collision of two distinguishable particle, the asymptotic solution takes the form

$$\psi(\boldsymbol{r}) = \exp(ikz) + f(\chi)\frac{\exp(ikr)}{r} \tag{4.113}$$

where k is the wave number

$$k := \frac{\sqrt{2m_r E}}{\hbar}. \tag{4.114}$$

Once $f(\chi)$ is known, the differential cross section is calculated as

$$\sigma(\chi) = |f(\chi)|^2 . \tag{4.115}$$

According to the book [93], the scattering amplitude obtained from Eq.(4.112) reads

$$f(\chi) = \frac{1}{k}\sum_{l=0}^{\infty}(2l+1)\exp(i\delta_l)\sin\delta_l P_l(\cos\chi), \tag{4.116}$$

where δ_l is the phase shift and $P_l(x)$ are Legendre polynomials. Then the differential cross section takes the form

$$\begin{aligned}\sigma(\chi) = |f|^2 = f(\chi)f^*(\chi) &= \frac{1}{k}\sum_{l=0}^{\infty}(2l+1)\exp(i\delta_l)\sin\delta_l P_l(\cos\chi) \\ &\times\frac{1}{k}\sum_{l'=0}^{\infty}(2l'+1)\exp(-i\delta_{l'})\sin\delta_{l'}P_{l'}(\cos\chi) \\ &= \frac{1}{k^2}\sum_{l=0}^{\infty}\sum_{l'=0}^{\infty}(2l+1)(2l'+1) \\ &\times\exp(i\delta_l - i\delta_{l'})\sin\delta_{l'}\sin\delta_l P_l(\cos\chi)P_{l'}(\cos\chi).\end{aligned} \tag{4.117}$$

In case of indistinguishable particle, the wave function must be symmetric for bosons and antisymmetric for fermions. Then the asymptotic solution of (4.112) reads

$$\psi(\boldsymbol{r}) = \exp(ikz) \pm \exp(-ikz) + (f(\chi) \pm f(\pi-\chi))\frac{\exp(ikr)}{r}. \tag{4.118}$$

If the total spin of interacting particles is odd, the differential cross section is related to the scattering amplitude as

$$\sigma'(\chi) = |f(\chi) - f(\pi-\chi)|^2 . \tag{4.119}$$

If the sum is even, then

$$\sigma''(\chi) = |f(\chi) + f(\pi - \chi)|^2 . \tag{4.120}$$

If s is the spin of the particles, the numbers of combinations of the even and odd sums of spins are different for bosons and fermions so that the differential cross sections considering all combinations read

$$\sigma^{(\mathrm{B})}(g,\chi) = \frac{s}{2s+1}\sigma'(g,\chi) + \frac{s+1}{2s+1}\sigma''(g,\chi) \tag{4.121}$$

for bosons, and

$$\sigma^{(\mathrm{F})}(g,\chi) = \frac{s+1}{2s+1}\sigma'(g,\chi) + \frac{s}{2s+1}\sigma''(g,\chi) \tag{4.122}$$

for fermions. The scattering amplitude again is obtained from (4.112) in the form (4.116) with the difference that only the odd terms are considered in σ'

$$\sigma'(g,\chi) = \frac{2}{k^2}\left|\sum_{l=1,3,5,\ldots}^{\infty}(2l+1)\exp(i\delta_l)\sin\delta_l P_l(\cos\chi)\right|^2 , \tag{4.123}$$

and only the even terms are considered in σ''

$$\sigma''(g,\chi) = \frac{2}{k^2}\left|\sum_{l=0,2,4,\ldots}^{\infty}(2l+1)\exp(i\delta_l)\sin\delta_l P_l(\cos\chi)\right|^2 . \tag{4.124}$$

Calculation of phase shift

Eq.(4.112) is written in the spherical coordinates

$$\frac{1}{r^2}\frac{\partial}{\partial r}\left(r^2\frac{\partial\psi}{\partial r}\right) + \frac{1}{r^2}\left[\frac{1}{\sin\chi}\frac{\partial}{\partial\chi}\left(\sin\chi\frac{\partial\psi}{\partial\chi}\right)\right] + \frac{2m_r}{\hbar^2}\left[E - V(r)\right]\psi = 0 \tag{4.125}$$

The solution of (4.125) is presented as

$$\psi = \sum_{l=0}^{\infty} A_l P_l(\cos\chi) R_l(r). \tag{4.126}$$

where $P_l(x)$ are Legendre polynomials. Substituting (4.126) into (4.125), the following equation for the radial part is obtained

$$\frac{1}{r^2}\frac{\mathrm{d}}{\mathrm{d}r}\left(r^2\frac{\mathrm{d}R_l}{\mathrm{d}r}\right) + \left[k^2 - \frac{l(l+1)}{r^2} - \frac{2m_r}{\hbar^2}V(r)\right]R_l = 0. \tag{4.127}$$

For large r, Eq.(4.127) is reduced to

$$\frac{\mathrm{d}}{\mathrm{d}r}\left(r^2\frac{\mathrm{d}R_l}{\mathrm{d}r}\right) + k^2 r^2 R_l = 0. \tag{4.128}$$

Then

$$R_l = \frac{1}{r}\sin\left(kr - \frac{l\pi}{2} + \delta_l\right). \tag{4.129}$$

Let us write Eq.(4.127) in the form

$$\frac{\mathrm{d}}{\mathrm{d}r}\left(r^2\frac{\mathrm{d}R_l}{\mathrm{d}r}\right) + r^2 U_l(r) R_l = 0, \tag{4.130}$$

where the function $U_l(r)$ including the potential $V(r)$ reads

$$U_l(r) = k^2 - \frac{l(l+1)}{r^2} - \frac{2m_r}{\hbar^2}V(r). \tag{4.131}$$

The integration of Eq.(4.130) was performed by the normalized Numerov method [116] introducing the following notations

$$r_m = m\,\Delta r, \quad T_m = -\Delta r^2 U_l(r_m)/12, \quad m = 1, 2, 3..., \tag{4.132}$$

where r_m are uniformly distributed knots of the radial variable r, and Δr is the integration step. Then, Eq.(4.130) is integrated by the scheme

$$R_l(r_m) = \frac{2 + 10T_m}{1 - T_m} - \frac{1}{R_l(r_{m-1})}, \tag{4.133}$$

assuming any value of $R_l(r_1)$ for the first knot. The integration is carried out up to a sufficiently large r_m and then the phase shift is calculated in accordance with Eq.(4.113a) in Ref. [93]

$$\tan\delta_l(k) = \frac{kj_l'(kr_m) - \gamma_l j_l(kr_m)}{kn_l'(kr_m) - \gamma_l n_l(kr_m)}, \tag{4.134}$$

where $j_l(z)$ is the spherical Bessel function and $n_l(z)$ is the spherical Neumann function, while $j_l'(z)$ and $n_l'(z)$ are their derivatives. The quantity γ_l is given as

$$\gamma_l = \frac{1}{R_l}\frac{\mathrm{d}R_l}{\mathrm{d}r}\bigg|_{r=r_m} \approx \frac{2[R_l(r_m) - R_l(r_{m-1})]}{\Delta r[R_l(r_m) + R_l(r_{m-1})]}. \tag{4.135}$$

The value of the last knot r_m used in Eq.(2.33) should be large enough for the solution of Eq.(4.135) to become periodic but still small enough to avoid an accumulation of local truncation error.

The above described procedure works well for small values of l, but it fails to calculate the phase shift for large l. In this case, the semi-classical WKB method [93,117] is applied. According to Eq.(3.66) of [117], the expression

$$\delta_l = \int_{r_0}^{\infty}\sqrt{U_l}\,\mathrm{d}r - \int_{r_1}^{\infty}\sqrt{k^2 - \frac{(l+1/2)^2}{r^2}}\,\mathrm{d}r \tag{4.136}$$

provides a good approximation of the phase shift for large values of l. Here, r_0 and r_1 are calculated as

$$U_l(r_0) = 0, \quad r_1 = (l + 1/2)/k. \tag{4.137}$$

It is easier to calculate the first integral in Eq.(4.136) using the variable $\xi = r_0/r$. After some manipulations proposed by Pack [118], Eq.(4.136) takes the following form

$$\delta_l = kr_0 \int_0^1 f(\xi)\sqrt{1-\xi^2}\,\mathrm{d}\xi + \frac{\pi}{2}\left[\sqrt{l(l+1)} - kr_0\right], \tag{4.138}$$

where

$$f(\xi) = \frac{1}{\xi^2}\left(\frac{1}{k}\sqrt{\frac{U_l}{1-\xi^2}} - 1\right). \tag{4.139}$$

Then, the integral is calculated by the following quadrature formula

$$\delta_l = kr_0 \sum_{i=1}^{N_\xi} w_i f(\xi_i) + \frac{\pi}{2}\left[\sqrt{l(l+1)} - kr_0\right] \tag{4.140}$$

with the nodes and weights given as [118]

$$\xi_i = \cos\left(\frac{\pi i}{2N_\xi + 1}\right), \quad w_i = \frac{\pi(1-\xi_i^2)}{2N_\xi + 1}. \tag{4.141}$$

Thus, the phase shift is calculated by quantum mechanics using Eqs.(4.137)-(4.135) up to some value l_q and then the semi-classical approach given by Eqs. (4.139)-(4.141) is used for larger values of l. The value of l_q depends on the interaction energy E and species of interacting gases.

Transport cross sections in terms of phase shifts

The transport cross sections $Q_{ij}^{(n)}$ are functions of the energy E and calculated via the corresponding differential cross section $\sigma(E, \chi)$ by Eq.(4.107). According to the method of Meeks et al. [119], the differential (4.117) is substituted into (4.107) and the transport cross sections take the form

$$Q_{ij}^{(n)}(E) = \frac{4\pi}{k^2}\sum_{l=0}^{\infty}\sum_{m=0}^{\lfloor (n-1)/2 \rfloor} C_{lm}^{(n)} \sin^2\left(\delta_l - \delta_{l+n-2m}\right), \quad i \neq j. \tag{4.142}$$

The coefficients $C_{lm}^{(n)}$ are given as

$$C_{lm}^{(n)} = (2l+1)\left(\prod_{i=1}^{n-2m}\frac{l+i}{2l+2i-1}\right)$$

$$\times \sum_{\alpha_1=0}^{n-m} L(l, \alpha_1 - m + 1) \sum_{\alpha_2=0}^{\alpha_1} L(l, \alpha_2 - m + 2) \ldots \sum_{\alpha_n=0}^{\alpha_{n-1}} L(l, \alpha_n), \tag{4.143}$$

with the function $L(l, \alpha)$ defined as

$$L(l, \alpha) = \frac{(l + \alpha)^2}{(2l + 2\alpha - 1)(2l + 2\alpha + 1)}. \tag{4.144}$$

For indistinguishable bosons with spin equal to zero, the differential cross section in the form (4.124) is substituted into (4.107). Then the transport cross section reads

$$Q_{ii}^{(n)}(E) = \frac{8\pi}{k^2} \sum_{l=0(even)}^{\infty} \sum_{m=0}^{\lfloor (n-1)/2 \rfloor} C_{lm}^{(n)} \sin^2 (\delta_l - \delta_{l+n-2m}) . \tag{4.145}$$

Chapter 5

RESULTS

5.1 Computational scheme and numerical error

To calculate the shift phase by Eq.(4.134), the value of r_m must be chosen so as to provide the best accuracy. Table 5.1 provides the values of r_m for mixture helium-neon for various ranges of the energy E.

For other mixtures, we used the following relation between the r_m and the energy E

$$r_m = \min\left\{\frac{F}{\sqrt{E}}, 100r_0\right\} \tag{5.1}$$

where F is equal to $1000r_0\mathrm{K}^{1/2}$ for pure argon and to $2000r_0\mathrm{K}^{1/2}$ for mixtures neon-argon and helium-argon. An increase of the value of r_m by the factor 1.5 and reducing it by a factor 0.75 did not change the transport coefficients within the relative uncertainty 10^{-5},

The value of l where the quantum method, see Eq.(4.134), is substituted by the semi-classical method, see Eq.(4.138), depends on the energy E. Table 5.2 provides the maximum value of l_q to apply the quantum approach for the pure gases and Table 5.3 given

Table 5.1: Value of r_m used Eq.(4.134) vs. interval of the interaction energy E. The quantity r_0 is the potential zero-point, $V(r_0) = 0$.

He-He		Ne-Ne and He-Ne	
$E(K)$	$r_m/r_0^{a)}$	$E(K)$	$r_m/r_0^{b),c)}$
$(0, 10^2]$	100	$(0, 10^2]$	100
$(10^2, 10^3]$	50	$(10^2, 10^3]$	50
$(10^3, 10^4]$	30	$(10^3, 5\times10^3]$	20
$(10^4, 10^5]$	12	$(5\times10^3, 10^4]$	10
$(10^5, 5\times10^4]$	6	$(10^4, 10^5]$	5
$(5\times10^4, 10^5)$	3		

$^{a)}r_0 = 0.2641$ nm for He-He
$^{b)}r_0 = 0.2761$ nm for Ne-Ne
$^{c)}r_0 = 0.2699$ nm for Ne-Ne

Table 5.2: Number of phase shifts l_q calculated by quantum mechanics for pure gases vs. interval of the interaction energy E. The phases shifts for $l > l_q$ were calculated by the WKB method.

He-He		Ne-Ne		Ar-Ar	
$E(K)$	l_q	$E(K)$	l_q	$E(K)$	l_q
(0, 0.1]	7	(0, 0.05]	15	(0, 0.05]	20
(0.1, 1]	20	(0.05, 0.1]	20	(0.05, 0.1]	30
(1, 10]	25	(0.1, 1]	40	(0.1, 1]	40
(10, 10^2]	40	(1, 20]	60	(1, 10]	90
(10^2, 10^3]	60	(20, 10^2]	90	(10, 20]	150
(10^3, 10^4]	90	(10^2, 10^3]	120	(20, 100]	200
(10^4, 10^5]	100	(10^3, 2×10^3]	150	(100, 10^5]	230
		(2×10^3, 10^4]	180		
		(10^4, 10^5]	200		

Table 5.3: Number of phase shifts l_q calculated by quantum mechanics for mixtures vs. interval of the interaction energy E. The phases shifts for $l > l_q$ were calculated by the WKB method.

He-Ne		He-Ar		Ne-Ar	
$E(K)$	l_q	$E(K)$	l_q	$E(K)$	l_q
(0, 0.05]	7	(0, 0.05]	22	(0, 0.05]	20
(0.05, 0.1]	9	(0.05, 0.1]	30	(0.05, 0.1]	30
(0.1, 0.5]	19	(0.1, 1]	50	(0.1, 1]	40
(0.5, 5]	30	(1, 10]	70	(1, 10]	80
(5, 10]	40	(10, 20]	130	(10, 20]	140
(10, 60]	70	(20, 50]	150	(20, 100]	190
(60, 10^3]	100	(50, 100]	170	(100, 10^5]	230
(10^3, 10^4]	120	(100, 10^5]	230		
(10^4,10^5]	200				

the value of l_q for mixtures. When the l value is lager than l_q, the WKB method was used. An increase of the l_q by the factor 1.2 also did not change the transport coefficients within the relative uncertainty 10^{-5},

According to Eqs.(4.142) and (4.145), the cross sections represent series with respect to the number l. In numerical calculations, the series was truncated when the contribution of ten successive terms did not exceed the relative value 10^{-10}. Figures 5.1 and 5.2 show some cross sections Q_{ij}^q for interactions between the same species and between different species, respectively. As one can see, the transport cross section tends to a finite value. This implies that collisions with high energies do not have a big contribution in the calculations. There are many peaks of the cross sections at the low energies. It means that to calculate the Omega integrals (4.104), the nodes of energy must be very dense

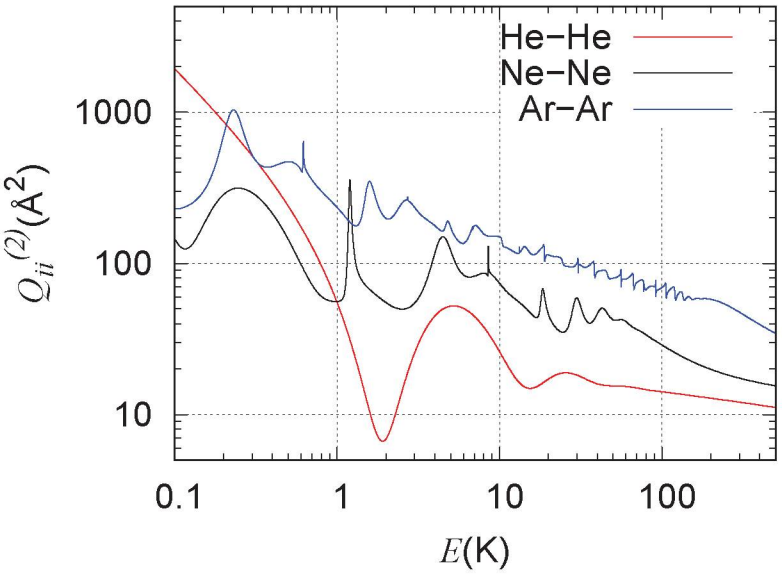

Figure 5.1: Transport cross section $Q_{ii}^{(2)}$ for interactions between identical particles vs. energy.

at low energy and less dense at high energies. To meet such a requirement, we used the following nodes of the energy

$$E_m = 2(1.001^m - 1), \quad m = 1, 2, 3, ..., 12000, \tag{5.2}$$

where the energy is given in K. When a denser mesh of the energy was used, the results did not change within the relative error of 10^{-5} for temperatures $T < 20$ K while for $T \geq 20$ K this variation did not exceed 10^{-6}.

The integration step Δr defined by Eq. (4.132) can also be a source of error. Test calculations were carried out increasing it by a factor of 2 and reducing it by a factor of 0.5. The relative variation of the results was within 10^{-6}.

The quadrature defined by Eq. (4.140) was tested for $N_\xi = 200$ and $N_\xi = 400$, resulting in a relative difference smaller than 10^{-10}.

In order to reduce the calculation time, calculated the values of Q_{ij}^q and stored them in a file. Then, the Omega integrals and the transport coefficients were calculated for many values of the temperature.

The transport coefficients were calculated up to the 10^{th} order of the approximation with respect to the Sonine polynomials. It is important to estimate the error of this approximation. Tables 5.4 - 5.15 show the results for different values of the approximation order N. A comparison between the results for $N = 8$ and $N = 10$ shows that the

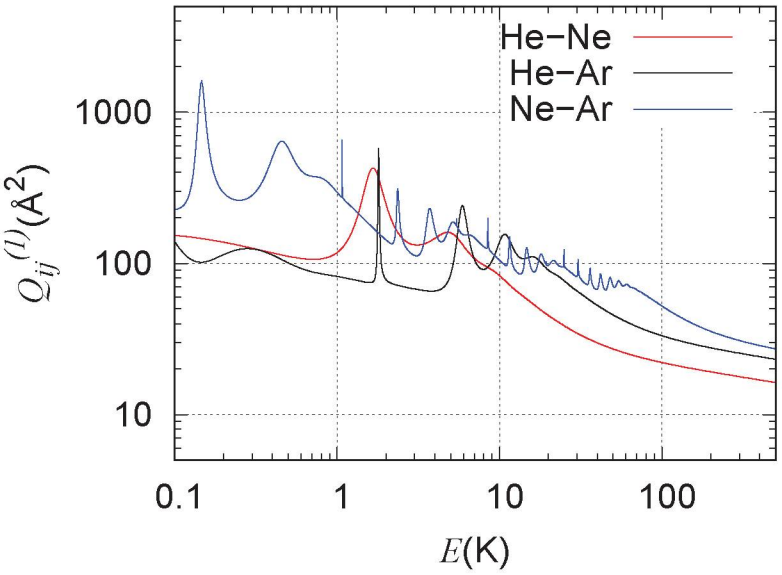

Figure 5.2: Transport cross section $Q_{ij}^{(1)}$ $(i \neq j)$ for interactions between distinguishable particles vs. energy.

Table 5.4: Viscosity μ at $x_1 = 0.5$ vs. order of approximation N for helium-neon mixture.

	μ (μPa·s)			
T(K)	N=4	N=6	N=8	N=10
5	0.925588	0.925594	0.925595	0.925595
10	1.81959	1.81959	1.81960	1.81960
20	3.42887	3.42891	3.42891	3.42891
100	13.2566	13.2567	13.2567	13.2567
1000	64.3415	64.3422	64.3422	64.3423
3000	139.483	139.485	139.485	139.485
5000	202.547	202.549	202.549	202.549

uncertainty has a maximum value of 0.046%, for the thermal diffusion factor at 5K for helium-argon. For all others coefficients and mixtures, the convergence has been achieved at $N = 8$.

Analyzing all numerical errors together we estimated the total numerical error to be around 5×10^{-5}.

5.2 Numerical data

The coefficients of viscosity, thermal conductivity, diffusion, and thermal diffusion for helium-neon, helium-argon, and neon-argon mixtures were calculated in the temperature ranges from 5K to 5000K for the helium-neon mixture and from 20K to 5000K for the

Table 5.5: Thermal conductivity κ at $x_1 = 0.5$ vs. order of approximation N for helium-neon mixture.

	κ (mW/(m·K))			
T(K)	N=4	N=6	N=8	N=10
5	3.05565	3.05597	3.05607	3.05609
10	6.05870	6.05891	6.05894	6.05896
20	11.3196	11.3216	11.3218	11.3218
100	39.9904	39.9919	39.9919	39.9920
1000	196.709	196.735	196.739	196.740
3000	437.171	437.219	437.226	437.227
5000	643.942	644.004	644.013	644.015

Table 5.6: Diffusions coefficient D_{12} at $x_1 = 0.5$ and standard pressure (101325 Pa) vs. order of approximation N for helium-neon mixture.

	$D_{12} \times 10^6$ (m^2/s)			
T(K)	N=4	N=6	N=8	N=10
5	0.048360	0.048367	0.048368	0.048368
10	0.223697	0.223698	0.223700	0.223701
20	0.938068	0.938177	0.938184	0.938184
100	17.3509	17.3509	17.3509	17.3509
1000	860.550	860.601	860.610	860.612
3000	5752.45	5752.74	5752.79	5752.80
5000	14126.6	14127.3	14127.4	14127.4

Table 5.7: Convergence of thermal diffusion factor $-\alpha_T$ at $x_1 = 0.5$ for helium-neon mixture.

T(K)	N=4	N=6	N=8	N=10
5	-0.320266	-0.319860	-0.319760	-0.319746
10	-0.205050	-0.205052	-0.205028	-0.205014
20	0.020834	0.021274	0.021310	0.021311
100	0.298782	0.298802	0.298800	0.298802
1000	0.289018	0.289287	0.289330	0.289339
3000	0.252815	0.253038	0.253074	0.253082
5000	0.232369	0.232565	0.232598	0.232605

Table 5.8: Viscosity μ at $x_1 = 0.5$ vs. order of approximation N for helium-argon mixture.

	μ (μPa·s)			
T(K)	N=4	N=6	N=8	N=10
5	0.71752	0.71771	0.71774	0.71775
10	1.29128	1.29154	1.29158	1.29159
20	2.42778	2.42783	2.42786	2.42787
100	9.54307	9.54310	9.54313	9.54314
1000	55.6483	55.6498	55.6500	55.6501
3000	119.075	119.078	119.078	119.078
5000	171.201	171.205	171.205	171.205

Table 5.9: Thermal conductivity κ at $x_1 = 0.5$ vs. order of approximation N for helium-argon mixture.

	κ (mW/(m·K))			
T(K)	N=4	N=6	N=8	N=10
5	1.96688	1.97585	1.97758	1.97785
10	3.58906	3.60101	3.60616	3.60792
20	6.54480	6.54585	6.54816	6.54978
100	24.1613	24.1617	24.1627	24.1634
1000	126.995	127.049	127.060	127.062
3000	281.503	281.610	281.633	281.639
5000	413.796	413.939	413.969	413.978

Table 5.10: Diffusions coefficient D_{12} at $x_1 = 0.5$ and standard pressure (101325 Pa) vs. order of approximation N for helium-argon mixture.

	$D_{12} \times 10^6$ (m^2/s)			
T(K)	N=4	N=6	N=8	N=10
5	0.03451	0.03460	0.03462	0.03462
10	0.12556	0.12591	0.12603	0.12607
20	0.53025	0.53041	0.53057	0.53066
100	11.3829	11.3837	11.3843	11.3845
1000	576.156	576.254	576.276	576.282
3000	3802.95	3803.56	3803.71	3803.76
5000	9277.06	9278.42	9278.76	9278.86

Table 5.11: Convergence of thermal diffusion factor $-\alpha_{\mathrm{T}}$ at $x_1 = 0.5$ for helium-argon mixture.

T(K)	N=4	N=6	N=8	N=10
5	0.47949	0.49121	0.49309	0.49332
10	-0.07531	-0.06510	-0.06125	-0.06000
20	-0.10504	-0.10438	-0.10335	-0.10270
100	0.31720	0.31727	0.31740	0.31747
1000	0.38255	0.38334	0.38351	0.38355
3000	0.34110	0.34183	0.34200	0.34205
5000	0.31614	0.31681	0.31697	0.31701

Table 5.12: Viscosity μ at $x_1 = 0.5$ vs. order of approximation N for neon-argon mixture.

	μ (μPa·s)			
T(K)	N=4	N=6	N=8	N=10
5	0.817003	0.817004	0.817006	0.817007
10	1.42620	1.42620	1.42620	1.42620
20	2.49312	2.49312	2.49312	2.49312
100	10.7313	10.7313	10.7313	10.7313
1000	61.6296	61.6301	61.6301	61.6301
3000	129.681	129.682	129.682	129.682
5000	184.798	184.800	184.800	184.800

Table 5.13: Thermal conductivity κ at $x_1 = 0.5$ vs. order of approximation N for neon-argon mixture.

	κ (mW/(m·K))			
T(K)	N=4	N=6	N=8	N=10
5	0.908122	0.908129	0.908139	0.908141
10	1.58697	1.58698	1.58698	1.58698
20	2.80651	2.80653	2.80653	2.80654
100	12.1022	12.1022	12.1022	12.1022
1000	67.8406	67.8431	67.8432	67.8433
3000	143.306	143.312	143.313	143.313
5000	204.683	204.691	204.692	204.692

Table 5.14: Diffusions coefficient D_{12} at $x_1 = 0.5$ and standard pressure (101325 Pa) vs. order of approximation N for neon-argon mixture.

	$D_{12} \times 10^6$ (m^2/s)			
T(K)	N=4	N=6	N=8	N=10
5	0.015925	0.015925	0.015925	0.015925
10	0.055814	0.055814	0.055814	0.055814
20	0.198136	0.198136	0.198136	0.198136
100	4.49569	4.49569	4.49569	4.49569
1000	251.009	251.011	251.011	251.011
3000	1617.30	1617.31	1617.31	1617.31
5000	3882.43	3882.46	3882.47	3882.47

Table 5.15: Convergence of thermal diffusion factor $-\alpha_{\mathrm{T}}$ at $x_1 = 0.5$ for neon-argon mixture.

T(K)	N=4	N=6	N=8	N=10
5	0.128752	0.128770	0.128794	0.128798
10	0.131152	0.131164	0.131165	0.131165
20	0.090355	0.090359	0.090360	0.090361
100	0.075686	0.075686	0.075687	0.075688
1000	0.197609	0.197662	0.197666	0.197666
3000	0.182996	0.183058	0.183064	0.183065
5000	0.172741	0.172798	0.172803	0.172804

helium-argon and neon-argon mixtures. Note that the ionization energies of the gases considered here are 24.5874eV (285325K), 21.5645eV (250246K) and 15.7596eV (182883K) for helium, neon and argon, respectively. Thus, no ionization happens in the considered range of temperature. The results are presented in the Tables 5.16 - 5.27, where x_1 represents the mole fraction of the lighter component, and it varies between 10^{-10} and $1-10^{-10}$. The results for the viscosity and the thermal conductivity at $x_1 = 0$ and $x_1 = 1$ are not given because those are the same as given by Refs. [73–75].

Table 5.16: Viscosity μ (μPa·s) vs. temperature T(K) and mole fraction x_1 for helium-neon mixture

	μ				
T	x_1=0.1	0.25	0.5	0.75	0.9
5.	1.00682	0.967576	0.925595	0.955716	1.06327
10.	1.77765	1.78670	1.81960	1.89842	1.99499
20.	3.21303	3.29844	3.42891	3.49766	3.45582
25.	3.98706	4.08123	4.20474	4.21149	4.08009
50.	7.85231	7.85838	7.72304	7.25071	6.67061
100.	14.2718	14.0024	13.2567	11.9206	10.6652
200.	23.7825	23.1413	21.5907	19.1231	16.9660
273.15	29.4596	28.6371	26.6784	23.6042	20.9380
300.	31.3887	30.5099	28.4216	25.1495	22.3137
373.15	36.3429	35.3291	32.9248	29.1599	25.8948
400.	38.0711	37.0131	34.5034	30.5711	27.1583
500.	44.1817	42.9770	40.1113	35.6031	31.6750
600.	49.8911	48.5605	45.3822	40.3552	35.9548
700.	55.2973	53.8557	50.3961	44.8926	40.0524
800.	60.4631	58.9218	55.2049	49.2582	44.0039
900.	65.4315	63.7995	59.8449	53.4820	47.8348
1000.	70.2338	68.5185	64.3423	57.5859	51.5637
2000.	112.544	110.243	104.396	94.4886	85.3434
3000.	149.089	146.447	139.485	127.236	115.625
4000.	182.509	179.662	171.894	157.770	144.072
5000.	213.864	210.905	202.549	186.871	171.355

Table 5.17: Thermal conductivity κ (mW/(m·K)) vs. temperature T(K) and mole fraction of helium x_1 for helium-neon mixture

	κ				
T	x_1=0.1	0.25	0.5	0.75	0.9
5.	1.75426	2.09060	3.05609	4.96827	7.13540
10.	3.19810	4.03419	6.05896	9.50973	12.9710
20.	5.85264	7.56062	11.3218	16.9467	21.8804
25.	7.23551	9.28101	13.7136	20.1649	25.6528
50.	13.9589	17.1808	24.0212	33.5640	41.2732
100.	25.0104	29.7807	39.9920	54.1959	65.5349
200.	41.5476	48.8721	64.6654	86.6667	104.173
273.15	51.5010	60.5404	80.0212	107.123	128.655
300.	54.8927	64.5394	85.3180	114.208	137.149
373.15	63.6212	74.8734	99.0688	132.653	159.290
400.	66.6712	78.4971	103.909	139.161	167.110
500.	77.4741	91.3755	121.176	162.431	195.099
600.	87.5902	103.488	137.493	184.485	221.661
700.	97.1863	115.016	153.083	205.606	247.125
800.	106.369	126.080	168.090	225.979	271.708
900.	115.213	136.760	182.618	245.734	295.565
1000.	123.772	147.118	196.740	264.967	318.808
2000.	199.535	239.577	323.988	439.348	530.154
3000.	265.400	320.838	437.227	595.847	720.603
4000.	325.914	396.081	543.021	742.971	900.206
5000.	382.908	467.391	644.015	884.147	1073.01

Table 5.18: Diffusion coefficient D_{12} (m^2/s) at the standard pressure (101325 Pa) vs. temperature T(K) and mole fraction x_1 for helium-neon mixture

	$D_{12} \times 10^5$						
T	$x_1 = 10^{-10}$	0.1	0.25	0.5	0.75	0.9	$1 - 10^{-10}$
5.	0.048533	0.048511	0.048470	0.048368	0.048184	0.047983	0.047764
10.	0.224351	0.224260	0.224094	0.223701	0.223036	0.222363	0.221682
20.	0.939277	0.939101	0.938802	0.938184	0.937347	0.936681	0.936137
25.	1.45057	1.45026	1.44972	1.44861	1.44712	1.44595	1.44500
50.	5.22158	5.21772	5.21110	5.19722	5.17815	5.16296	5.15059
100.	17.5053	17.4798	17.4371	17.3509	17.2387	17.1535	17.0865
200.	56.8315	56.7258	56.5519	56.2115	55.7841	55.4686	55.2250
273.15	96.1901	96.0057	95.7040	95.1176	94.3881	93.8529	93.4413
300.	112.684	112.467	112.113	111.426	110.574	109.949	109.469
373.15	162.889	162.577	162.068	161.084	159.866	158.976	158.293
400.	183.187	182.838	182.267	181.166	179.803	178.808	178.045
500.	267.230	266.729	265.912	264.338	262.395	260.978	259.892
600.	364.043	363.373	362.285	360.187	357.601	355.716	354.271
700.	473.049	472.198	470.813	468.147	464.861	462.466	460.631
800.	593.795	592.748	591.047	587.772	583.734	580.791	578.536
900.	725.910	724.656	722.619	718.695	713.858	710.333	707.631
1000.	869.084	867.612	865.220	860.612	854.932	850.790	847.616
2000.	2863.82	2859.68	2852.94	2839.92	2823.82	2812.05	2803.01
3000.	5796.00	5788.53	5776.36	5752.80	5723.59	5702.18	5685.71
4000.	9594.19	9582.93	9564.56	9528.97	9484.72	9452.22	9427.17
5000.	14216.7	14201.3	14176.2	14127.4	14066.7	14021.97	13987.5

Table 5.19: Thermal diffusion factor α_{T} vs. temperature T(K) and mole fraction x_1 for helium-neon mixture

	$-\alpha_{\mathrm{T}}$						
T	$x_1 = 10^{-10}$	0.1	0.25	0.5	0.75	0.9	$1 - 10^{-10}$
5.	0.213852	0.228057	0.254505	0.319746	0.438047	0.568505	0.712534
10.	0.138463	0.147788	0.164743	0.205015	0.273938	0.344825	0.417544
20.	0.018407	0.018968	0.019841	0.021311	0.022487	0.022635	0.022152
25.	0.066702	0.069916	0.075409	0.086951	0.103052	0.116232	0.127252
50.	0.182613	0.190730	0.204520	0.233132	0.272102	0.303099	0.328348
100.	0.241740	0.250996	0.266651	0.298802	0.341803	0.375333	0.402211
200.	0.259980	0.269063	0.284442	0.316022	0.358128	0.390801	0.416877
273.15	0.260333	0.269254	0.284365	0.315399	0.356753	0.388811	0.414371
300.	0.259821	0.268692	0.283719	0.314578	0.355692	0.387555	0.412953
373.15	0.257765	0.266519	0.281347	0.311789	0.352327	0.383725	0.408741
400.	0.256892	0.265609	0.280372	0.310680	0.351030	0.382277	0.407169
500.	0.253503	0.262099	0.276654	0.306520	0.346256	0.377012	0.401501
600.	0.250174	0.258672	0.273054	0.302549	0.341772	0.372116	0.396273
700.	0.247037	0.255449	0.269682	0.298858	0.337638	0.367630	0.391500
800.	0.244111	0.252448	0.266549	0.295443	0.333833	0.363516	0.387136
900.	0.241387	0.249657	0.263639	0.292280	0.330321	0.359726	0.383124
1000.	0.238846	0.247054	0.260929	0.289339	0.327062	0.356217	0.379414
2000.	0.219981	0.227745	0.240848	0.267626	0.303130	0.330556	0.352377
3000.	0.207331	0.214794	0.227380	0.253082	0.287151	0.313479	0.334435
4000.	0.197599	0.204824	0.217004	0.241870	0.274838	0.300330	0.320635
5000.	0.189578	0.196601	0.208439	0.232605	0.264659	0.289462	0.309233

Table 5.20: Viscosity μ (μPa·s) vs. temperature T(K) and mole fraction x_1 for helium-argon mixture

	μ				
T	x_1=0.1	0.25	0.5	0.75	0.9
20.	2.12263	2.21574	2.42787	2.76363	3.07390
25.	2.54873	2.67790	2.96031	3.36593	3.67845
50.	4.48262	4.75993	5.31726	5.95920	6.22427
100.	8.37594	8.78596	9.54314	10.2187	10.2087
200.	16.1256	16.5166	17.1147	17.2655	16.5464
273.15	21.1786	21.5063	21.9161	21.6726	20.5192
300.	22.9010	23.2064	23.5531	23.1821	21.8896
373.15	27.2911	27.5444	27.7434	27.0720	25.4454
400.	28.8069	29.0444	29.1980	28.4317	26.6963
500.	34.0930	34.2868	34.3073	33.2460	31.1553
600.	38.9344	39.1039	39.0367	37.7515	35.3653
700.	43.4445	43.6039	43.4822	42.0242	39.3852
800.	47.6981	47.8583	47.7065	46.1132	43.2536
900.	51.7467	51.9156	51.7522	50.0525	46.9973
1000.	55.6270	55.8108	55.6501	53.8666	50.6361
2000.	88.9814	89.4765	89.7339	87.7775	83.4328
3000.	117.1846	118.104	119.078	117.517	112.663
4000.	142.7393	144.126	145.945	145.057	140.021
5000.	166.5857	168.464	171.205	171.176	166.184

Table 5.21: Thermal conductivity κ (mW/(m·K)) vs. temperature T(K) and mole fraction of helium x_1 for helium-argon mixture

	κ				
T	x_1=0.1	0.25	0.5	0.75	0.9
20.	2.28323	3.51273	6.54978	12.1890	18.6821
25.	2.75438	4.26059	7.93344	14.5917	22.0214
50.	4.88938	7.62708	14.0719	24.9991	36.1724
100.	8.92255	13.5373	24.1634	41.4673	58.3106
200.	16.4864	23.7944	40.5271	67.4853	93.3828
273.15	21.3647	30.2930	50.7664	83.7889	115.511
300.	23.0321	32.5184	54.2864	89.4191	123.177
373.15	27.3003	38.2416	63.3898	104.044	143.140
400.	28.7808	40.2371	66.5827	109.195	150.185
500.	33.9720	47.2798	77.9286	127.577	175.381
600.	38.7628	53.8401	88.5978	144.961	199.270
700.	43.2533	60.0377	98.7541	161.583	222.157
800.	47.5101	65.9507	108.504	177.597	244.242
900.	51.5788	71.6332	117.923	193.110	265.665
1000.	55.4922	77.1239	127.062	208.201	286.530
2000.	89.5447	125.646	209.012	344.690	476.030
3000.	118.744	167.964	281.639	466.870	646.566
4000.	145.435	207.046	349.375	581.570	807.258
5000.	170.512	244.045	413.978	691.522	961.764

Table 5.22: Diffusion coefficient D_{12} (m^2/s) at the standard pressure (101325 Pa) vs. temperature T(K) and mole fraction x_1 for helium-argon mixture

	$D_{12} \times 10^5$						
T	$x_1 = 10^{-10}$	0.1	0.25	0.5	0.75	0.9	$1 - 10^{-10}$
20.	0.531278	0.531190	0.531031	0.530665	0.530050	0.529416	0.528741
25.	0.838779	0.838665	0.838461	0.838001	0.837264	0.836554	0.835855
50.	3.24773	3.24686	3.24530	3.24177	3.23610	3.23061	3.22525
100.	11.4472	11.4380	11.4217	11.3845	11.3250	11.2682	11.2137
200.	38.0465	37.9930	37.8997	37.6948	37.3844	37.1036	36.8456
273.15	64.6710	64.5679	64.3894	64.0034	63.4308	62.9218	62.4597
300.	75.8155	75.6912	75.4769	75.0151	74.3337	73.7304	73.1843
373.15	109.693	109.506	109.183	108.493	107.486	106.601	105.8059
400.	123.373	123.159	122.793	122.013	120.876	119.880	118.984
500.	179.922	179.605	179.064	177.917	176.256	174.809	173.511
600.	244.920	244.488	243.752	242.195	239.953	238.003	236.257
700.	317.964	317.406	316.457	314.455	311.577	309.079	306.844
800.	398.735	398.043	396.865	394.384	390.823	387.735	384.973
900.	486.977	486.141	484.720	481.731	477.442	473.725	470.401
1000.	582.474	581.487	579.809	576.282	571.225	566.842	562.923
2000.	1905.04	1902.20	1897.37	1887.21	1872.63	1859.96	1848.59
3000.	3836.18	3831.02	3822.25	3803.76	3777.12	3753.89	3733.00
4000.	6326.30	6318.50	6305.22	6277.15	6236.61	6201.17	6169.21
5000.	9346.38	9335.68	9317.44	9278.86	9223.00	9174.03	9129.79

Table 5.23: Thermal diffusion factor α_{T} vs. temperature T(K) and mole fraction x_1 for helium-argon mixture

	$-\alpha_{\mathrm{T}}$						
T	$x_1 = 10^{-10}$	0.1	0.25	0.5	0.75	0.9	$1 - 10^{-10}$
20.	-0.062735	-0.068044	-0.077923	-0.102699	-0.150022	-0.206323	-0.273797
25.	-0.026715	-0.029122	-0.033636	-0.045101	-0.067332	-0.093930	-0.125586
50.	0.111890	0.119874	0.134263	0.167959	0.224635	0.282143	0.340648
100.	0.216479	0.231144	0.257331	0.317469	0.415021	0.509644	0.601679
200.	0.268431	0.285495	0.315753	0.384305	0.493194	0.596572	0.695333
273.15	0.278400	0.295703	0.326342	0.395583	0.505183	0.608894	0.707719
300.	0.280178	0.297495	0.328150	0.397398	0.506944	0.610547	0.709225
373.15	0.282519	0.299794	0.330364	0.399380	0.508470	0.611566	0.709701
400.	0.282800	0.300044	0.330558	0.399442	0.508310	0.611183	0.709098
500.	0.282430	0.299535	0.329800	0.398116	0.506076	0.608082	0.705165
600.	0.280914	0.297868	0.327867	0.395592	0.502635	0.603792	0.700081
700.	0.278939	0.295745	0.325487	0.392640	0.498809	0.599169	0.694723
800.	0.276793	0.293460	0.322957	0.389572	0.494922	0.594539	0.689414
900.	0.274611	0.291146	0.320413	0.386523	0.491105	0.590032	0.684277
1000.	0.272453	0.288865	0.317916	0.383550	0.487415	0.585695	0.679356
2000.	0.254473	0.269939	0.297341	0.359355	0.457771	0.551197	0.640494
3000.	0.241505	0.256311	0.282560	0.342047	0.436672	0.526740	0.613041
4000.	0.231310	0.245592	0.270928	0.328412	0.420033	0.507442	0.591375
5000.	0.222815	0.236655	0.261220	0.317012	0.406095	0.491257	0.573189

Table 5.24: Viscosity μ (μPa·s) vs. temperature T(K) and mole fraction x_1 for neon-argon mixture

T	μ				
	x_1=0.1	0.25	0.5	0.75	0.9
20.	;2.14222	;2.26074	;2.49316	;2.78335	;2.99498
25.	;2.56421	;2.71318	;3.01221	;3.39930	;3.69202
50.	;4.53726	;4.90247	;5.63522	;6.57805	;7.28208
100.	;8.57597	;9.31365	;10.7316	;12.4230	;13.5775
200.	;16.5103	;17.5406	;19.4645	;21.6660	;23.1146
273.15	;21.6428	;22.7520	;24.8218	;27.1998	;28.7827
300.	;23.3890	;24.5196	;26.6324	;29.0693	;30.7010
373.15	;27.8357	;29.0195	;31.2448	;33.8433	;35.6117
400.	;29.3702	;30.5732	;32.8404	;35.4999	;37.3200
500.	;34.7199	;35.9985	;38.4299	;41.3267	;43.3440
600.	;39.6187	;40.9800	;43.5886	;46.7350	;48.9541
700.	;44.1821	;45.6322	;48.4278	;51.8311	;54.2537
800.	;48.4862	;50.0294	;53.0185	;56.6827	;59.3084
900.	;52.5828	;54.2223	;57.4089	;61.3355	;64.1629
1000.	;56.5092	;58.2467	;61.6331	;65.8222	;68.8496
2000.	;90.2523	;92.9847	;98.3544	;105.075	;109.983
3000.	;118.765	;122.449	;129.689	;138.749	;145.365
4000.	;144.582	;149.171	;158.178	;169.433	;177.641
5000.	;168.657	;174.113	;184.810	;198.153	;207.869

Table 5.25: Thermal conductivity κ (mW/(m·K)) vs. temperature T(K) and mole fraction of neon x_1 for neon-argon mixture

T	κ				
	x_1=0.1	0.25	0.5	0.75	0.9
20.	;1.81361	;2.14168	;2.80659	;3.67972	;4.34897
25.	;2.17532	;2.58127	;3.41113	;4.51547	;5.37339
50.	;3.86649	;4.70093	;6.42617	;8.76046	;10.6024
100.	;7.28357	;8.86935	;12.1026	;16.3773	;19.6681
200.	;13.9165	;16.4721	;21.6231	;28.3221	;33.4019
273.15	;18.1975	;21.2643	;27.4455	;35.4848	;41.5821
300.	;19.6550	;22.8908	;29.4162	;37.9085	;44.3528
373.15	;23.3707	;27.0375	;34.4453	;44.1063	;51.4491
400.	;24.6542	;28.4714	;36.1882	;46.2597	;53.9187
500.	;29.1340	;33.4869	;42.3058	;53.8427	;62.6304
600.	;33.2416	;38.1028	;47.9667	;60.8917	;70.7467
700.	;37.0715	;42.4212	;53.2878	;67.5412	;78.4160
800.	;40.6862	;46.5086	;58.3436	;73.8770	;85.7325
900.	;44.1284	;50.4104	;63.1847	;79.9572	;92.7605
1000.	;47.4286	;54.1587	;67.8475	;85.8237	;99.5463
2000.	;75.8199	;86.6020	;108.512	;137.239	;159.133
3000.	;99.8332	;114.194	;143.323	;181.430	;210.417
4000.	;121.588	;139.253	;175.030	;221.742	;257.216
5000.	;141.883	;162.668	;204.707	;259.503	;301.057

Table 5.26: Diffusion coefficient D_{12} (m^2/s) at the standard pressure (101325 Pa) vs. temperature T(K) and mole fraction x_1 for neon-argon mixture

T	D		
	$x_1 = 10^{-10}$	0.1	0.25
20. ;0.198361 ;0.198324 ;0.198262 ;0.198136 ;0.197972 ;0.197848 ;0.197751			
25. ;0.302126 ;0.302090 ;0.302032 ;0.301914 ;0.301764 ;0.301652 ;0.301565			
50. ;1.17069 ;1.17068 ;1.17066 ;1.17063 ;1.17058 ;1.17055 ;1.17052			
100. ;4.49818 ;4.49779 ;4.49712 ;4.49569 ;4.49372 ;4.49214 ;4.49086			
200. ;16.0043 ;15.9984 ;15.9883 ;15.9672 ;15.9386 ;15.9162 ;15.89841			
273.15 ;27.6714 ;27.6572 ;27.6329 ;27.5827 ;27.5155 ;27.4635 ;27.4224			
300. ;32.5588 ;32.5408 ;32.5100 ;32.4466 ;32.3620 ;32.2968 ;32.2453			
373.15 ;47.4041 ;47.3740 ;47.3228 ;47.2177 ;47.0787 ;46.9723 ;46.8885			
400. ;53.3909 ;53.3557 ;53.2961 ;53.1740 ;53.0126 ;52.8894 ;52.7924			
500. ;78.0899 ;78.0338 ;77.9390 ;77.7458 ;77.4922 ;77.2994 ;77.1482			
600. ;106.387 ;106.307 ;106.172 ;105.898 ;105.539 ;105.267 ;105.055			
700. ;138.087 ;137.981 ;137.801 ;137.437 ;136.962 ;136.604 ;136.324			
800. ;173.038 ;172.903 ;172.675 ;172.213 ;171.613 ;171.160 ;170.807			
900. ;211.117 ;210.951 ;210.671 ;210.105 ;209.370 ;208.817 ;208.385			
1000. ;252.222 ;252.023 ;251.688 ;251.011 ;250.134 ;249.473 ;248.958			
2000. ;814.789 ;814.174 ;813.142 ;811.067 ;808.389 ;806.380 ;804.820			
3000. ;1624.29;1623.13;1621.20;1617.31;1612.31;1608.55;1605.64			
4000. ;2656.69;2654.90;2651.90;2645.88;2638.13;2632.33;2627.83			
5000. ;3897.59;3895.08;3890.89;3882.47;3871.63;3863.52;3857.23			

Table 5.27: Thermal diffusion factor α_{T} vs. temperature T(K) and mole fraction x_1 for neon-argon mixture

T	$x_1 = 10^{-10}$	0.1	0.25	
20.	;0.072459;0.075432;0.080397;0.090364;0.103280;0.113061;0.120734			
25.	;0.050061;0.052119;0.055562;0.062504;0.071568;0.078488;0.083957			
50.	;0.013040;0.013659;0.014707;0.016867;0.019775;0.022059;0.023902			
100.	;0.058602;0.061394;0.066098;0.075693;0.088379;0.098144;0.105884			
200.	;0.119513;0.124741;0.133491;0.151126;0.174056;0.191443;0.205077			
273.15	;0.138177;0.143988;0.153700;0.173225;0.198543;0.217701;0.232708			
300.	;0.142507;0.148436;0.158343;0.178253;0.204059;0.223581;0.238871			
373.15	;0.150463;0.156588;0.166816;0.187362;0.213978;0.234106;0.249869			
400.	;0.152425;0.158592;0.168890;0.189574;0.216366;0.236627;0.252493			
500.	;0.157107;0.163358;0.173797;0.194759;0.221907;0.242434;0.258508			
600.	;0.159364;0.165639;0.176117;0.197158;0.224404;0.245003;0.261133			
700.	;0.160377;0.166649;0.177121;0.198149;0.225375;0.245955;0.262068			
800.	;0.160705;0.166960;0.177404;0.198373;0.225520;0.246036;0.262096			
900.	;0.160636;0.166867;0.177272;0.198160;0.225197;0.245626;0.261615			
1000.	;0.160330;0.166534;0.176894;0.197689;0.224600;0.244930;0.260839			
2000.	;0.154321;0.160250;0.170144;0.189980;0.215602;0.234921;0.250018			
3000.	;0.148773;0.154485;0.164010;0.183089;0.207694;0.226219;0.240679			
4000.	;0.144261;0.149799;0.159029;0.177502;0.201295;0.219188;0.233141			
5000.	;0.140487;0.145879;0.154863;0.172828;0.195943;0.213308;0.226837			

5.3 Uncertainty related to potential

As has been already mentioned, the uncertainty related to the He-He potential on the viscosity and thermal conductivity of pure helium given in Ref. [75] is 5×10^{-4} for $T \leq$50K and 2×10^{-5} for $T >$ 50K. Its contribution into the uncertainty of the viscosity and thermal conductivity coefficients of the mixture considered here is smaller by the factor x_{He}^2, because the main terms in the mixture expressions for μ and κ contain the integral $\Omega_{11}^{(2,2)}$ based on the He-He potential with the factor x_{He}^2. Thus, the relative uncertainty of μ and κ related to the He-He potential reads

$$\frac{\Delta\mu_{\text{He-He}}}{\mu} = \frac{\Delta\kappa_{\text{He-He}}}{\kappa} = x_{\mathrm{He}}^2 \begin{cases} 0.05\% & \text{for} \quad T \leq 50 \text{ K}, \\ 0.002\% & \text{for} \quad T > 50 \text{ K}. \end{cases} \tag{5.3}$$

The uncertainty related to the Ne-Ne potential was estimated by Bich *et al.* [73] as 0.1% except for the lowest temperature. However, the authors of [73] did not estimate the uncertainty for low temperatures nor did they indicate the temperature range for the estimated uncertainty of 0.1 %. To estimate the uncertainty related to the Ne-Ne potential, the viscosity μ and thermal conductivity κ for pure helium were calculated in the temperature range $5\leq T/\mathrm{K} \leq 50$ for the potentials proposed by Hellmann *et al.* [63] and by Cybulski and Toczylowski [57]. It was found that the relative difference of μ and κ for these two potentials is within 0.5 % for $5 \leq T/\mathrm{K} \leq 50$. Thus, the uncertainty of μ and κ related to the Ne-Ne potential was assumed to be given by

$$\frac{\Delta\mu_{\text{Ne-Ne}}}{\mu} = \frac{\Delta\kappa_{\text{Ne-Ne}}}{\kappa} = x_{\mathrm{Ne}}^2 \begin{cases} 0.5\% & \text{for} \quad T \leq 50 \text{ K}, \\ 0.1\% & \text{for} \quad T > 50 \text{ K}, \end{cases} \tag{5.4}$$

where, the factor x_{Ne}^2 has been introduced for the same reason as the factor x_{He}^2 in Eq.(5.3).

The uncertainty related to the Ar-Ar potential was estimated by Vogel *et al.* [74] as 0.1%. Again, the authors did not estimate the uncertainty for low temperatures nor did they indicate the temperature range for the estimated uncertainty of 0.1 %. To estimate the uncertainty related to the Ar-Ar potential, the viscosity μ and thermal conductivity κ for pure helium were calculated in the temperature range $5\leq T/\mathrm{K} \leq 50$ for the potentials proposed by Jager *et al.* [66] and by Cybulski and Toczylowski [57]. It was found that the relative difference of μ and κ for these two potentials is within 0.5 % for $5 \leq T/\mathrm{K} \leq 50$. Thus, the uncertainty of μ and κ related to the Ar-Ar potential was assumed to be given

by

$$\frac{\Delta\mu_{\text{Ar-Ar}}}{\mu} = \frac{\Delta\kappa_{\text{Ar-Ar}}}{\kappa} = x_{\text{Ar}}^2 \begin{cases} 0.5\% & \text{for} \quad T \leq 50 \text{ K}, \\ 0.1\% & \text{for} \quad T > 50 \text{ K}, \end{cases} \tag{5.5}$$

where, the factor x_{Ar}^2 has been introduced for the same reason as the factor x_{He}^2 in Eq.(5.3).

To evaluate the uncertainty related to the potential between helium and neon, additional calculations were carried out based on the potential by Cybulski and Toczylowski [57]. A difference of the results based on the He-Ne potential by Cacheiro [61] with those based on the potential given in Ref. [57] was assumed as the uncertainty related to the He-Ne potential. It depends on both temperature and molar fraction. Its maximum value for each coefficient is as follows

$$\frac{\Delta\mu_{\text{He-Ne}}}{\mu} = 0.08\%, \quad \frac{\Delta\kappa_{\text{He-Ne}}}{\kappa} = 0.06\%, \tag{5.6}$$

$$\frac{\Delta D_{12,\text{He-Ne}}}{D_{12}} = 0.12\%, \quad \Delta\alpha_{\text{T,He-Ne}} = 8 \times 10^{-4}. \tag{5.7}$$

The uncertainty of the thermal diffusion factor α_{T} is given by its absolute value because the relative uncertainty becomes extremely large near the inversion point.

To evaluate the uncertainty related to the potential between helium and argon, we have used the same idea. A difference of the results based on the He-Ar potential by Cacheiro [61] with those based on the potential given in Ref. [57] was assumed as the uncertainty related to the He-Ar potential. It depends on both temperature and molar fraction. Its maximum value for each coefficient is as follows

$$\frac{\Delta\mu_{\text{He-Ar}}}{\mu} = 0.02\%, \quad \frac{\Delta\kappa_{\text{He-Ar}}}{\kappa} = 0.03\%, \tag{5.8}$$

$$\frac{\Delta D_{12,\text{He-Ar}}}{D_{12}} = 0.05\%, \quad \Delta\alpha_{\text{T,He-Ar}} = 5 \times 10^{-4}. \tag{5.9}$$

Again, the uncertainty of the thermal diffusion factor α_{T} is given by its absolute value because the relative uncertainty becomes extremely large near the inversion point.

For the uncertainty related to the potential between neon and argon, we have used the same method. A difference of the results based on the Ne-Ar potential by Cacheiro [61] with those based on the potential given in Ref. [57] was assumed as the uncertainty related

to the Ne-Ar potential. It depends on both temperature and molar fraction. Its maximum value for each coefficient is as follows

$$\frac{\Delta\mu_{\text{Ne-Ar}}}{\mu} = 0.02\%, \quad \frac{\Delta\kappa_{\text{Ne-Ar}}}{\kappa} = 0.03\%, \tag{5.10}$$

$$\frac{\Delta D_{12,\text{Ne-Ar}}}{D_{12}} = 0.05\%, \quad \Delta\alpha_{\text{T,Ne-Ar}} = 1.8 \times 10^{-4}. \tag{5.11}$$

The combined uncertainties for viscosity μ or thermal conductivity κ can be determined using the expression

$$\frac{\Delta c}{c} = \sqrt{\left(\frac{\Delta c_{11}}{c}\right)^2 + \left(\frac{\Delta c_{22}}{c}\right)^2 + \left(\frac{\Delta c_{12}}{c}\right)^2}, \quad c = \mu, \kappa. \tag{5.12}$$

It is plotted against the temperature in Figure 5.3 for helium-neon, Figure 5.6 for helium-argon and Figure 5.9 for neon-argon mixtures. As expected, the coefficients μ and κ for the molar fraction $x_1 = 0.9$ have uncertainties about 0.08 % for low temperatures and about 0.01 % for $T \geq 100$ K. In this case, the contributions of the uncertainties related to the potentials Ne-Ne and He-Ne are small. For the mixture with molar fraction $x_1 = 0.9$, the combined uncertainty is one order higher, i.e., it is 0.4 % at the low temperature and 0.09 % for $T \geq 100$ K.

The total uncertainties of the diffusion coefficient D_{12} and thermal diffusion factor α_{T} are related only to the potential He-Ne, He-Ar and Ne-Ar because the main term of their expressions contains the integral $\Omega_{12}^{(1,1)}$ based on this potential. The uncertainties of D_{12} and α_{T} are plotted in Figures 5.4 and 5.5 for helium-neon, Figures 5.7 and 5.8 for helium-argon, and Figures 5.10 and 5.11 for neon-argon, respectively. These uncertainties weakly depend on the molar fraction and vary significantly with the temperature. For the helium-neon mixture, the diffusion coefficient uncertainty is about 0.13 % at the low temperature and within 0.04 % for $T > 100$ K. For the helium-argon mixture, the uncertainty is about 0.05 %, reaching -0.01% at 10 K. For the neon-argon mixture, the uncertainty is close to 0.05 % for temperatures above 50 K, and about 0.02 % for other temperatures.

The uncertainty of the thermal diffusion factor of the helium-neon is smaller than 4×10^{-4} for $T \geq 100$ K that corresponds to the relative uncertainty of 0.4 %. For the low temperature, the uncertainty is three times larger and reaches the value $\Delta\alpha_{\text{T}} = 1.5 \times 10^{-3}$ that corresponds to 0.7 % for $T = 5$ K. Near the inversion point $T = 18.7$ K, the relative

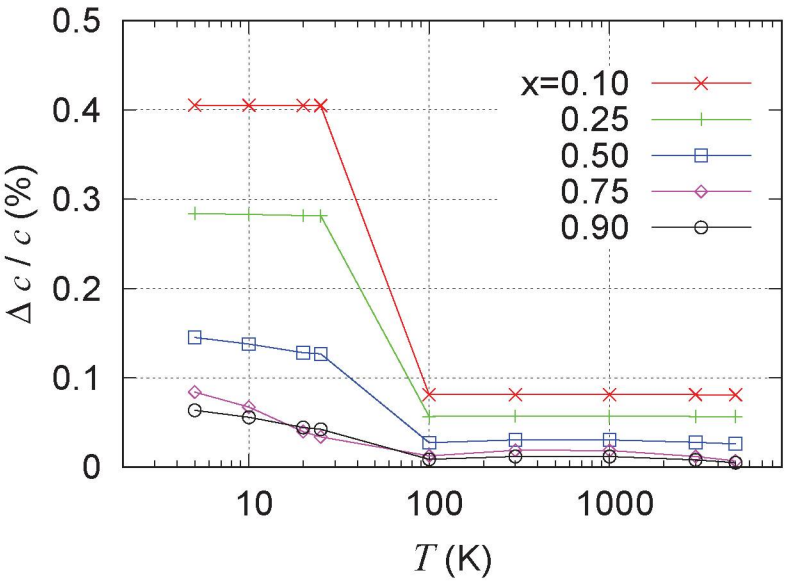

Figure 5.3: Combined relative uncertainty of viscosity μ and thermal conductivity κ related to potentials for helium-neon mixture ($c = \mu,\kappa$).

uncertainty becomes extremely large. For the helium-argon mixture, the uncertainty is lower than 5×10^{-4} for temperature above 100 K. For lower temperatures, it reaches 3×10^{-3}, which is the inversion point of the coefficient. For the neon-argon mixture, we have not observed an inversion for the sign of the thermal diffusion factor. In this situation, the uncertainty is always lower than 2×10^{-4}.

Summarizing, we conclude that practically in all cases considered here the uncertainty related to the potentials is orders of magnitude larger than the numerical error. The only situation where both potential uncertainty and numerical error contribute equally (approximately 2×10^{-5}) is $x_1 = 0.9$ and $T \geq 100$ K.

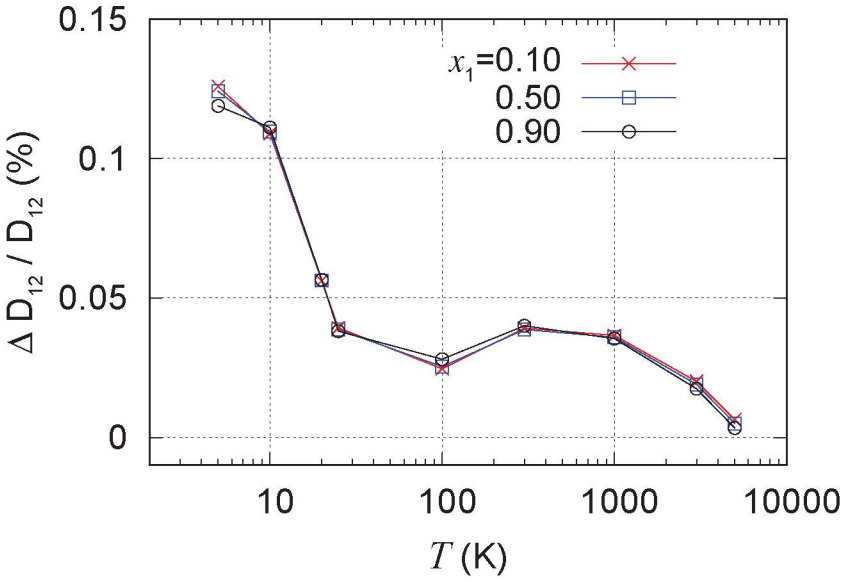

Figure 5.4: Relative uncertainty of diffusions coefficient D_{12} related to potential for helium-neon mixture.

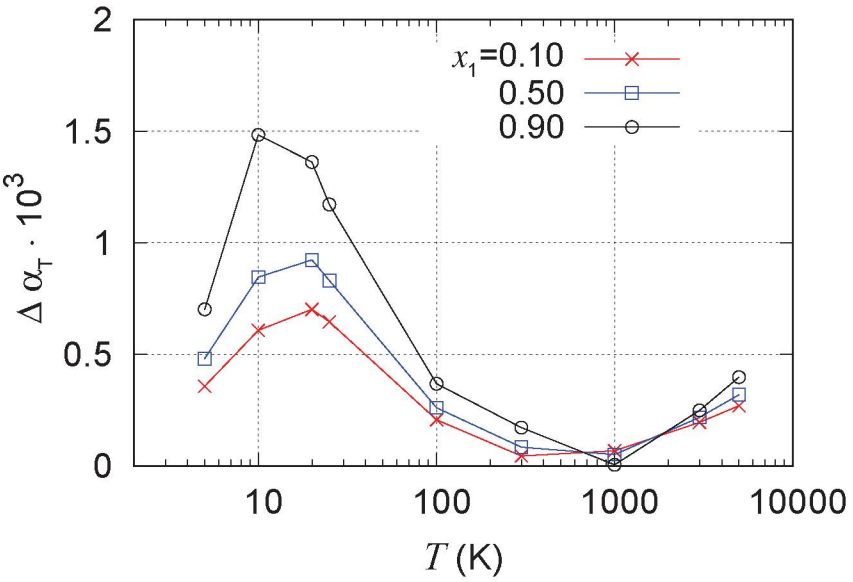

Figure 5.5: Uncertainty of thermal diffusion factor α_{T} related to potential for helium-neon mixture.

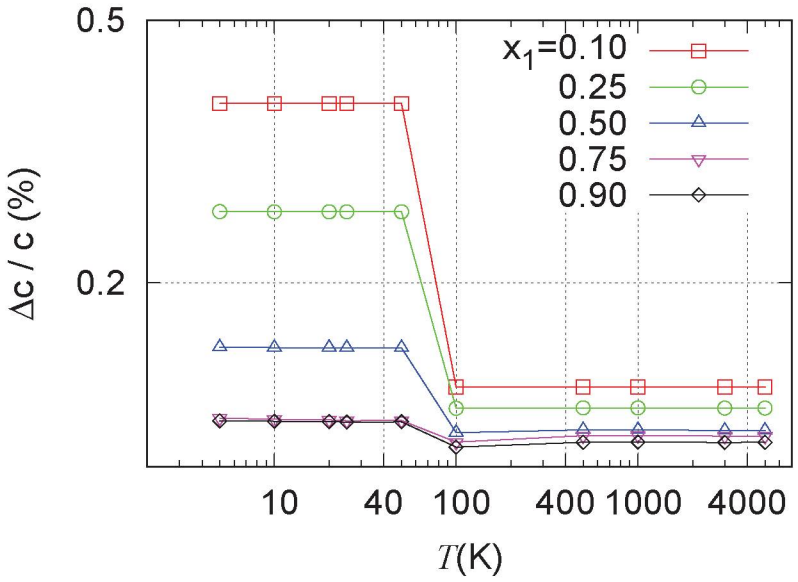

Figure 5.6: Combined relative uncertainty of viscosity μ and thermal conductivity κ related to potentials for helium-argon mixture ($c = \mu, \kappa$).

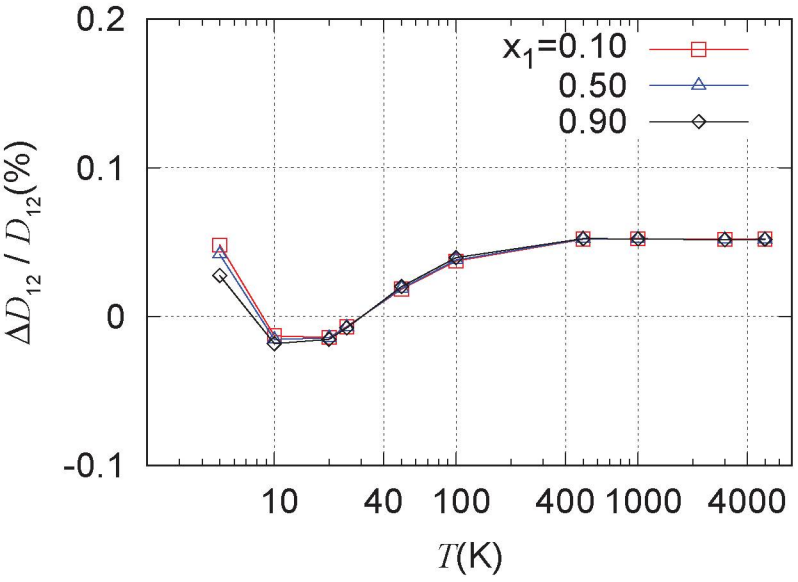

Figure 5.7: Relative uncertainty of diffusions coefficient D_{12} related to potential for helium-argon mixture.

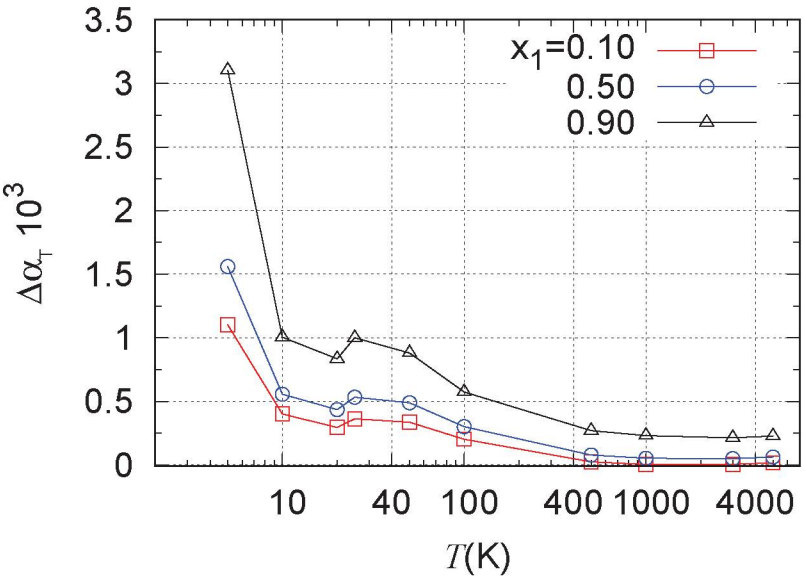

Figure 5.8: Uncertainty of thermal diffusion factor α_T related to potential for helium-argon mixture.

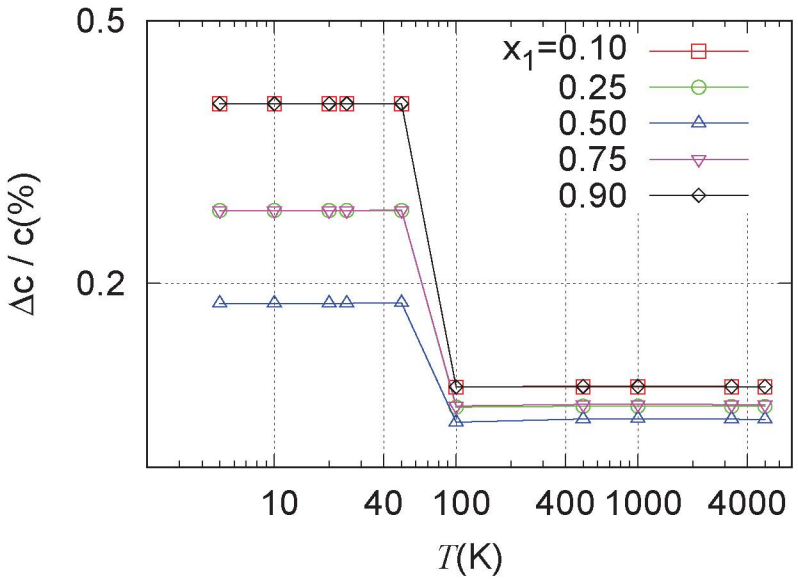

Figure 5.9: Combined relative uncertainty of viscosity μ and thermal conductivity κ related to potentials for neon-argon mixture ($c = \mu, \kappa$).

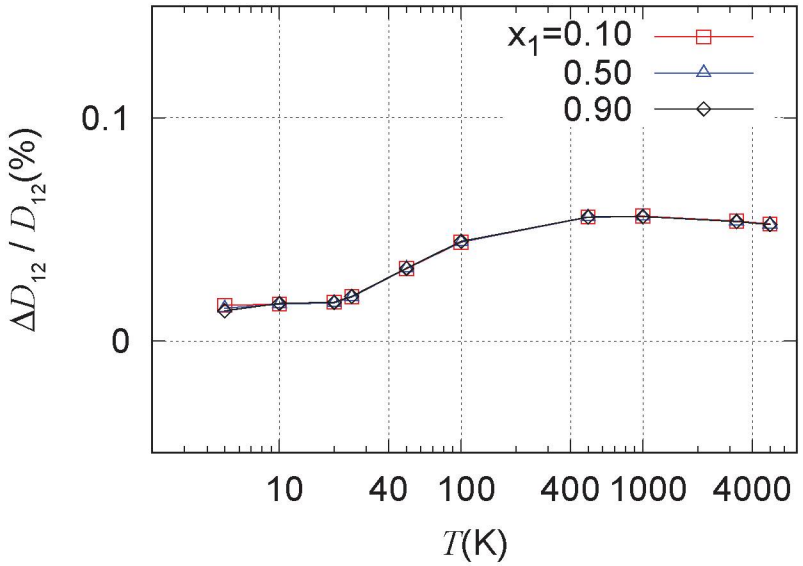

Figure 5.10: Relative uncertainty of diffusions coefficient D_{12} related to potential for neon-argon mixture.

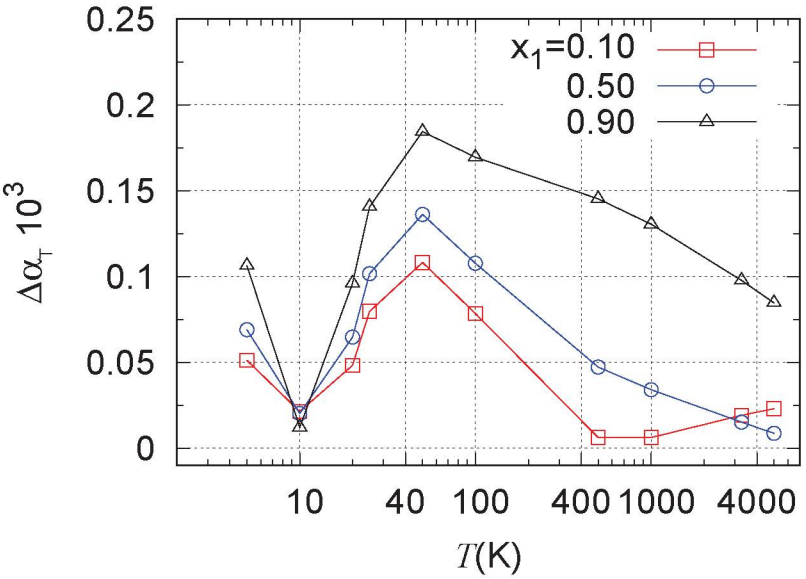

Figure 5.11: Uncertainty of thermal diffusion factor α_{T} related to potential for neon-argon mixture.

5.4 Discussions

To analyze the obtained data, the viscosity, thermal conductivity, diffusion and thermal diffusion factor are plotted against the temperature in Figures 5.12, 5.13, 5.14, and 5.15, respectively. In all cases, the viscosity, thermal conductivity and diffusion increase with the temperature. The viscosity of neon-argon mixture shown in Figure 5.12 has a different dependence on the molar fraction than the mixtures helium-neon and helium-argo. Indeed, the mixture with a small atomic mass ratio m_2/m_1, i.e. neon-argon, the viscosity of the lighter species μ_{Ne} is always larger than that of the heavier one μ_{Ar}. The viscosity of the mixture of these two species always varies between μ_{Ar} and μ_{Ne}. In contrast, the mixture with a large atomic mass ratio m_2/m_1, i.e. helium-neon and helium-argon, the viscosity of the lighter species is smaller than that of the heavier one in some specific temperature range. The values of viscosity of these mixtures are inverted at low temperatures. In this case, the viscosity of the mixture does not always vary between the single gas viscosities.

The thermal conductivity has the same qualitative behavior for all mixtures considered here. More specifically, the lighter species always has a larger thermal conductivity. The thermal conductivity of mixture always varies between conductivities of the corresponding single gases.

The diffusion coefficient depicted in Figure 5.14 is weakly affected by the molar fraction of the mixture.

Figure 5.15 shows the behavior of the thermal diffusion factor. In case of the He-Ne and He-Ar mixture, this quantity is negative within a significant range of temperature T and is positive at low temperatures. Such an inversion of the thermal diffusion in liquids was reported in some previously published papers [120,121]. To the best of our knowledge, the same phenomenon in gases has not been observed yet. The thermal diffusion factor of neon-argon mixture is always negative, but its dependence on the temperature is not monotone, i.e. it has a maximum (minimum of the magnitude) at about $T = 40$ K and a minimum (maximum of the magnitude) at about $T = 800$ K. Such a behavior is explained by that fact that the thermal diffusion factor is determined by both molecular mass ratio and cross section ratio of two species. According to Figure 5.1, the cross section of helium drastically increases by decreasing the temperature, while the cross sections of neon and argon tend to constant values. Thus, the large difference of the cross sections could be

the reason of the sign inversion at a low temperature.

5.5 Comparison with other works

5.5.1 Helium-Neon mixture

The paper by Kestin *et al.* [91] reports expressions and values of the transport coefficients for mixtures of the noble gases. The uncertainty of the coefficients was evaluated by comparison with experimental data published before 1984. For the specific helium-neon mixture, the authors of Ref. [91] provided the uncertainties 0.5 %, 0.7 %, 1 % and 8% for μ, κ, D_{12} and α_{T}, respectively. Note, that the uncertainties of the present work are smaller in all cases. Song et al. [76, 77] calculated these coefficients using only the first order of the Sonine polynomial expansion ($N = 1$). They did not provide an estimation of their uncertainties. The deviations of the present results from those reported in [76,77,91] are plotted on Figures 5.16-5.19.

The deviation of the viscosity from the data by Kestin *et al.* [91] shown in Figure 5.16 by the solid lines with symbols is within the uncertainty of 0.5 % declared in Ref. [91] only in the range $80 \leq T/\mathrm{K} \leq 700$. Out of this range, the uncertainty exceeds 0.5 % and reaches the value of 2 % for T=50 K and 3000 K. The deviation of the viscosity data by Song *et al.* [76] varies in the range from 1 % to 4 %. Such a deviation cannot be explained just by the low order of the Sonine expansion used by the authors of Ref. [76]. The probable reason is a large numerical error of the phase shifts calculated by Eq. (5) in Ref. [76].

A comparison of the present results on the thermal conductivity with those reported in Refs. [76, 91] and demonstrated in Figure 5.17 leads to much the same conclusion as that for the viscosity. The deviation of the present calculation from values recommended by Kestin *et al.* [91] is smaller than the uncertainty of 0.7% given in Ref. [91] only in the temperature range $80 \leq T/\mathrm{K} \leq 400$. At the lowest temperature $T = 50$ K, the difference is about 1.5 %, while it reaches 3.5 % at the highest temperature $T = 3000$ K. The difference between our results and those of Song *et al.* [76], varies from 3 % to 5 % depending upon the molar fraction.

The deviation between diffusion coefficient values reported in Ref. [91] and those obtained in the present work, and illustrated in Figure 5.18, varies between -0.5% to +6%, typically larger than the 1% given in Ref. [91]. Deviations of the values reported in Ref. [77] from those obtained in the present paper is within 2 %.

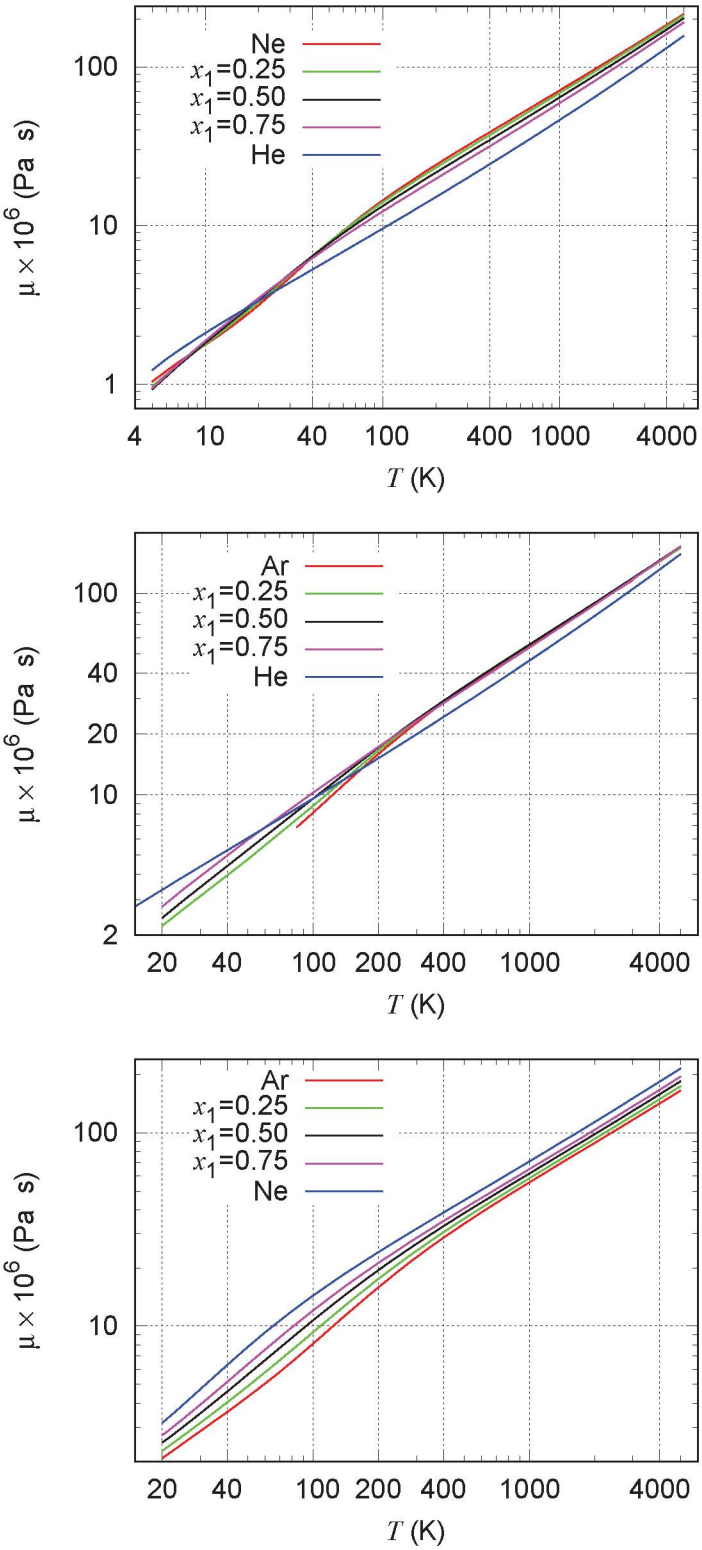

Figure 5.12: Viscosity vs. temperature T: upper He-Ne, middle He-Ar, lower Ne-Ar

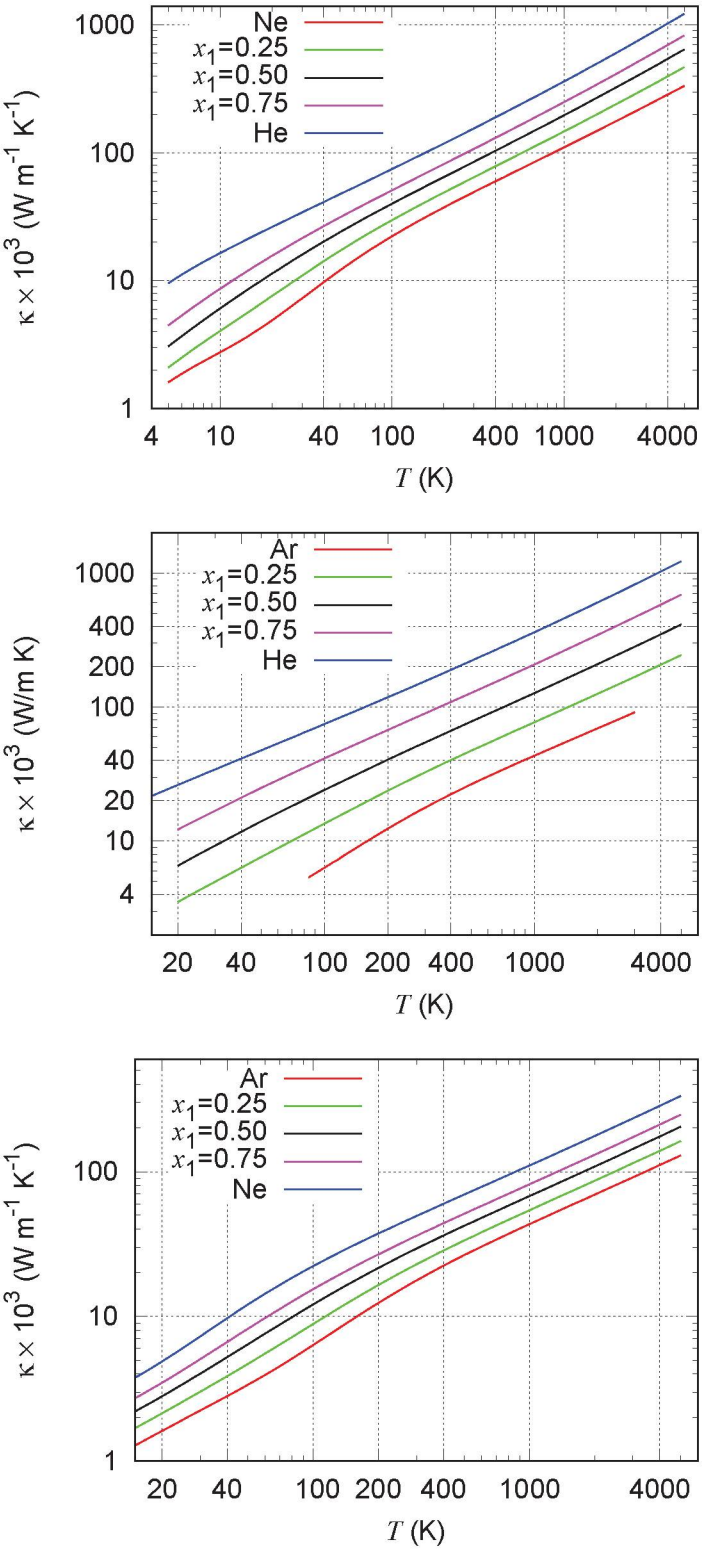

Figure 5.13: Thermal conductivity vs. temperature T: upper He-Ne, middle He-Ar, lower Ne-Ar

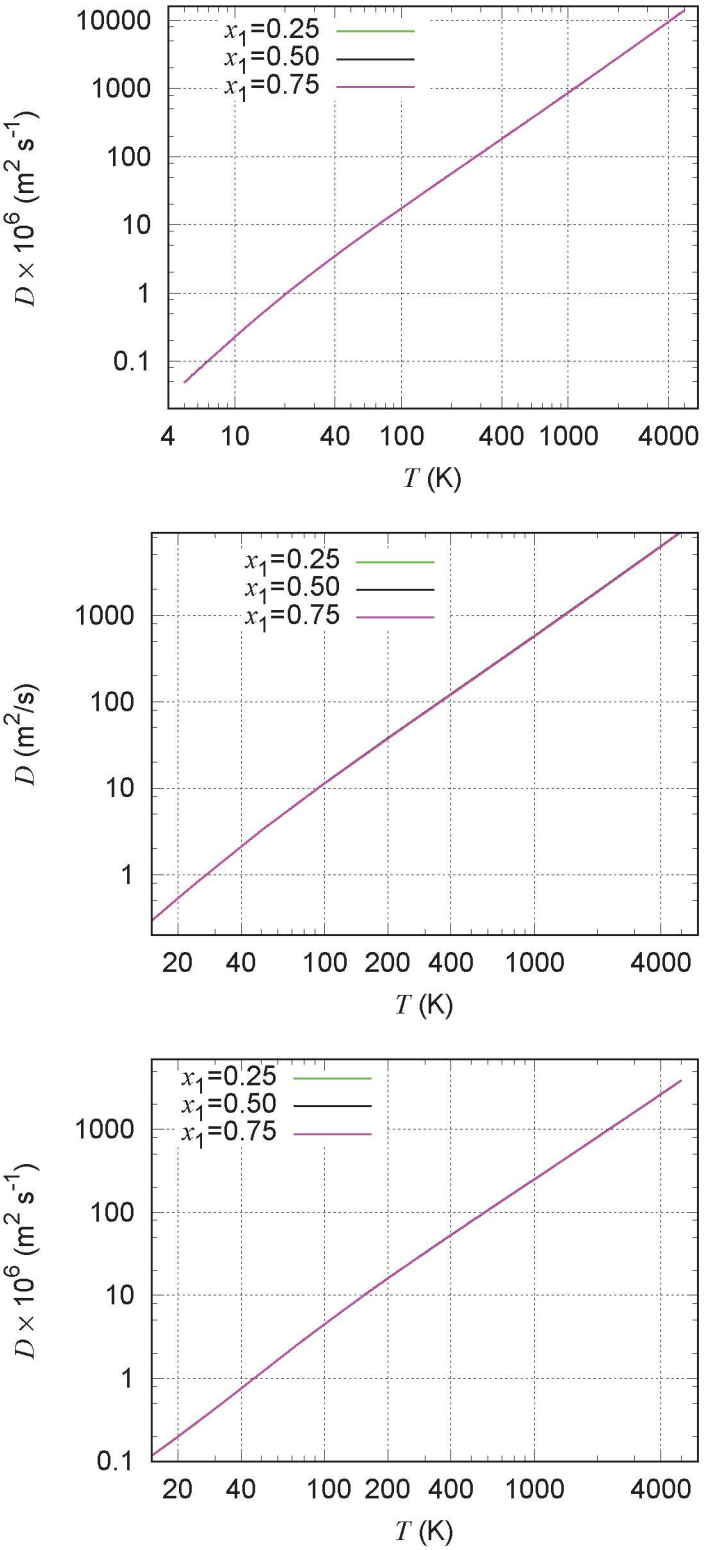

Figure 5.14: Diffusion vs. temperature T: upper He-Ne, middle He-Ar, lower Ne-Ar

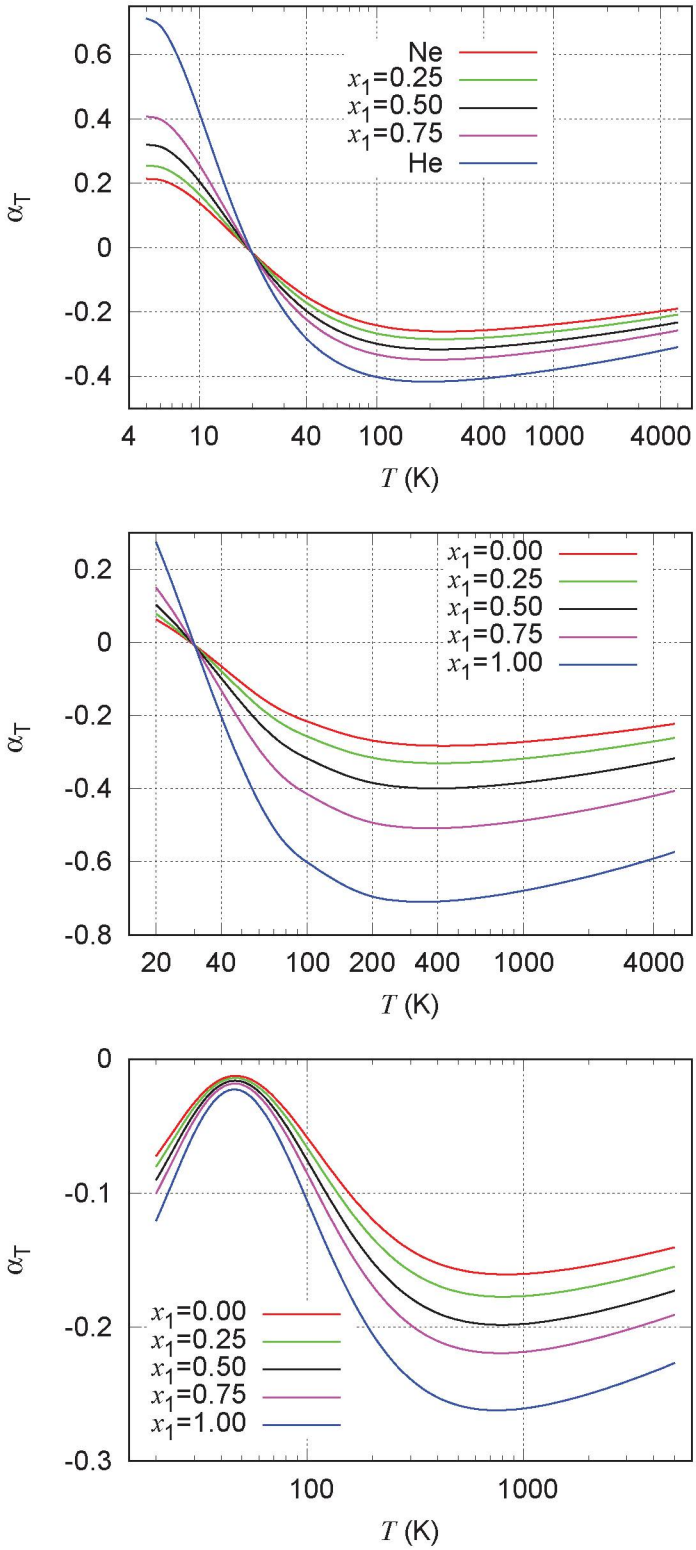

Figure 5.15: Thermal diffusion factor vs. temperature T: upper He-Ne, middle He-Ar, lower Ne-Ar

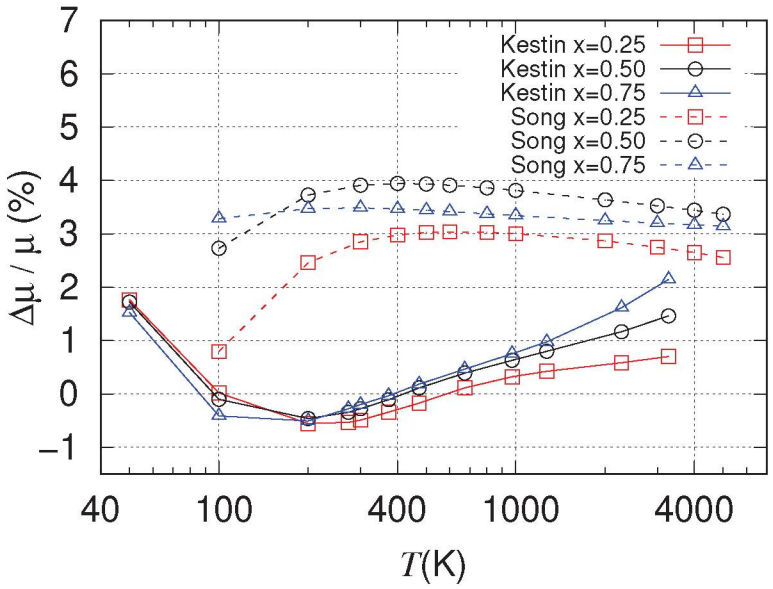

Figure 5.16: Deviation of viscosity of helium-neon mixture calculated in the present work from that reported in Refs. [76,91], $\Delta\mu/\mu = (\mu_{\text{present}} - \mu_{\text{other}})/\mu_{\text{present}}$, solid line with symbols - Ref. [91], dashed line with symbols - Ref. [76]; squares - $x_1 = 0.25$, circles - $x_1 = 0.5$, triangles - $x_1 = 0.75$.

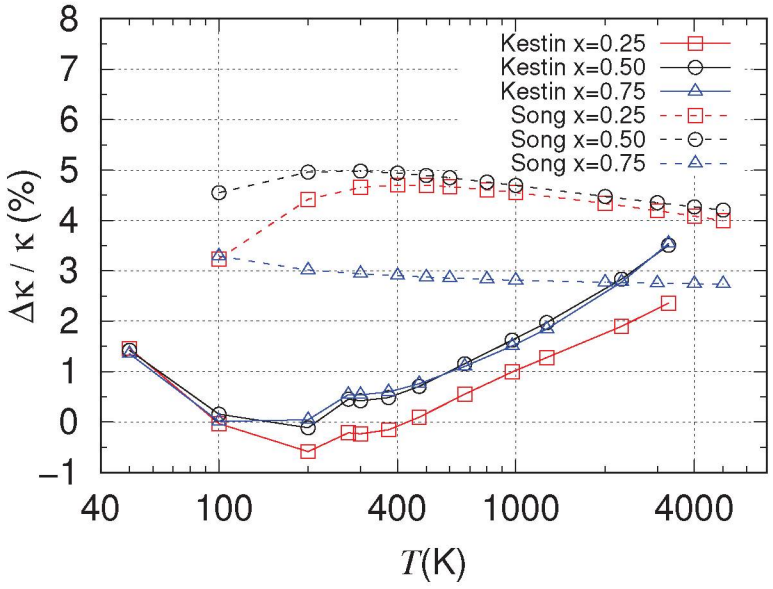

Figure 5.17: Deviation of thermal conductivity of helium-neon mixture calculated in the present work from that reported in Refs. [76, 91], $\Delta\kappa/\kappa = (\kappa_{\text{present}} - \kappa_{\text{other}})/\kappa_{\text{present}}$, solid line - Ref. [91], dashed line - Ref. [76]; squares - $x_1 = 0.25$, circles - $x_1 = 0.5$, triangles - $x_1 = 0.75$.

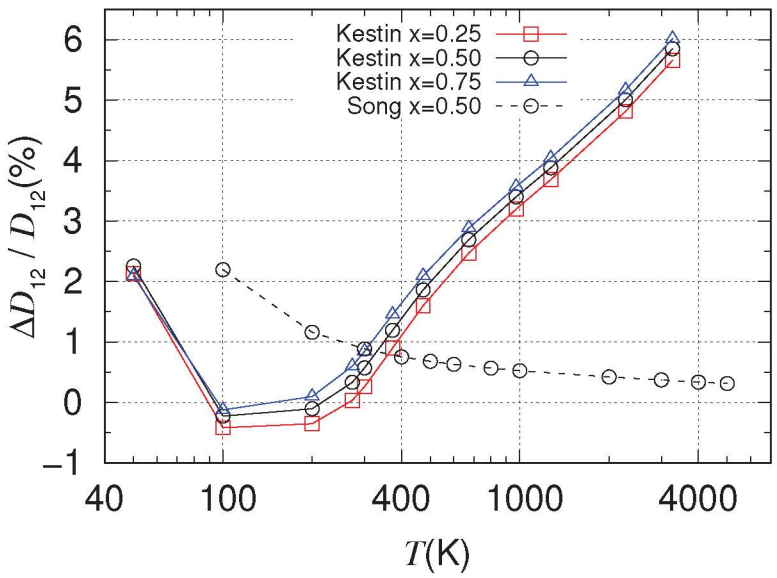

Figure 5.18: Deviation of diffusion coefficient of helium-neon mixture calculated in the present work from that reported in Refs. [77, 91], $\Delta D_{12}/D_{12} = (D_{12,\text{present}} - D_{12,\text{other}})/D_{12,\text{present}}$, solid line - Ref. [91], dashed line - Ref. [77]; squares - $x_1 = 0.25$, circles - $x_1 = 0.5$, triangles - $x_1 = 0.75$.

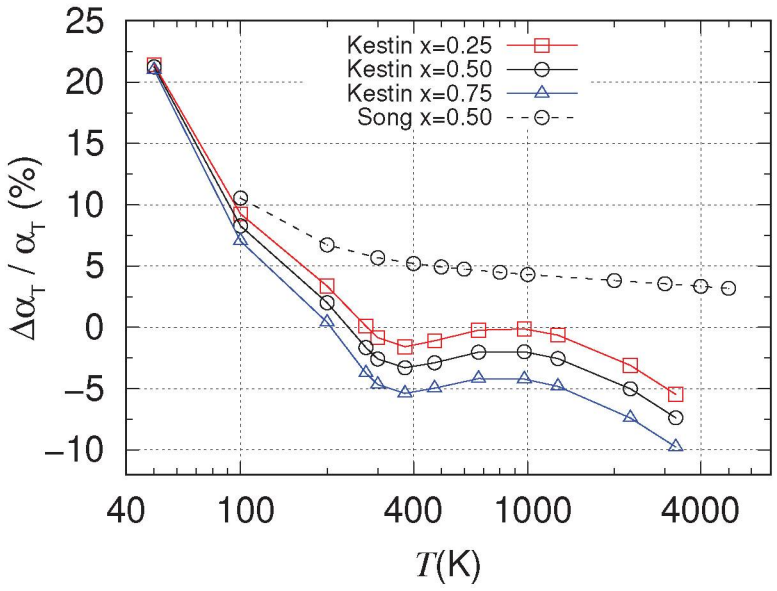

Figure 5.19: Deviation of thermal diffusion factor of helium-neon mixture calculated in the present work from that reported in Refs. [77,91], $\Delta\alpha_T/\alpha_T = (\alpha_{T,\text{ present}} - \alpha_{T,\text{ other}})/\alpha_{T,\text{present}}$, solid line - Ref. [91], dashed line - Ref. [77]; squares - $x_1 = 0.25$, circles - $x_1 = 0.5$, triangles - $x_1 = 0.75$.

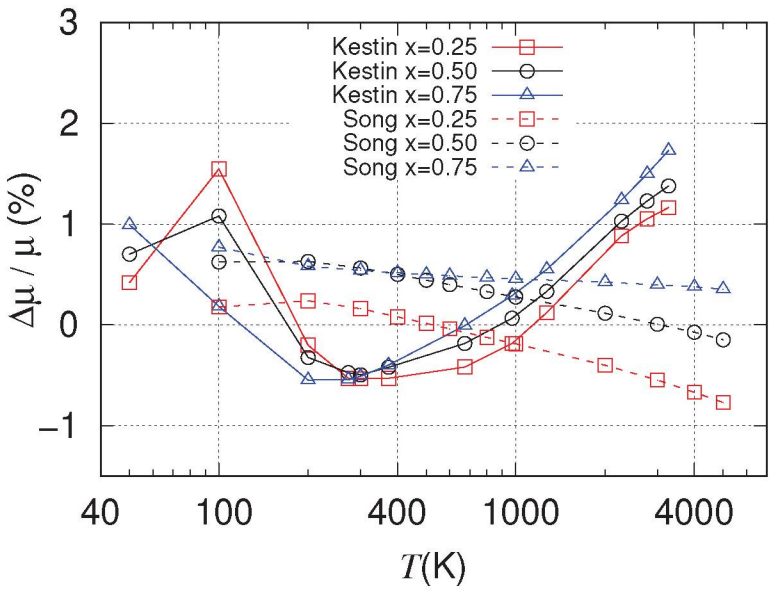

Figure 5.20: Deviation of viscosity of helium-argon mixture calculated in the present work from that reported in Refs. [76, 91], $\Delta\mu/\mu = (\mu_{\text{present}} - \mu_{\text{other}})/\mu_{\text{present}}$, solid line with symbols - Ref. [91], dashed line with symbols - Ref. [76]; squares - $x_1 = 0.25$, circles - $x_1 = 0.5$, triangles - $x_1 = 0.75$.

The uncertainty of 8 % for the thermal diffusion factor α_{T} obtained in Ref. [91] is largest among all coefficients considered here. Its deviation from our results plotted in Figure 5.19 varies from -10 % at the high temperature $T = 3000$ K up to 22 % at the low temperature $T = 50$ K. This probably occurs because the available experimental data were obtained only in the temperature range of 100K to 1000K, which implies that outside this temperature interval, the results are extrapolated. Also, the quantum effects can affect the results obtained by them. The difference between our results and those reported in Ref. [77] ranges in a smaller interval, namely, from 3% at the high temperature $T = 5000$ K up to 22 % at the low temperature.

5.5.2 Helium-Argon mixture

For the helium-argon mixture, the paper by Kestin *et al.* [91] reports the uncertainties 0.4 %, 0.7 %, 1 % and 3% for μ, κ, D_{12} and α_{T}, respectively. Song et al. [76, 77] did not provide an estimation of their uncertainties for this mixture too. The deviations of the present results from those reported in [76, 77, 91] are plotted on Figures 5.20-5.23.

The deviation of the viscosity from the data by Kestin *et al.* [91] shown in Figure 5.20 by the solid lines with symbols is within the uncertainty of 0.5 % declared in Ref. [91]

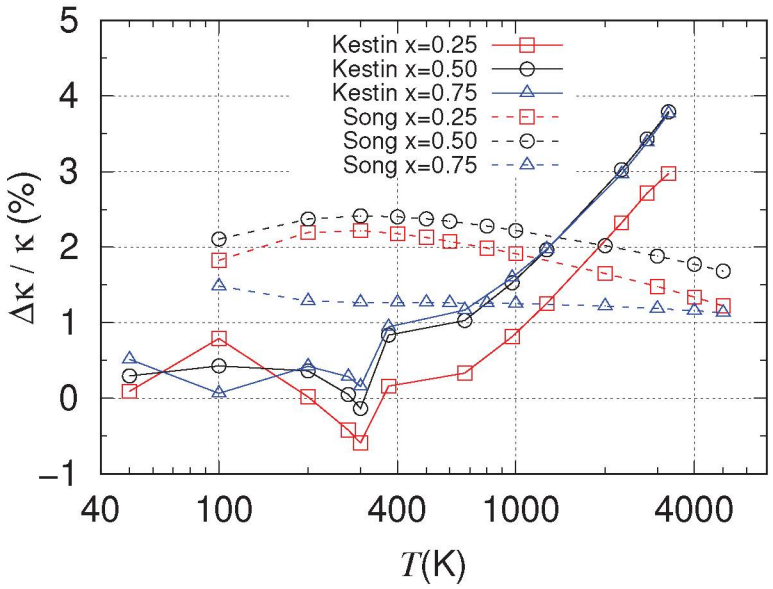

Figure 5.21: Deviation of thermal conductivity of helium-argon mixture calculated in the present work from that reported in Refs. [76, 91], $\Delta\kappa/\kappa = (\kappa_{\text{present}} - \kappa_{\text{other}})/\kappa_{\text{present}}$, solid line - Ref. [91], dashed line - Ref. [76]; squares - $x_1 = 0.25$, circles - $x_1 = 0.5$, triangles - $x_1 = 0.75$.

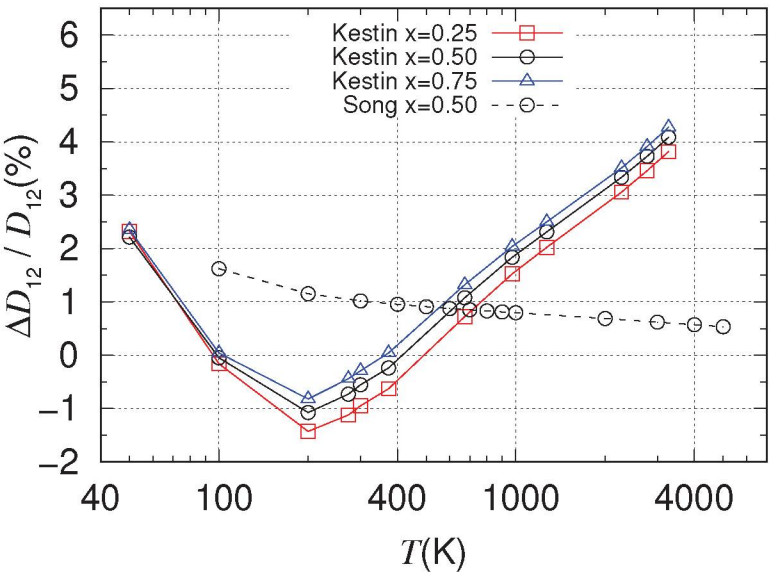

Figure 5.22: Deviation of diffusion coefficient of helium-argon mixture calculated in the present work from that reported in Refs. [77, 91], $\Delta D_{12}/D_{12} = (D_{12,\text{present}} - D_{12,\text{other}})/D_{12,\text{present}}$, solid line - Ref. [91], dashed line - Ref. [77]; squares - $x_1 = 0.25$, circles - $x_1 = 0.5$, triangles - $x_1 = 0.75$.

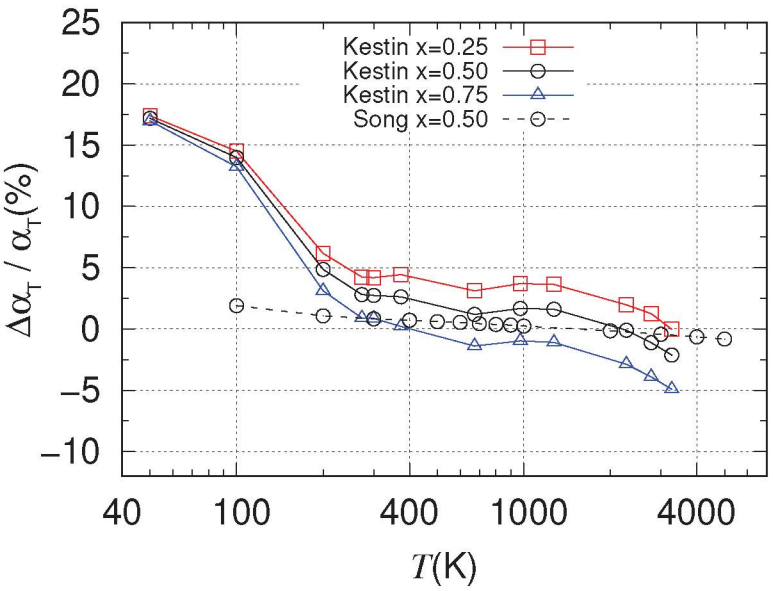

Figure 5.23: Deviation of thermal diffusion factor of helium-argon mixture calculated in the present work from that reported in Refs. [77, 91], $\Delta\alpha_{\rm T}/\alpha_{\rm T} = (\alpha_{\rm T,\ present} - \alpha_{\rm T,\ other})/\alpha_{\rm T,present}$, solid line - Ref. [91], dashed line - Ref. [77]; squares - $x_1 = 0.25$, circles - $x_1 = 0.5$, triangles - $x_1 = 0.75$.

only in the range $200 \leq T/\mathrm{K} \leq 1000$. Out of this range, the uncertainty exceeds 0.5 % and reaches the value of 1.7 % for T=3000 K. The deviation of the viscosity data by Song *et al.* [76] varies in the range from -0.8 % to 0.8 %, which is better compared with the helium-neon coefficients.

A comparison of the present results on the thermal conductivity with those reported in Refs. [76, 91] and demonstrated in Figure 5.21 leads to much the same conclusion as that for the viscosity. The deviation of the present calculation from values recommended by Kestin *et al.* [91] is smaller than the uncertainty of 0.7% given in Ref. [91] only in the temperature range $80 \leq T/\mathrm{K} \leq 300$. However. the difference is about 4 % at the highest temperature $T = 3000$ K. The difference between our results and those of Song *et al.* [76], reaches 2.5 % for $x_1 = 0.5$.

The deviation between diffusion coefficient values reported in Ref. [91] and those obtained in the present work, and illustrated in Figure 5.22, varies between -1.5% to +4%. For the values reported in Ref. [77], the deviation from those obtained in the present paper is about 1.6 % for 100 K and 0.5 % for 5000 K.

The divergences for the thermal diffusion factor $\alpha_{\rm T}$ obtained in Ref. [91] is largest among all coefficients considered here. Its deviation from our results plotted in Figure

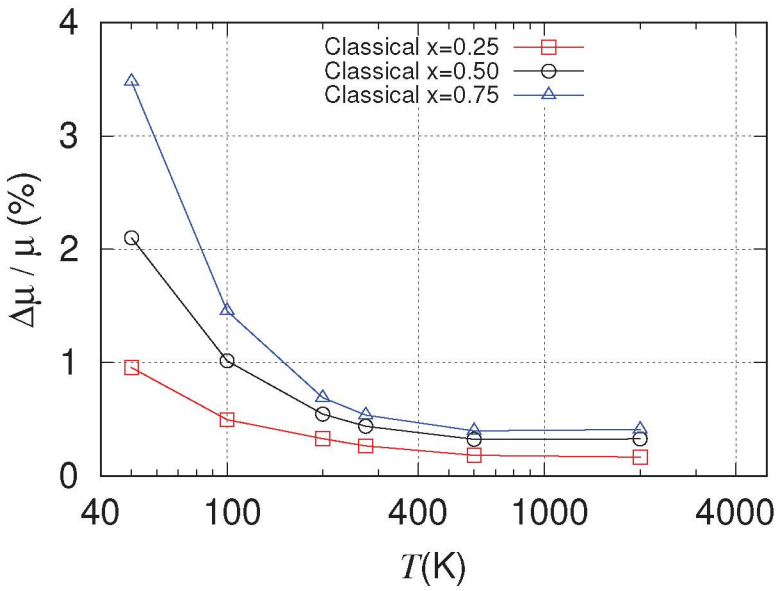

Figure 5.24: Deviation of viscosity of helium-argon mixture calculated in the present work from that reported in Ref. [113], $\Delta\mu/\mu = (\mu_{\text{present}} - \mu_{\text{other}})/\mu_{\text{present}}$; squares - $x_1 = 0.25$, circles - $x_1 = 0.5$, triangles - $x_1 = 0.75$.

5.23 varies from -5 % at the high temperature $T = 3000$ K up to 18 % at the low temperature $T = 50$ K. The difference between our results and those reported in Ref. [77] ranges in a smaller interval, namely, from 2% at the low temperature $T = 100$ K to -0.8 % at the higher temperature.

For this mixture, we have also compared its results with the ones calculated previously in [113], which were calculated classically. The divergences are given in Figures 5.24 - 5.27. As one can see, for all coefficients and mole fractions, the divergence grows at low temperatures, and can be over 11 % for the thermal diffusion factor. Even for the mixture with more argon, it can be seen a divergence in the results.

5.5.3 Neon-Argon mixture

For the neon-argon mixture, the paper by Kestin *et al.* [91] reports the uncertainties 0.3 %, 0.5 %, 0.7 % and 5% for μ, κ, D_{12} and α_{T}, respectively. Song et al. [76, 77] did not provide an estimation of their uncertainties for this mixture too. The deviations of the present results from those reported in [76, 77, 91] are plotted on Figures 5.28-5.31.

The deviation of the viscosity from the data by Kestin *et al.* [91] shown in Figure 5.28 by the solid lines with symbols is within the uncertainty of 0.3 % declared in Ref. [91] only in the range $200 \leq T/\text{K} \leq 1000$. Out of this range, the uncertainty exceeds 0.5 % and

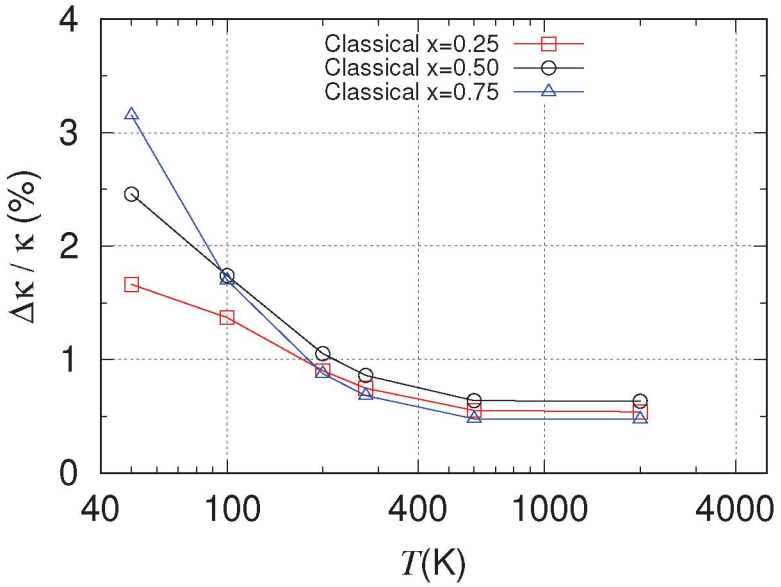

Figure 5.25: Deviation of thermal conductivity of helium-argon mixture calculated in the present work from that reported in Ref. [113], $\Delta\kappa/\kappa = (\kappa_{\text{present}} - \kappa_{\text{other}})/\kappa_{\text{present}}$; squares - $x_1 = 0.25$, circles - $x_1 = 0.5$, triangles - $x_1 = 0.75$.

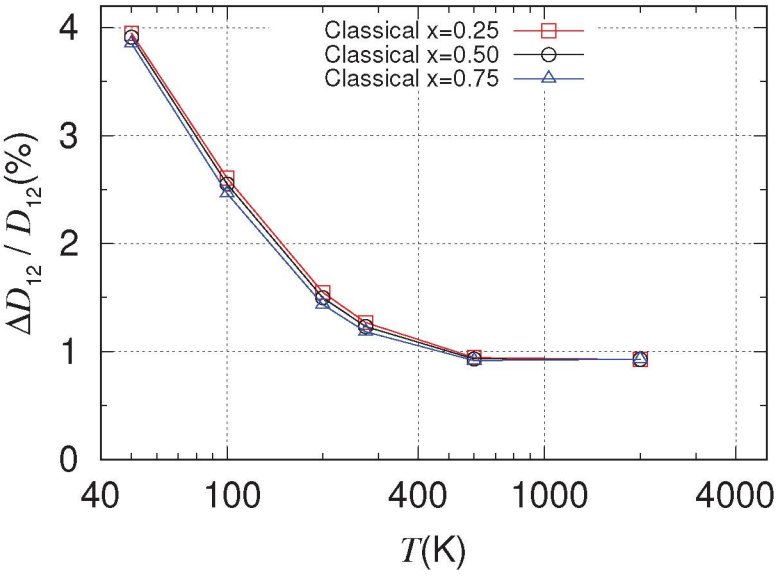

Figure 5.26: Deviation of diffusion coefficient of helium-argon mixture calculated in the present work from that reported in Ref. [113], $\Delta D_{12}/D_{12} = (D_{12,\text{present}} - D_{12,\text{other}})/D_{12,\text{present}}$; squares - $x_1 = 0.25$, circles - $x_1 = 0.5$, triangles - $x_1 = 0.75$.

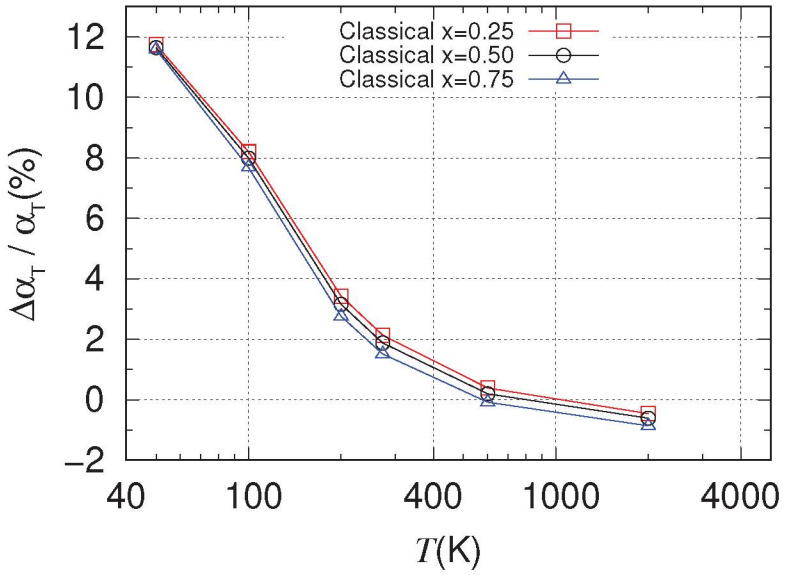

Figure 5.27: Deviation of thermal diffusion factor of helium-argon mixture calculated in the present work from that reported in Ref. [113], $\Delta\alpha_{\mathrm{T}}/\alpha_{\mathrm{T}} = (\alpha_{\mathrm{T,\ present}} - \alpha_{\mathrm{T,\ other}})/\alpha_{\mathrm{T,present}}$; squares - $x_1 = 0.25$, circles - $x_1 = 0.5$, triangles - $x_1 = 0.75$.

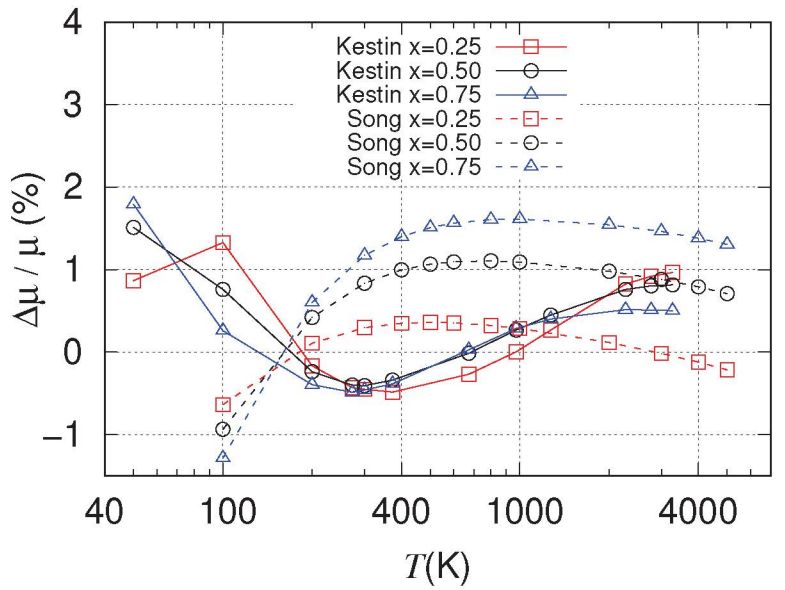

Figure 5.28: Deviation of viscosity of neon-argon mixture calculated in the present work from that reported in Refs. [76,91], $\Delta\mu/\mu = (\mu_{\mathrm{present}} - \mu_{\mathrm{other}})/\mu_{\mathrm{present}}$, solid line with symbols - Ref. [91], dashed line with symbols - Ref. [76]; squares - $x_1 = 0.25$, circles - $x_1 = 0.5$, triangles - $x_1 = 0.75$.

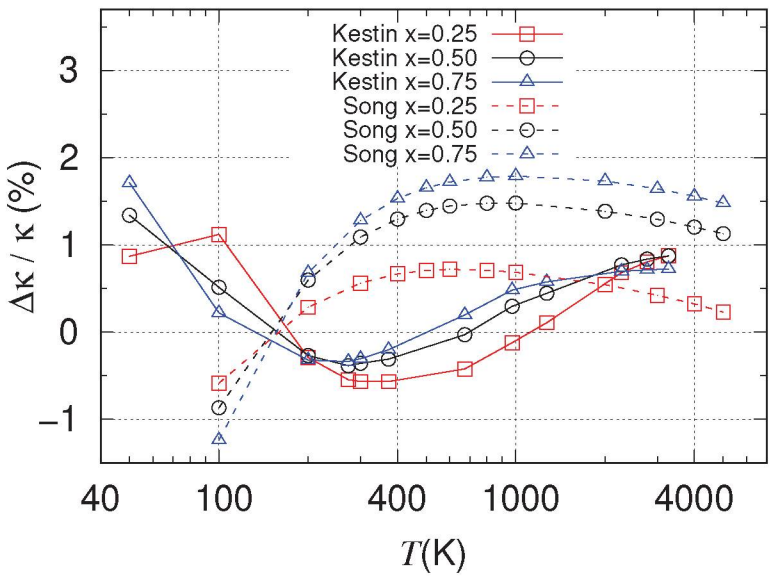

Figure 5.29: Deviation of thermal conductivity of neon-argon mixture calculated in the present work from that reported in Refs. [76, 91], $\Delta\kappa/\kappa = (\kappa_{\text{present}} - \kappa_{\text{other}})/\kappa_{\text{present}}$, solid line - Ref. [91], dashed line - Ref. [76]; squares - $x_1 = 0.25$, circles - $x_1 = 0.5$, triangles - $x_1 = 0.75$.

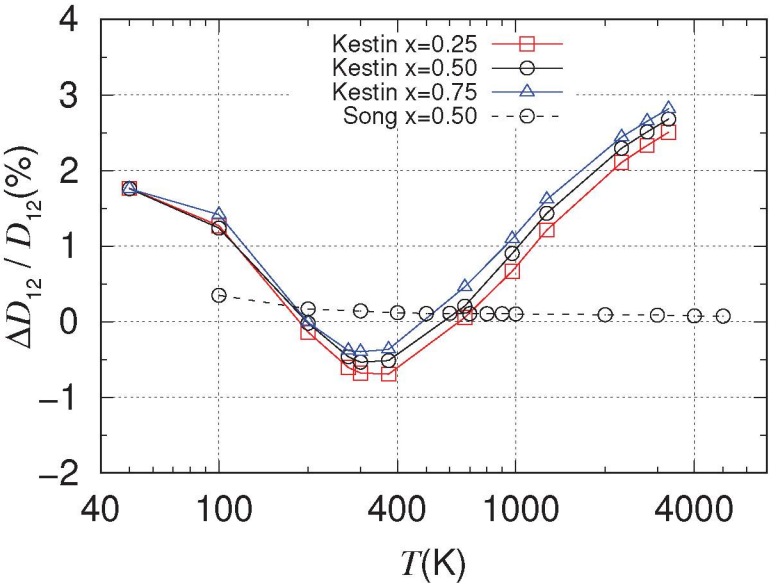

Figure 5.30: Deviation of diffusion coefficient of neon-argon mixture calculated in the present work from that reported in Refs. [77, 91], $\Delta D_{12}/D_{12} = (D_{12,\text{present}} - D_{12,\text{other}})/D_{12,\text{present}}$, solid line - Ref. [91], dashed line - Ref. [77]; squares - $x_1 = 0.25$, circles - $x_1 = 0.5$, triangles - $x_1 = 0.75$.

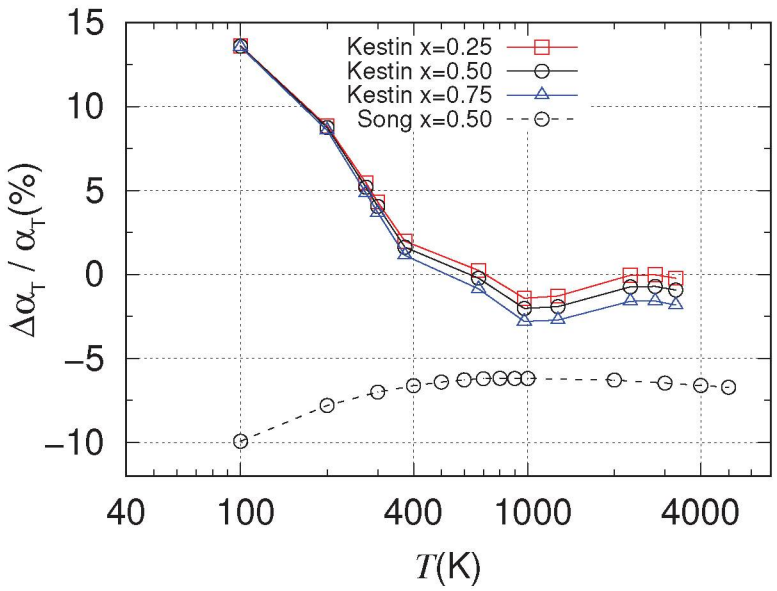

Figure 5.31: Deviation of thermal diffusion factor of neon-argon mixture calculated in the present work from that reported in Refs. [77,91], $\Delta\alpha_{\rm T}/\alpha_{\rm T} = (\alpha_{\rm T,\ present} - \alpha_{\rm T,\ other})/\alpha_{\rm T,present}$; solid line - Ref. [91], dashed line - Ref. [77]; squares - $x_1 = 0.25$, circles - $x_1 = 0.5$, triangles - $x_1 = 0.75$.

reaches the value of 1.85 % for T=3000 K. The deviation of the viscosity data by Song *et al.* [76] varies in the range from -1 % to 1.6 %.

A comparison of the present results on the thermal conductivity with those reported in Refs. [76, 91] and demonstrated in Figure 5.29 leads to much the same conclusion as that for the viscosity. The deviation of the present calculation from values recommended by Kestin *et al.* [91] is smaller than the uncertainty of 0.5% given in Ref. [91] only in the temperature range $100 \leq T/\mathrm{K} \leq 1000$. However. the difference is about 2 % at the lowest temperature $T = 50$ K. The difference between our results and those of Song *et al.* [76], reaches 1.8 % for $x_1 = 0.75$.

The deviation between diffusion coefficient values reported in Ref. [91] and those obtained in the present work, and illustrated in Figure 5.30, varies between -0.8% to +3%. For the values reported in Ref. [77], the deviation from those obtained in the present thesis is about 0.5 % for 100 K and 0.1 % for 5000 K.

The divergences for the thermal diffusion factor $\alpha_{\rm T}$ obtained in Ref. [91] is largest among all coefficients considered here. Its deviation from our results plotted in Figure 5.31 varies from -2 % at the high temperature $T = 3000$ K up to 15 % at the low temperature $T = 50$ K. The difference between our results and those reported in Ref. [77]

ranges in a smaller interval, namely, from -10% at the low temperature $T = 100$ K to -7 % at the higher temperature.

Chapter 6

FINAL STATEMENTS

6.1 Conclusions

The transport coefficients, namely, viscosity, thermal conductivity, diffusion and thermal diffusion, for helium-neon, helium-argon, and neon-argon mixtures have been calculated with a high precision using *ab initio* potentials over the temperature range from 20 K to 5000 K using the Chapman-Enskog method. The 10^{th} order of the expansion with respect to the Sonine polynomials has been taken into account. According to this method, the transport coefficients are expressed in terms of the Omega integrals containing the transport cross sections as integrants. The cross sections have been calculated applying the quantum theory of scattering. The main contributions into the uncertainty of the obtained results come from the potentials for the He-Ne, He-Ar and Ne-Ar used here. A deep analysis of all errors related to the numerical procedure has been performed. The main contributions into the numerical errors are the truncation of the expansion with respect to the Sonine polynomials, the quadratures used to calculate the Omega integrals, the truncation of the transport coefficients with respect to the phase shifts, and finite difference scheme to calculate the phase shifts. It has been shown that the total numerical error for all coefficients is several orders smaller than the potential uncertainty. The calculations have been carried out for many values of both temperature and molar fraction of the mixtures.

For the helium-neon mixture, the relative uncertainties of the viscosity and thermal conductivity vary from 0.09 % at the high temperature up to 0.4 % at the low one. The relative uncertainty of the diffusion coefficient is about 0.04 % in the temperature interval from $T = 20$ K to 5000 K. It increases up to 0.13 % at the low temperatures. The absolute uncertainty of the thermal diffusion factor is smaller than 0.5×10^{-3} for $T \geq 100$ K. It

reaches the maximum value of 1.5×10^{-3} for $T = 10$ K. It has been detected the sign inversion of this coefficient at $T = 18.7$ K. As a result, the relative uncertainty drastically increases near this point so that only its absolute value is reported.

For the helium-argon mixture, the relative uncertainties of the viscosity and thermal conductivity vary from 0.09 % at the high temperature up to 0.4 % at the low one. The relative uncertainty of the diffusion coefficient is about 0.05 % for the whole temperature range. The absolute uncertainty of the thermal diffusion factor is smaller than 0.5×10^{-3} for $T \geq 100$ K. It reaches the maximum value of 3×10^{-3} for $T = 5$ K. It has been also observed the inversion on the sign of the factor at low temperatures.

For the neon-argon mixture, the relative uncertainties of the viscosity and thermal conductivity vary from 0.09 % at the high temperature up to 0.4 % at the low one. The relative uncertainty of the diffusion coefficient is about 0.05 % in the temperature interval from $T = 100$ K to 5000 K. It decreases to 0.02 % at the low temperatures. The absolute uncertainty of the thermal diffusion factor is smaller than 0.2×10^{-3} for all temperatures, reaching 0.025×10^{-3} at $T = 10$ K. The thermal diffusion factor of this mixture is always negative.

A comparison of the present results with data published previously showed that, at the moment, the results reported in the present work are the most precise for dilute gaseous mixtures. Moreover, the temperature range considered here is larger in comparison with other papers that reported the transport coefficients for the mixtures considered in this work.

6.2 Publications on this work

This work resulted in two papers published in the Journal of Chemical Physics [113, 122]. Main results were presented at the 2nd European Conference on Non-Equilibrium Gas Flows (Eindhoven, The Netherlands) in 2015 and at the 31st International Symposium on Rarefied Gas Dynamics (Glasgow, United Kingdom) in July, 2018. At least other two papers based on the results of the present work will be submitted.

6.3 Recommendations for future work

The developed numerical codes can be used to calculate the transport coefficients for any other mixture of monatomic gases for arbitrary potential and any order of approxi-

mation in the Sonine polynomials expansion. In order to use these codes for the isotope helium-3, some modification will be made in calculations of the phase shifts taking into account that this isotope is a fermion, while helium-4 is a boson. The same methodology can be used to calculate the transport coefficients for ternary mixtures, e.g., helium-neon-argon. In this case, the final expressions of the transport coefficients must be adapted, while the procedure to calculate the Omega integrals is the same. In the present work, the average atomic mass of neon and argon have been considered. However, the uncertainty related to the isotopic composition can be close to that related to the potential. Thus, the influence of this factor on the transport coefficients is also worth to study in the future.

Appendix A

UNIVERSAL CONSTANTS

Table A.1: Universal constants according to CODATA-2014, Ref. [123].

Constant	Symbol	Value
Bohr radius	a_0	$0.529\ 177\ 210\ 92(17) \times 10^{-10}$ m
Hartree energy	E_h	$4.359\ 744\ 34(19) \times 10^{-18}$J
Boltzmann constant	k_{B}	$1.380\ 648\ 8(13) \times 10^{-23}$ J / K
Reduced Planck constant	$\hbar$	$1.054\ 571\ 726(47) \times 10^{-34}$ J $\cdot$ s
Atomic unit for weight	u	$1.660\ 538\ 921(73) \times 10^{-27}$ kg
Loschmidt constant	N_L	$2.651\ 646\ 7(15) \times 10^{25}$ m^{-3}

Bibliography

[1] R. Shah and D. Sekulic, *Fundamentals of Heat Exchanger Design* (John Wiley & Sons, New Jersey, 2003).

[2] A. Nienow, M. Edwards, and N. Harnby, *Mixing in the Process Industries* (Butterworth-Heinemann, 1992), 2 edn.

[3] W. Isalski, *Separation of gases* (Oxford University Press, 1989).

[4] R. Jaaniso and O. Tan, *Semiconductor Gas Sensors* (Elsevier, 2013).

[5] E. Hirschel, *Basics of Aerothermodynamics* (Springer, 2015), 2 edn.

[6] L. D. Landau and E. M. Lifshitz, *Fluid Mechanics* (Pergamon, New York, 1989).

[7] L. I. Sedov, *Mechanics of Continuous Media* (World Scientific, 1997).

[8] J. Happel and H. Brenner, *Low Reynolds number hydrodynamics* (Noordhoff International Publishing Leyden, 1973).

[9] J. O. Hirschfelder, C. F. Curtiss, and R. B. Bird, *The Molecular Theory of Gases and Liquids* (Wiley, New York, 1954).

[10] M. N. Kogan, *Rarefied Gas Dynamics* (Plenum, New York, 1969).

[11] C. Cercignani, *Rarefied Gas Dynamics. From Basic Concepts to Actual Calculations* (Cambridge University Press, Cambridge, 2000).

[12] G. A. Bird, *Molecular Gas Dynamics and the Direct Simulation of Gas Flows* (Oxford University Press, Oxford, 1994).

[13] F. Sharipov, *Rarefied Gas Dynamics. Fundamentals for Research and Practice* (Wiley-VCH, Berlin, 2016).

[14] A. Volkov and F. Sharipov, "Flow of a monatomic rarefied gas over a circular cylinder: Calculations based on the *ab initio* potential method." Int. J. Heat Mass Transfer. **114**, 47–61 (2017).

[15] F. Sharipov, "Modelling of transport phenomena in gases based on quantum scattering." Physica A **508**, 797–805 (2018).

[16] F. Sharipov, "Gaseous mixtures in vacuum systems and microfluidics," J. Vac. Sci. Technol. A **31**, 050 806 (2013).

[17] A. van Itterbeek and O. van Paemel, "Measurements on the viscosity of neon, hydrogen, deuterium and helium as a function of the temperature, between room temperature and liquid hydrogen temperatures," Physica **7**, 265–272 (1940).

[18] J. M. J. Coremans, A. van Itterbeek, J. J. M. Beenakker, H. F. P. Knaap, and P. Zandbergen, "The viscosity of gaseous He, Ne, H_2 and D_2 below 80°K," Physica **24**, 557–576 (1958).

[19] J. Kestin and W. Leidenfrost, "The viscosity of Helium," Physica **25**, 537–555 (1959).

[20] E. Thornton, "Viscosity and thermal conductivity of binary gas mixtures: Xenon-Krypton, Xenon-Argon, Xenon-Neon and Xenon-Helium," Proc. Phys. Soc. London **76**, 104 (1960).

[21] E. Thornton, "Viscosity and thermal conductivity of binary gas mixtures: Krypton-Argon, Krypton-Neon, and Krypton-Helium," Proc. Phys. Soc. London **77**, 1166 (1961).

[22] E. Thornton and W. Baker, "Viscosity and thermal conductivity of binary gas mixtures: Argon-Neon, Argon-Helium, and Neon-Helium," Proc. Phys. Soc. London **80**, 1171 (1962).

[23] D. Clifton, "Measurements of the Viscosity of Krypton," J. Chem. Phys. **38**, 1123–1131 (1963).

[24] J. Kestin, S. Ro, and W. Wakeham, "Viscosity of the noble gases in the temperature range 25-700 C," J. Chem. Phys. **56**, 4119–4124 (1972).

[25] P. Tekasakul, J. A. Bentz, R. V. Tompson, and S. K. Loyalka, "The spinning rotor gauge: Measurements of viscosity, velocity slip coefficients, and tangential momentum accommodation coefficients," J. Vac. Sci. Technol. A **14**, 2946–2952 (1996).

[26] J. A. Bentz, R. V. Thompson, and S. K. Loyalka, "Viscosity and velocity slip coefficient for gas mixture: measurements with a spinning rotor," J. Vac. Sci. Technol. A **17**, 235–241 (1999).

[27] J. Wilhelm and E. Vogel, "Viscosity Measurements on Gaseous Argon, Krypton, and Propane," Int. J. of Thermophys. **21**, 301–318 (2000).

[28] J. A. Bentz, R. V. Thompson, and S. K. Loyalka, "Measurements of viscosity, velocity slip coefficients, and tangential momentum accommodation coefficients using a modified spinning rotor gauge," J. Vac. Sci. Technol. A **19**, 317–324 (2001).

[29] C. Evers, H. Lösch, and W. Wagner, "An Absolute Viscometer-Densimeter and Measurements of the Viscosity of Nitrogen, Methane, Helium, Neon, Argon, and Krypton over a Wide Range of Density and Temperature," Int. J. Thermophysics **23**, 1411–1439 (2002).

[30] W. F. May, M. R. Moldover, R. F. Berg, and J. J. Hurly, "Transport properties of argon at zero density from viscosity-ratio measurements," Metrologia **43**, 247–258 (2006), erratum: Metrologia **43**, 183 (2006).

[31] E. Vogel, "Reference Viscosity of Argon at Low Density in the Temperature Range from 290K to 680K," Int. J. Thermophys. **31**, 447–461 (2010).

[32] R. Berg and M. Moldover, "Recommended viscosities of 11 Dilute Gases at 25° C," J. Phys. Chem. Ref. Data **41**, 043 104 (2012).

[33] R. F. Berg and W. C. Burton, "Noble gas viscosities at 25° C," Mol. Phys. **111**, 195–199 (2013).

[34] R. F. Berg, E. F. May, and M. R. Moldover, "Viscosity Ratio Measurements with Capillary Viscometers," J. Chem. Eng. Data **59**, 116–124 (2014).

[35] H. Lin, X. J. Feng, J. T. Zhang, and C. Liu, "Using a two-capillary viscometer with preheating to measure the viscosity of dilute argon from 298.15 K to 653.15 K," J. Chem. Phys. **141**, 234 311 (2014).

[36] J. De Groot, J. Kestin, and H. Sookiazian, "Instrument to measure the thermal conductivity of gases," Physica **75**, 454–482 (1974).

[37] M. J. AssaeL, M. Dix, A. Lucas, and W. Wakeham, "Absolute determination of the thermal-conductivity of the noble-gases and 2 of their binary-mixtures as a function of density," Journal of the Chemical Society-Faraday Transactions I **77**, 439–464 (1981).

[38] J. Kestin, R. Paul, A. A. Clifford, and W. Wakeham, "Absolute determination of the thermal conductivity of the noble gases at room temperature up to 35 MPa," Physica A **100**, 349–369 (1980).

[39] R. Fleeter, J. Kestin, R. Paul, and W. Wakeham, "The thermal conductivity of mixtures of nitrogen with four noble gases at room temperature," Physica A **108**, 371–401 (1981).

[40] F. Uribe, E. Mason, and J. Kestin, "Thermal Conductivity of Nine Polyatomic Gases at Low Density," J. Phys. Chern. Ref. Data **19**, 1123–1136 (1990).

[41] T. Marrero and E. Mason, "Gaseous Diffusion Coefficients," J. Phys. Chem. Ref. Data **1**, 3–118 (1972).

[42] T. Kugler, B. Jager, E. Bich, M. H. Rausch, and A. P. Froba, "Measurement of bynary diffusion coefficients for neon-argon gas mixtures using Loschmidt cell combined with holographic interferometry," Int. J. Thermophys. **34**, 47–63 (2013).

[43] E. H. Kennard, *Kinetic Theory of Gases* (McGraw-Hill Book Company, Inc., New York, 1938).

[44] S. Chapman and T. G. Cowling, *The Mathematical Theory of Non-Uniform Gases* (University Press, Cambridge, 1952).

[45] J. H. Ferziger and H. G. Kaper, *Mathematical Theory of Transport Processes in Gases* (North-Holland Publishing Company, Amsterdam, 1972).

[46] F. Sharipov and G. Bertoldo, "Numerical solution of the linearized Boltzmann equation for an arbitrary intermolecular potential," J. Comp. Phys. **228**, 3345–3357 (2009).

[47] O. I. Dodulad, Y. Y. Kloss, D. O. Savichkin, and F. G. Tcheremissine, "Knudsen pumps modeling with Lennard-Jones and ab initio intermolecular potentials," Vacuum **109**, 360–367 (2014).

[48] F. Sharipov and J. L. Strapasson, " *Ab initio* simulation of transport phenomena in rarefied gases," Phys. Rev. E **86**, 031 130 (2012).

[49] A. Venkattraman and A. A. Alexeenko, "Binary scattering model for Lennard-Jones potential: Transport coefficients and collision integrals for non-equilibrium gas flow simulations," Phys. Fluids **24**, 027 101 (2012).

[50] F. Sharipov and G. Bertoldo, "Poiseuille flow and thermal creep based on the Boltzmann equation with the Lennard-Jones potential over a wide range of the Knudsen number," Phys. Fluids **21**, 067 101 (2009).

[51] J. L. Strapasson and F. Sharipov, " *Ab initio* simulation of heat transfer through a mixture of rarefied gases," Int. J. Heat Mass Transfer **71**, 91–97 (2014).

[52] F. Sharipov and J. L. Strapasson, " *Ab initio* simulation of rarefied gas flow through a thin orifice," Vacuum **109**, 246–252 (2014).

[53] F. Sharipov and C. F. Dias, " *Ab initio* simulation of planar shock waves," Computers and Fluids **150**, 115–122 (2017).

[54] S. Boyes, "The interatomic potential of argon," Chem. Phys. Lett. **221**, 467–472 (1994).

[55] R. Aziz, A. Janzen, and M. Moldover, "*Ab-initio* calculations for helium: a standard for transport property measurements," Phys. Rev. Lett. **74**, 1586–1589 (1995).

[56] A. R. Janzen and R. A. Aziz, "An accurate potential energy curve for helium based on *ab initio* calculations," J. Chem. Phys. **107**, 914–919 (1997).

[57] S. M. Cybulski and R. R. Toczylowski, "Ground state potential energy curves for He_2, Ne_2, Ar_2, He-Ne, He-Ar, and Ne-Ar: A coupled-cluster study," J. Chem. Phys. **111**, 10 520–10 528 (1999).

[58] F. M. Tao, "*Ab initio* calculation of the interaction potential for the krypton dimer: The use of bond function basis sets," J. Chem. Phys. **111**, 2407–2413 (1999).

[59] T. P. Haley and S. M. Cybulski, "Ground state potential energy curves for He-Kr, Ne-Kr, Ar-Kr, and Kr_2: Coupled-cluster calculations and comparison with experiment," J. Chem. Phys. **119**, 5487–5496 (2003).

[60] P. Slavíček, R. Kalus, P. Paška, I. Odvárková, P. Hobza, and A. Malijevský, "State-of-the-art correlated ab initio potential energy curves for heavy rare gas dimers: Ar_2, Kr_2, and Xe_2," J. Chem. Phys. **119**, 2102–2119 (2003).

[61] J. Cacheiro, B. Fernández, D. Marchesan, S. Coriani, C. Hättig, and A. Rizzo, "Coupled cluster calculations of the ground state potential and interaction induced electric properties of the mixed dimers of helium, neon and argon," Mol. Phys. **102**, 101–110 (2004).

[62] R. Hellmann, E. Bich, and E. Vogel, "*Ab initio* potential energy curve for the helium atom pair and thermophysical properties of dilute helium gas. I. Helium-helium interatomic potential," Mol. Phys. **105**, 3013–3023 (2007).

[63] R. Hellmann, E. Bich, and E. Vogel, "*Ab initio* potential energy curve for the neon atom pair and thermophysical properties of the dilute neon gas. I. Neon-neon interatomic potential and rovibrational spectra," Mol. Phys. **106**, 133–140 (2008).

[64] J. B. Mehl, "*Ab initio* properties of gaseous helium," C. R. Phys. **10**, 859–865 (2009).

[65] A. Baranowska, S. B. Capelo, and B. Fernandez, "New basis sets for the evaluation of interaction energies: an ab initio study of the He-He, Ne-Ne, Ar-Ar, He-Ne, He-Ar and Ne-Ar van der Waals complex internuclear potentials and ro-vibrational spectra," Phys. Chem. Chem. Phys. **12**, 13 586–13 596 (2010).

[66] B. Jäger, R. Hellmann, E. Bich, and E. Vogel, "*Ab initio* pair potential energy curve for the argon atom pair and thermophysical properties of the dilute argon gas. I. Argon-argon interatomic potential and rovibrational spectra," Mol. Phys. **107**, 2181–2188 (2009), erratum in Mol. Phys. **108**, 105 (2010).

[67] M. Przybytek, W. Cencek, J. Komasa, G. Łach, B. Jeziorski, and K. Szalewicz, "Relativistic and quantum electrodynamics effects in the helium pair potential," Phys. Rev. Lett. **104**, 183 003 (2010), Erratum in Phys. Rev. Lett. **108** , 129902 (2012).

[68] J. M. Waldrop, B. Song, K. Patkowski, and X. Wang, "Accurate *ab initio* potential for the krypton dimer and transport properties of the low-density krypton gas," J. Chem. Phys. **142**, 204 307 (2015).

[69] B. Jäger, R. Hellmann, E. Bich, and E. Vogel, "State-of-the-art *ab initio* potential energy curve for the krypton atom pair and thermophysical properties of dilute krypton gas," J. Chem. Phys. **144**, 114 304 (2016).

[70] R. Hellmann, J. B, and E. Bich, "State-of-the-art ab initio potential energy curve for the xenon atom pair and related spectroscopic and thermophysical properties," J. Chem. Phys. **147**, 034 304 (2017).

[71] B. Jäger and E. Bich, "Thermophysical properties of krypton-helium gas mixtures from *ab initio* pair potentials," J. Chem. Phys. **146**, 214 302 (2017).

[72] E. Bich, R. Hellmann, and E. Vogel, " *Ab initio* potential energy curve for the helium atom pair and thermophysical properties of the dilute helium gas. II. Thermophysical standard values for low-density helium," Mol. Phys. **105**, 3035–3049 (2007).

[73] E. Bich, R. Hellmann, and E. Vogel, " *Ab initio* potential energy curve for the neon atom pair and thermophysical properties for the dilute neon gas. II. Thermophysical properties for low-density neon," Mol. Phys. **106**, 813–825 (2008).

[74] E. Vogel, B. Jaeger, R. Hellmann, and E. Bich, "Ab initio pair potential energy curve for the argon atom pair and thermophysical properties for the dilute argon gas. II. Thermophysical properties for low-density argon," Mol. Phys. **108**, 3335–3352 (2010).

[75] W. Cencek, M. Przybytek, J. Komasa, J. B. Mehl, B. Jeziorski, and K. Szalewicz, "Effects of adiabatic, relativistic, and quantum electrodynamics interactions on the pair potencial and thermophysical properties of helium," J. Chem. Phys. **136**, 224 303 (2012).

[76] B. Song, X. Wang, J. Wu, and Z. Liu, "Prediction of transport properties of pure noble gases and some of their binary mixtures by ab initio calculations," Fluid Phase Equilibria **290**, 55–62 (2010).

[77] B. Song, X. Wang, J. Wu, and Z. Liu, "Calculations of the thermophysical properties of binary mixtures of noble gases at low density from ab initio potentials," Mol. Phys. **109**, 1607–1615 (2011).

[78] B. Song, X. Wang, and Z. Liu, "Thermal Conductivity of Pure Noble Gases at Low Density from Ab Initio Prandtl Number," Int. J. Thermophys. **34**, 402–411 (2013).

[79] B. Song, X. Wang, K. Kang, and Z. Liu, "Highly accurate transport properties of Helium-4, Helium-3, and their binary mixtures by *Ab initio* potential," Cryogenics **61**, 1–7 (2014).

[80] D. G. Anderson, "Numerical solution of the Krook kinetic equation," J.Fluid Mech. **25**, 271–287 (1966).

[81] C. Cercignani, *The Boltzmann Equation and its Application* (Springer-Verlag, New York, 1988).

[82] R. K. Pathria and P. D. Beale, *Statistical Mechanics* (Elsevier, Amsterdam, 2011), 3 edn.

[83] F. Mandl, *Statistical Physics* (Wiley, 1991), 2 edn.

[84] C. L. Pekeris and Z. Alterman, "Solution of the Boltzmann-Hilbert integral equation. II. The coefficients of viscosity and heat conduction," Proc. Natl. Acad. Sci. **43**, 998–1007 (1957).

[85] C. L. Pekeris, "Solution of the Boltzmann-Hilbert integral equation," Proc. Natl. Acad. Sci. **41**, 661–669 (1955).

[86] F. Sharipov, "Numerical simulation of rarefied gas flow through a thin orifice," J. Fluid Mech. **518**, 35–60 (2004).

[87] S. Varoutis, D. Valougeorgis, O. Sazhin, and F. Sharipov, "Rarefied gas flow through short tubes into vacuum," J. Vac. Sci. Technol. A **26**, 228–238 (2008).

[88] S. Varoutis, D. Valougeorgis, and F. Sharipov, "Simulation of gas flow through tubes of finite length over the whole range of rarefaction for various pressure drop ratios," J. Vac. Sci. Technol. A. **22**, 1377–1391 (2009).

[89] E. L. Tipton, R. V. Tompson, and S. K. Loyalka, "Chapman-Enskog solutions to arbitrary order in Sonine polynomials II: Viscosity in a binary, rigid-sphere, gas mixture," Eur. J. Mech. B-Fluids **28**, 335–352 (2009).

[90] E. L. Tipton, R. V. Tompson, and S. K. Loyalka, "Chapman-Enskog solutions to arbitrary order in Sonine polynomials III: Diffusion, thermal diffusion, and thermal conductivity in a binary, rigid-sphere, gas mixture," Eur. J. Mech. B-Fluids **28**, 353–386 (2009).

[91] J. Kestin, K. Knierim, E. A. Mason, B. Najafi, S. T. Ro, and M. Waldman, "Equilibrium and transport properties of the noble gases and their mixture at low densities," J. Phys. Chem. Ref. Data **13**, 229–303 (1984).

[92] L. D. Landau and E. M. Lifshitz, *Quantum mechanics - Nonrelatitivistic theory* (Pergamon Press, Oxford, 1958).

[93] J. Joachain, *Quantum Collision Theory* (North-Holland Publishing Company, Amsterdam, 1975).

[94] J. Sakurai and J. Napolitano, *Modern Quantum Mechanics* (Addison-Wesley, San Francisco, 1994).

[95] J. Jones, "On the Determination of Molecular Fields. I. From the Variation of the Viscosity of a Gas with Temperature," Proc. R. Soc. A **106**, 441–462 (1924).

[96] T. Korona, H. L. Williams, R. Bukowski, B. Jeziorski, and K. Szalewicz, "Helium dimer potential from symmetry-adapted perturbation theory calculations using large Gaussian geminal and orbital basis sets," J. Chem. Phys. **106**, 5109–5122 (1997).

[97] J. J. Hurly and M. R. Moldover, "Ab Initio Values of the Thermophysical Properties of Helium as Standards," J. Res. Natl. Inst. Stand. Technol. **105**, 667–688 (2000).

[98] J. J. Hurly and J. B. Mehl, "^{4}He Thermophysical Properties: New Ab Initio Calculations," J.Res. Natl. Inst. Stand. Technol. **112**, 75–94 (2007).

[99] K. T. Tang and J. P. Toennies, "An improved simple model for the van der Waals potential based on universal damping functions for the dispersion coefficients," J. Chem. Phys. **80**, 3726–3741 (1984).

[100] R. Eggenberger, S. Gerber, H. Huber, and D. Searles, "Ab initio calculation of the second virial coefficient of neon and the potencial energy curve of Ne_2," Chem. Phys. **156**, 395–401 (1991).

[101] G. Grochola, S. Russo, and I. Snook, "An *ab initio* pair potential for Ne_2 and the equilibrium properties of neon," Molecular Physics **95**, 471–475 (1998).

[102] R. A. Aziz, "A highly accurate interatomic potential for argon," J. Chem. Phys. **99**, 4518–4525 (1993).

[103] A. E. Nasrabad and R. Laghaei, "Computational studies on thermodynamic properties, effective diameters, and free volume of argon using an ab initio potential," J. Chem. Phys. **125**, 084 510 (2006).

[104] K. Patkowski and K. Szalewicz, "Argon pair potential at basis set and excitation limits," J. Chem. Phys. **133**, 094 304 (2010).

[105] J. Meija, T. B. Coplen, M. Berglund, W. A. Brand, P. De Bievre, M. Groning, N. E. Holden, J. Irrgeher, R. D. Loss, T. Walczyk, and T. Prohaska, "Isotopic composition of the elements 2013 (IUPAC Technical Report)," Pure Appl. Chem. **88**, 293–306 (2016).

[106] J. De Laeter, J. Bohlke, P. De Bievre, H. Hidaka, H. Peiser, K. Rosman, and P. Taylor, "Atomic weights of the elements: Review 2000 - (IUPAC technical report)," Pure Appl. Chem. **75**, 683–800 (2003).

[107] J. Meija, T. B. Coplen, M. Berglund, W. A. Brand, P. De Bievre, M. Groening, N. E. Holden, J. Irrgeher, R. D. Loss, T. Walczyk, and T. Prohaska, "Atomic weights of the elements 2013 (IUPAC Technical Report)," Pure Appl. Chem. **88**, 265–291 (2016).

[108] D. Seibt, S. Herrmann, E. Vogel, E. Bich, and E. Hassel, "Simultaneous Measurements on Helium and Nitrogen with a Newly Designed Viscometer-Densimeter over a Wide Range of Temperature and Pressure," J. Chem. Eng. Data **54**, 2626–2637 (2009).

[109] R. Eggenberger, S. Gerber, H. Huber, D. Searles, and M. Welker, "Calculation of transport properties of neon in the liquid, supercritical, and gaseous state by

molecular dynamics simulations applying an ab initio pair potential," J. Phys. Chem. **97**, 1980–1984 (1993).

[110] L. Xiufeng and L. Xi, "Theoretical calculation of transport properties of the noble gases He and Ne and their binary mixtures at low density," Int. J, Theor. Phys. **35**, 1753–1765 (1996).

[111] R. V. Tompson, E. L. Tipton, and S. K. Loyalka, "Chapman-Enskog solutions to arbitrary order in Sonine polynomials V: Summational expressions for the viscosity-related bracket integrals," Eur. J. Mech. B-Fluids **29**, 153–179 (2010).

[112] M. Jeziorska, W. Cencek, K. Patkowski, B. Jeziorski, and K. Szalewicz, "Pair potential for helium from symmetry-adapted perturbation theory calculations and from supermolecular data," J. Chem. Phys. **127**, 124 303 (2007).

[113] F. Sharipov and V. Benites, "Transport coefficients of helium-argon mixture based on *Ab initio* potential," J. Chem. Phys. **143**, 154 104 (2015).

[114] L. A. Viehland, A. R. Janzen, and R. A. Aziz, "High approximations to the transport properties of pure atomic gases," J. Chem. Phys. **102**, 5444–5450 (1995).

[115] R. V. Tompson, E. L. Tipton, and S. K. Loyalka, "Chapman-Enskog solutions to arbitrary order in Sonine polynomials IV: Summational expressions for the diffusion- and thermal conductivity-related bracket integrals," Eur. J. Mech. B-Fluids **28**, 695–721 (2009).

[116] B. R. Johnson, "New numerical-methods applied to solving one-dimensional eigenvalue problem," J. Chem. Phys. **67**, 4086–4093 (1977).

[117] B. Shizgal, *Spectral Methods in Chemistry and Physics* (Springer, 2015).

[118] R. Pack, "Space-fixed vs body-fixed axes in atom-diatomic molecule scattering. Sudden approximations," J. Chem. Phys. **60**, 633–639 (1974).

[119] F. Meeks, T. Cleland, K. Hutchinson, and W. Taylor, "On the quantum cross sections in dilute gases," J. Chem. Phys. **100**, 3813–3820 (1994), erratum in J.Chem.Phys. **103**, 1239 (1994).

[120] F. S. Gaeta, G. Perna, G. Scala, and F. Bellucci, "Nonisothermal matter transport in sodium chloride and potassium chloride aqueous solutions. 1. Homogeneous system (thermal diffusion)." The Journal of Physical Chemistry **86**, 2967–2974 (1982).

[121] S. Di Lecce, T. Albrecht, and F. Bresme, "A computational approach to calculate the heat of transport of aqueous solutions," Sci Rep **7**, 44 833 (2017).

[122] F. Sharipov and V. Benites, "Transport coefficients of helium-neon mixtures at low density computed from *Ab initio* potentials," J. Chem. Phys. **147**, 224 302 (2017).

[123] P. J. Mohr, D. B. Newell, and B. N. Taylor, "CODATA Recommended Values of the Fundamental Physical Constants: 2014," J. Phys. Chem. Ref. Data **43**, 043 102 (2016).